NASA CONTRACTOR REPORT

NASA CR-656

NASA CR-656

N67 12275
(ACCESSION NUMBER)
108 (PAGES)
NASA CR. 656
(NASA CR OR TMX OR AD NUMBER)

(THRU)
(CODE)
76
(CATEGORY)

FACILITY FORM 602

CHARGE STORAGE EFFECTS IN MYLAR RESULTING FROM ELECTRON IRRADIATION

by L. K. Monteith, J. R. Hauser, and T. M. Royal

Prepared by
RESEARCH TRIANGLE INSTITUTE
Durham, N. C.
for Langley Research Center

NATIONAL AERONAUTICS AND SPACE ADMINISTRATION • WASHINGTON, D. C. • DECEMBER 1966

CHARGE STORAGE EFFECTS IN MYLAR RESULTING FROM

ELECTRON IRRADIATION

By L. K. Monteith, J. R. Hauser, and T. M. Royal

Distribution of this report is provided in the interest of information exchange.   Responsibility for the contents resides in the author or organization that prepared it.

Prepared under Contract No. NAS 1-5225 by
RESEARCH TRIANGLE INSTITUTE
Durham, N.C.

for Langley Research Center

NATIONAL AERONAUTICS AND SPACE ADMINISTRATION

FOREWORD

This report was prepared by the Research Triangle Institute, Research Triangle Park, North Carolina, on NASA Contract NAS1-5225, "Study of the Electron Irradiation Effects on Capacitor-Type Micrometeoroid Detectors". This work was administered under the direction of the Instrument Research Division at Langley Research Center. Charles C. Laney was project engineer for NASA.

This investigation began in June 1965 and was concluded in June 1966. It was performed by the Solid State Laboratory of the Research Triangle Institute under the general direction of Dr. R. M. Burger. L. K. Monteith, J. R. Hauser, and T. M. Royal are the authors of this report. The authors are indebted to H. B. Lyon for his contributions to the research effort.

This report is directly related to earlier reports: "Theoretical Analysis of Operational Characteristics of Micrometeoroid Capacitor Detectors" dated April 1964 and prepared under Contract NAS1-3343 and "Study on the Electron Irradiation Effects on Capacitor-Type Micrometeoroid Detectors", NASA CR-312, October 1965.

ABSTRACT

/2275

External charge transfer resulting from electron irradiation of mylar has been observed and a phenomenological model developed which includes space charge build-up, transport of charge during irradiation and the decay of space charge after ceasing irradiation. The spatial symmetry does not strongly influence the external charge transfer characteristics. The depth of trap filling and the spatial extent of trapped charge are the major factors in determining the external charge transfer. The model has been shown to be in reasonable agreement with the experimental observations.

Charge storage resulting from electron irradiation of a capacitor structure using mylar can result in spontaneous discharge events. The spontaneous discharge characteristics depend upon the irradiation electron energy and the flux rate. At flux rates comparable to the Van Allen flux rate, irregular discharge events with a pulse height less than 1 volt were observed. For flux rates in excess of 10^{12} e/cm^2-sec regular pulsing with a pulse height the order of 100 volts was observed. These can be interpreted as partial and complete liberation of the trapped charge respectively.

Author

CONTENTS

LIST OF ILLUSTRATIONS

LIST OF ILLUSTRATIONS (continued)

LIST OF ILLUSTRATIONS (continued)

x

LIST OF ILLUSTRATIONS (continued)

LIST OF SYMBOLS

A	area (cm^2)
$\overset{\circ}{A}$	angstrom unit (10^{-8} cm)
B	constant characterizing trap distributions
c_n	capture coefficient
$\bar{c}_n$	normalized capture coefficient
E	an energy measured below the conduction band (ev)
$\triangle E$	an energy interval at an energy E below the conduction band (ev)
E_t	trap energy measured from the conduction band
e	electron
E_m	maximum energy of the β-ray spectrum for a radioactive isotope (Mev)
E_{fn}	energy at quasi-fermi level
E_{fo}	equilibrium value of fermi-level for dark conductivity (ev)
F	electric field (volts/cm)
$\bar{F}$	normalized electric field
G	rate at which electrons are generated (cm^{-3})
$\bar{G}$	normalized rate at which electrons are generated
I_o	initial intensity of β-rays
I	intensity of β-rays after passing an absorbing material
I_{ext}	external current (amperes)
k	Boltzmann's constant (8.62×10^{-5} ev/°K)
L	dielectric thickness (mils)
L'	displacement amplitude (cm)
ℓ	dielectric thickness (cm)
n	free electron density (cm^{-3})
$\bar{n}_o$	normalized equilibrium free electron density

$\bar{n}$	normalized free electron density
n_{ts}	saturation value of n_t
n_r	number of electrons released from traps (e/cm^3)
n_t	trapped electron density (cm^{-3})
N_T	total trap density (cm^{-3})
$\bar{N}_T$	normalized total trap density
$\triangle n_t$	density of trapped electrons in an energy interval $\triangle E$
$\triangle N_T$	trap density at an energy E below the conduction band
n_{to}	equilibrium electron trap density (cm^{-3})
q	magnitude of electron charge (1.6×10^{-19} coulomb)
Q_{ext}	external charge transfer (coulomb)
Q_{traps}	total trapped charge (coulomb)
Q_{flux}	total incident charge (coulomb)
r	practical range of primary electron (cm)
s	attempt to escape frequency (sec^{-1})
t_s	time required to reach steady-state
T_c	thermal constant characterizing trap
$\bar{t}_s$	normalized time required to reach steady-state
$\bar{t}$	normalized time variable
T	temperature ($^\circ K$)
v	voltage (volt)
$\bar{x}$	normalized length variable
$\triangle x$	beam dimension in direction of beam displacement
x^*	zero electric field point
x	length variable

LIST OF SYMBOLS (continued)

α ratio of total external charge transfer to the total initial charge in traps

ϕ electron flux rate (e/cm^2-sec)

μ mobility (cm^2/volt sec)

$\Delta\tau$ time for $\frac{1}{2}$ cycle of the beam sweep

σ surface charge density

ϵ permittivity (farad/cm)

$\bar{\mu}_n$ normalized electron mobility

μ apparent absorption coefficient (cm^{-1})

ρ material density (gm/cm^3)

CHARGE STORAGE EFFECTS IN MYLAR

RESULTING FROM ELECTRON IRRADIATION

By L. K. Monteith, J. R. Hauser and T. M. Royal
Research Triangle Institute

SECTION I

INTRODUCTION

Under NASA Contract NAS1-3892, charge storage in polyethylene terephthalate* (PET) was observed resulting from irradiation with energetic electrons (Ref. 1). A phenomenological model which agrees with the kinetics of the space charge decay was developed. The model combined the concepts of charge release from traps with electrostatics to obtain an estimate of the internal electric field which resulted from space charge build-up. The assumptions used to arrive at a reasonable model were such that only minimum values could be inferred. Under NASA Contract NAS1-5225, the model has been extended to include space charge build-up and transport of charge during irradiation and the decay of trapped charge after ceasing irradiation. Four spatial distributions of trapped charge have been included in the model and it has been possible to account for the release of charge from traps and the resulting changes in the trapped charge asymmetry for each distribution.

There has also been evidence obtained from many sources which demonstrates that the charge storage associated with electron irradiation can result in spontaneous discharge events (Refs. 2,3). Pulse heights and rates as a function of numerous irradiation parameters have been obtained experimentally. These data for PET indicate that there are at least two operative mechanisms associated with spontaneous discharge. Irregular pulse rates and pulse heights the order of a volt or less can be logically interpreted as discharges occurring either due to excessive charge build-up in a localized region or due to the ionization of a localized region where the field strength is less than that for most of the irradiated volume. Full discharge events are those for which most of the space charge is liberated. Data indicates that the irregular pulse rates and pulse heights are more likely at least for irradiation flux rates comparable to those expected in the Van Allen belts.

---

*　Dupont Mylar

SECTION II

IRRADIATION CHARGE BUILD-UP AND RELEASE

This section investigates the model used to describe the charge build-up and decay as a function of time. A one carrier model is used with the discussion in terms of electrons. It is assumed that a band model is applicable with traps in the forbidden band below the conduction levels.

The equations describing the free electron density n and the trapped electron density n_t are Poisson's equation, and continuity equations for trapped and free charges. For a single trap level, these equations are (neglecting carrier diffusion)

$$\nabla \cdot \vec{F} = \frac{q}{\epsilon} [n - n_o + n_t - n_{to}] , \qquad (1)$$

$$\frac{\partial n_t}{\partial t} = c_n n(N_T - n_t) - s n_t \exp(-E_t/kT) , \qquad (2)$$

$$\frac{\partial n}{\partial t} = G - \frac{\partial n_t}{\partial t} + \frac{\partial}{\partial x}(\mu n F) , \qquad (3)$$

where c_n is the capture coefficient, N_T is the total trap density, s is an attempt to escape frequency, E_t is the trap energy measured from the conduction band, and G is the rate at which electrons are generated per unit volume.

For distributed traps, the above continuity equation for trapped electrons applies only to a small increment $\triangle n_t$ of trapped electrons, i.e.,

$$\frac{\partial \triangle n_t}{\partial t} = c_n n(\triangle N_T - \triangle n_t) - s \triangle n_t e^{-E/kT} , \qquad (4)$$

where $\triangle n_t$ is the density of trapped electrons in an energy interval $\triangle E$ at an energy E below the conduction band, and $\triangle N_T$ is the trap density in this energy interval. A continuity equation for the total density of trapped electrons can be obtained by integrating the above equation over all trap energies. The form of the continuity equation obtained depends upon the assumed distribution of traps with energy below the conduction band. Three distributions are of special interest as approximations to the physical situation. These are:

2

(a) Single trap level

$$N_T = N_T \delta (E - E_t)$$ (5)

(b) Uniform trap density

$$\frac{\partial N_T}{\partial E} = \frac{B}{kT_c}$$ (6)

(c) Exponential trap density

$$\frac{\partial N_T}{\partial E} = \frac{B}{kT_c} \exp(-E/kT_c) \; .$$ (7)

The derivation of the continuity equation for trapped charge is given in Appendix A for the above distributions.

For a uniform trap distribution, the normalized equations describing electron build-up and decay are

$$\frac{\partial \bar{n}_t}{\partial \bar{t}} = \bar{c}_n \bar{n} (\bar{N}_T - \bar{n}_t) - \exp(\bar{n}_t) \; ,$$ (8)

$$\frac{\partial \bar{n}}{\partial \bar{t}} = - \frac{\partial \bar{n}_t}{\partial \bar{t}} + \bar{G} + \frac{\partial}{\partial \bar{x}}(\bar{\mu}_n \bar{n} \bar{F}) \; ,$$ (9)

$$\frac{\partial \bar{F}}{\partial \bar{x}} = - (\bar{n} - \bar{n}_o + \bar{n}_t) \; ,$$ (10)

A program has been written to solve these equations by a computer.

In considering the release of trapped electrons, it is useful to consider the various time constants associated with the terms in the continuity equations. There are three time constants of interest:

(1) the trapping time for free electrons,
(2) the release time constant of trapped electrons, and
(3) the transport time for free carriers out of the material.

The last two time constants depend upon the magnitude of trapped charge. For typical parameter values, it is found that the free carrier trapping time constant and the free carrier transport time constant are much less than the release time constant for trapped carriers. This indicates that the time behavior of the charge release is determined mainly by the nature of the traps.

3

The different physical processes (i.e., trapping, transport, and charge release) and associated time constants lead to difficulties in a straightforward attempt to solve the three above equations. It is found that the free electron concentration can change very rapidly by trapping and transport to reach a state of "quasi-equilibrium" where $\partial n/\partial t \ll \partial n_t/\partial t$. When this occurs, difficulty is encountered in the continuity equation for free electrons since $\partial n/\partial t$ is the small difference between large terms which are approximately equal.

The above conclusions have been verified by a computer solution of the equations for n and n_t. Regardless of the initial free electron concentration, it rapidly adjusts in times on the order of the electron transit time across the material to a value such that $\partial n/\partial t \ll \partial n_t/\partial t$. In studying the build-up and the decay of trapped electrons, the continuity equation for electrons has been replaced, therefore, by the equation

$$\frac{\partial \bar{n}_t}{\partial \bar{t}} = \bar{c}_n \bar{n} \, (\bar{N}_T - \bar{n}_t) - \exp(\bar{n}_t) \simeq \bar{G} + \frac{\partial}{\partial \bar{x}}(\bar{\mu}_n \bar{n}\bar{F}) \quad . \quad (11)$$

This leads to a differential equation for n as a function of $\bar{n}_t$ and $\bar{x}$ which is

$$\bar{\mu}_n \bar{F} \frac{\partial \bar{n}}{\partial \bar{x}} - [\bar{\mu}_n (\bar{n}_t + \bar{n} - \bar{n}_o) + \bar{c}_n (\bar{N}_T - \bar{n}_t)] \, \bar{n} + \bar{G} \exp(\bar{n}_t) = 0. \quad (12)$$

This equation combined with the continuity equation for trapped charge and Poisson's equation are the three equations used for calculating charge build-up and decay. It was also assumed that $n_t \gg n$ which is the case except at very large densities of trapped charge ($n_t \sim N_T$) or at very small densities of trapped charge.

The method of solving for the free and trapped charge is briefly described below. The initial trapped charge and the generation rate $\bar{G}$ are considered as known as well as the constants $\bar{c}_n$, $\bar{N}_T$, $\bar{\mu}_n$, and $\bar{n}_o$. With the initial trapped charge, Poisson's equation is solved for the electric field ($\bar{n} - \bar{n}_o \ll \bar{n}_t$). The boundary conditions on the electric field are

$$\int_o^1 \bar{F} \, d\bar{x} = 0 \, , \quad (13)$$

which corresponds to the shorted electrode case. With $\bar{F}$ known, the free electron concentration is calculated from the differential equation for $\bar{n}$. Then $\partial \bar{n}_t/\partial \bar{t}$ can be evaluated and this used to extrapolate to a new time to obtain $\bar{n}_t$ at a later time. The process is then repeated for any desired time interval. Further aspects and difficulties in the solution of the equations are discussed in Appendix B.

It can be seen from the basic equations for $\bar{n}_t \ll \bar{N}_T$ and for $\partial \bar{n}/\partial \bar{t} \ll \partial \bar{n}_t/\partial \bar{t}$ that the shape of the build-up and decay curves depend upon the combination of parameters

$$\frac{\bar{c}_n \bar{N}_T}{\bar{\mu}_n} = \left(\frac{\epsilon T_c}{qTB}\right) \frac{(N_T - n_{to})c_n}{\mu_n} , \qquad (14)$$

and

$$\bar{G} = \frac{T_c}{TBs} \exp(\bar{N}_T) \; G . \qquad (15)$$

This is an important consideration since it is possible to study all parameter variations by changing only these two quantities. These parameters are discussed in detail in Appendix C. A value $\bar{c}_n \bar{N}_T/\bar{\mu}_n = 1.7$ was principally used for the computer calculations. However, in a few instances, values of $\bar{c}_n \bar{N}_T/\bar{\mu}_n = 0.17$ and $\bar{c}_n \bar{N}_T/\bar{\mu}_n = 17$ were used to indicate the behavior expected with a variation of these parameters. Spatial distributions were chosen to approximate the physical processes which result in the slowing down of the irradiation electrons to thermal velocity. The following results are obtained considering only a uniform trap distribution with energy. For external charge transfer, the data are presented for times larger than 60 seconds following the start of trapped charge decay. This corresponds to the experimental procedures outlined in Appendix D.

EXTERNAL CHARGE TRANSFER FOR
VARIOUS DEPTHS OF TRAP FILLING

Using a uniform spatial distribution of trapped irradiation electrons as inferred from the results obtained under NASA Contract NAS1-3892 (Ref. 1), the external charge transfer for various depths of trap filling has been considered. The trapped charge is initially assumed to be uniformly distributed to a depth of one-half the total thickness of the sample. Ratios of the total external charge transfer to the total initial charge in traps α have also been calculated. The results are shown in Fig. 1. The salient feature of the results is the ln t behavior over some portion of each curve. Also, the external charge transfer reaches a maximum between 10^4 and 10^5 seconds with approximately 5 percent of the total initial charge in traps observed in the external circuit.

The corresponding external current as a function of time for the various depths of trap filling are shown in Fig. 2. It should be noted that the current does not have a simple 1/t behavior. Initially, the current decreases less rapidly that 1/t and only approximates 1/t for a portion of the decay time.
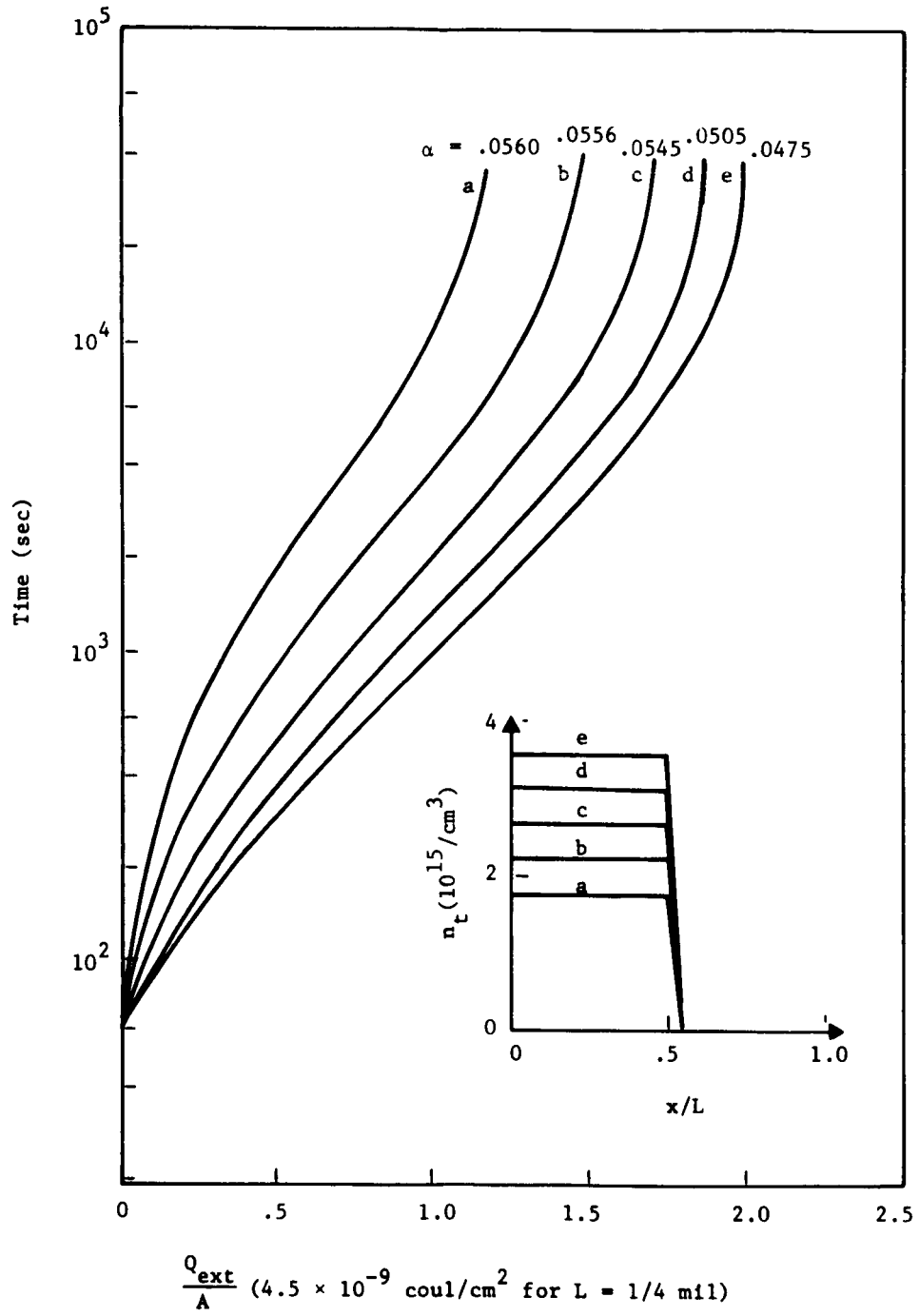
Figure 1. External charge transfer as a function of time for various trapped charge densities.

6
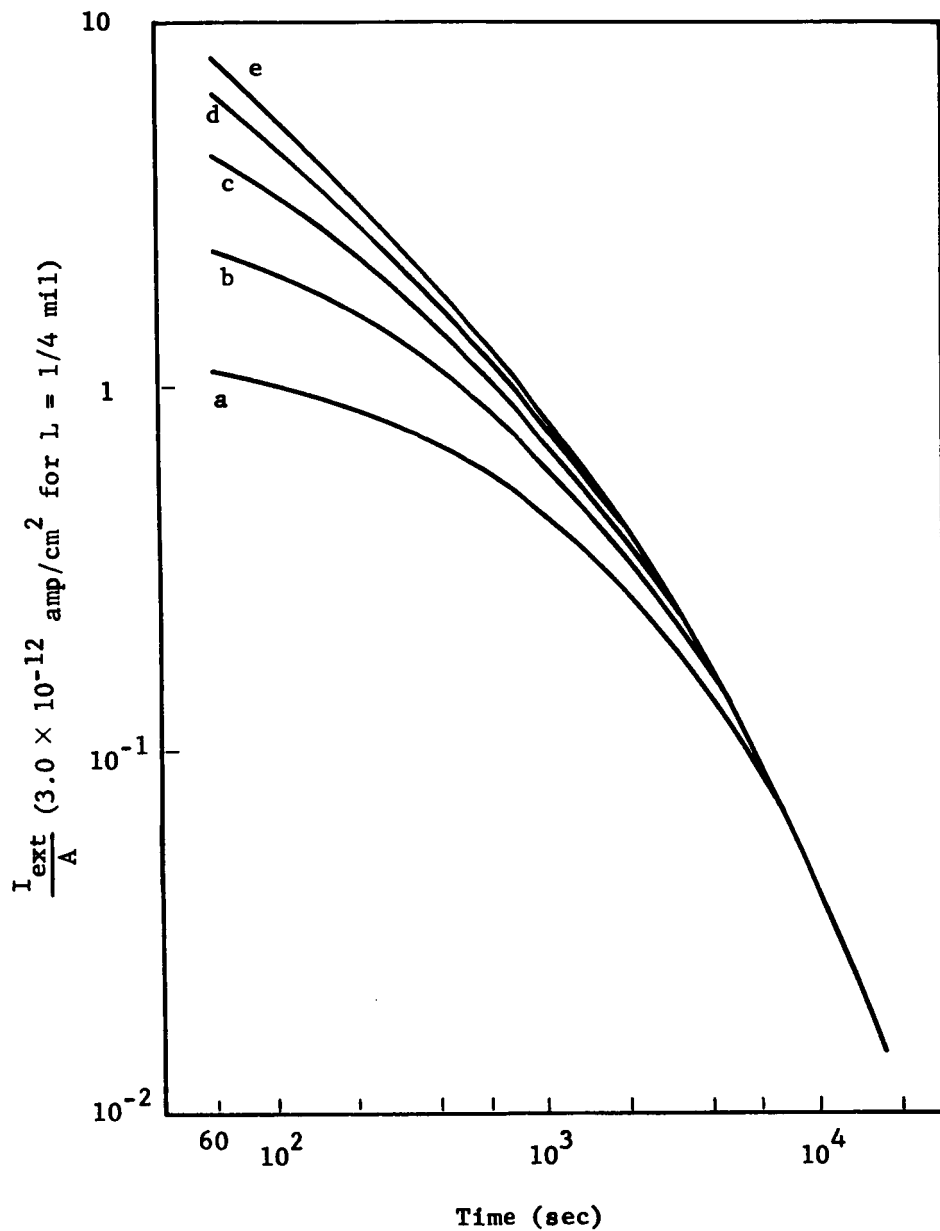
Figure 2. External current as a function of time for various trapped charge densities.

EXTERNAL CHARGE TRANSFER FOR VARIOUS
SPATIAL DEPTHS OF TRAPPED CHARGE

Using a uniform spatial distribution of trapped charge extending
from the irradiated boundary to various fractions of the total thick-
ness of the sample, the external charge transfer has been computed as
shown in Fig. 3. Again, the transfer of external charge has a ln t
behavior for some portion of each curve. The maximum fraction of the
initial trapped charge which can be detected by external charge trans-
fer has been calculated with a maximum value of 6 percent obtained when
the trapped charge is distributed uniformly to a depth slightly less
than one-half the sample thickness. The corresponding characteristics
for external current during space charge decay are shown in Fig. 4.

EFFECT OF CHANGING THE PARAMETER $\dfrac{\bar{c}_n \bar{N}_T}{\bar{\mu}_n}$

The spatial distributions as a function of time during space charge
decay for mobility values of 1, 0.1 and 0.01 cm^2/v-sec are shown in
Figs. 5, 6 and 7, respectively. The initial depth of trap filling and spa-
tial symmetry was identical for each case and the same as considered in
Fig. 1. The main affects of changing the mobility are (1) the rate of
space charge decay in the initial trapped charge region and (2) the
rate of charge build-up in the region beyond the initial trapped charge
region. For the high mobility case (Fig. 5), the carriers are trans-
ported to the boundaries essentially as they are released from traps
(i.e., no-retrapping). When this occurs, there is little change in
the symmetry of the trapped charge and the external charge transfer is
only a small portion of the initial trapped charge. For the low mobil-
ity case (Fig. 7), there is appreciable retrapping of the carriers in
the space charge region resulting in a slower rate of space charge
decay. In addition, essentially all the electrons released from traps
to the right of the zero field point are retrapped in the region be-
yond the initial space charge front. This approaches the simple model
considered in Appendix D.

Shown in Fig. 8 are the effects of mobility on retrapping in the
space charge region. The curves show the decay of charge from traps.
The high mobility case approaches the no-trapping release considered
under NASA Contract NAS1-3892 (Ref. 1). As the mobility decreases, re-
trapping reduces the rate of space charge decay.

The external charge transfer for the three mobility values are
shown in Fig. 9. Again, the curves show a ln t behavior for some portion
of time for each value of mobility. However, the maximum fraction of
the initial trapped charge detected as external charge increases with de-
creasing mobility. This fraction is approximately 0.2 percent and 7
percent for 1.0 cm^2/v-sec and 0.01 cm^2/v-sec, respectively. It is inter-
esting to note that the simple model in Appendix D predicts a fraction
of approximately 7 percent. An important conclusion that can be drawn

8
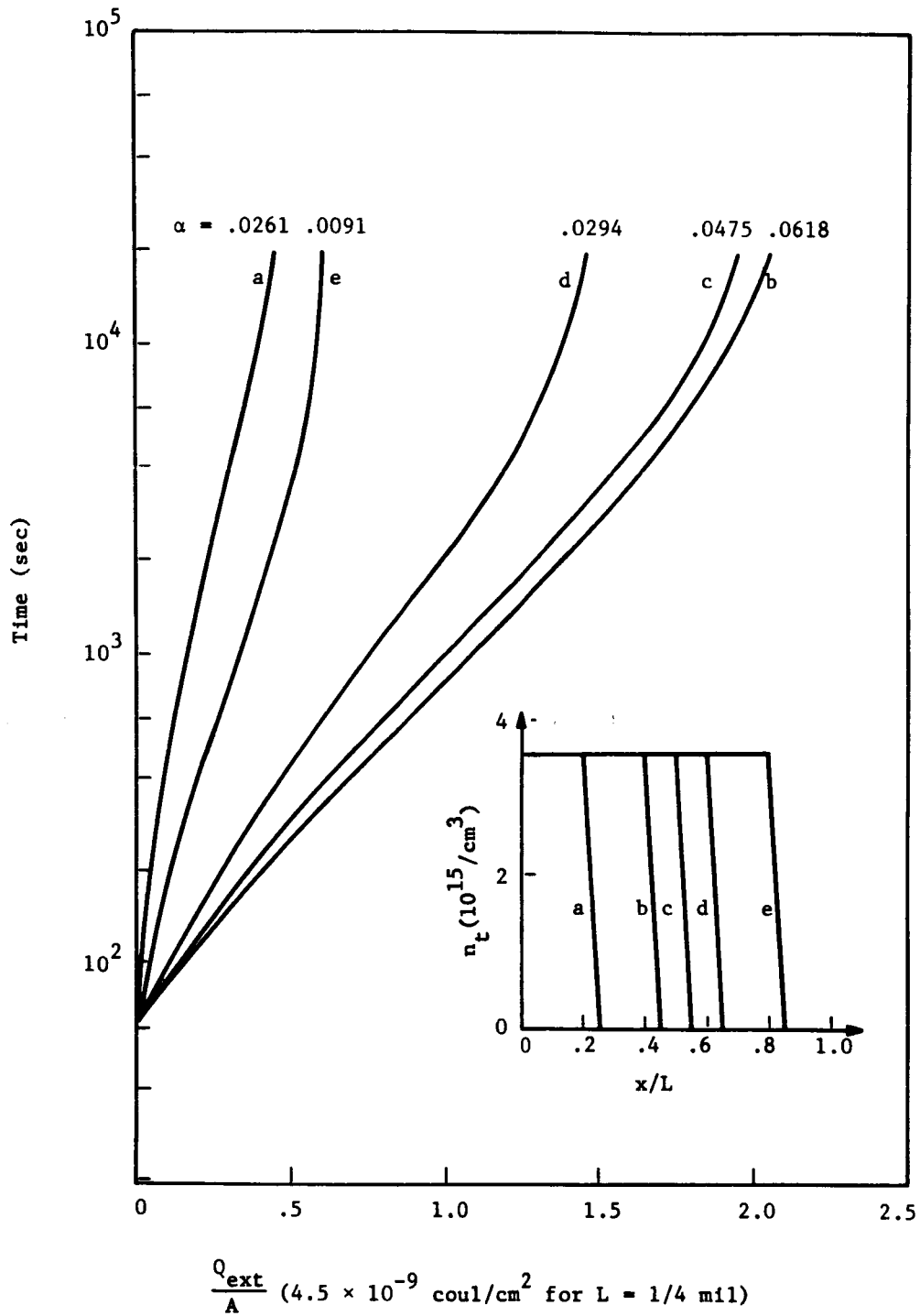
Figure 3.   External charge transfer as a function of time for various spatial depths of trapped charge

9
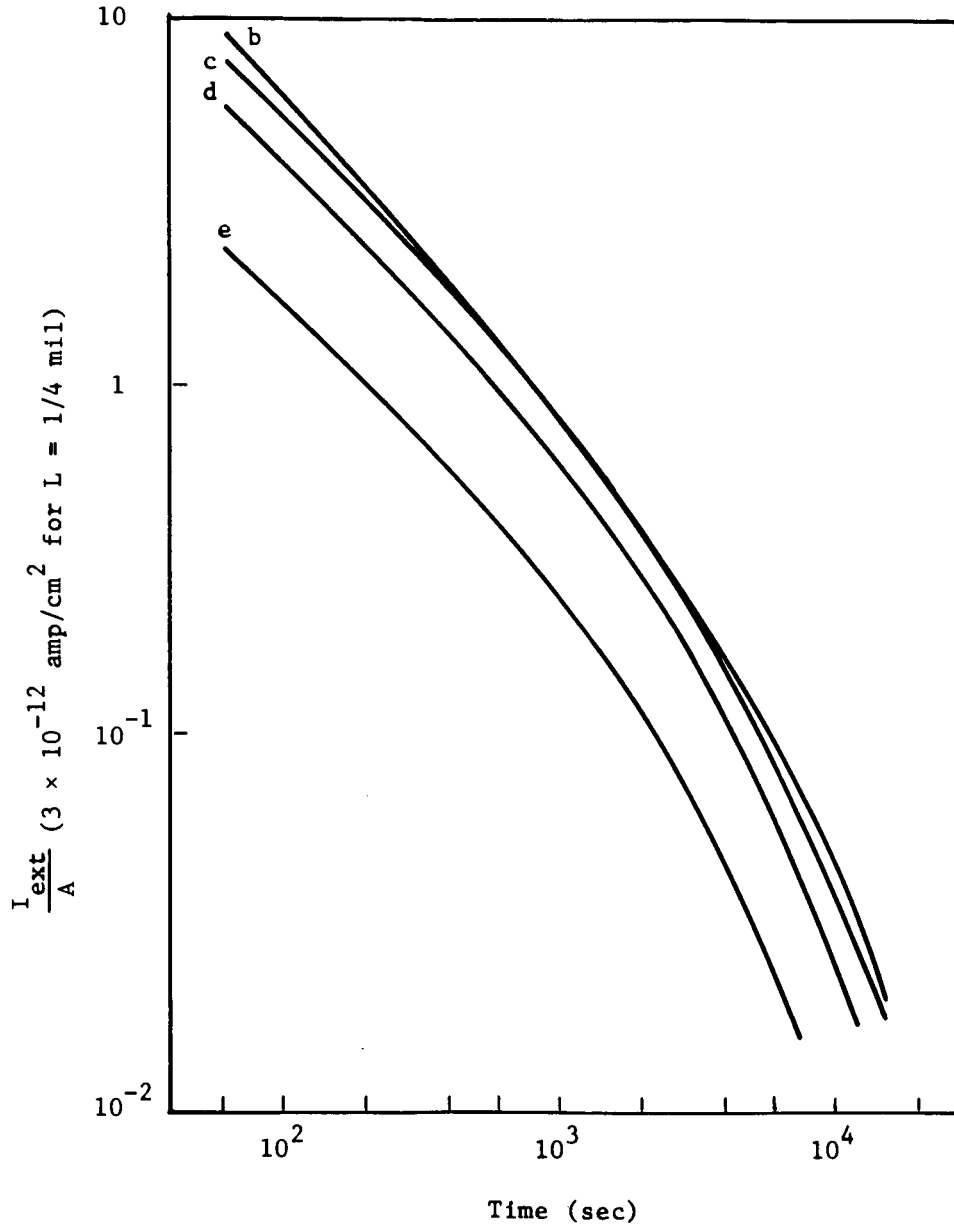
Figure 4. External current as a function of time for various spatial depths of trapped charge.

10
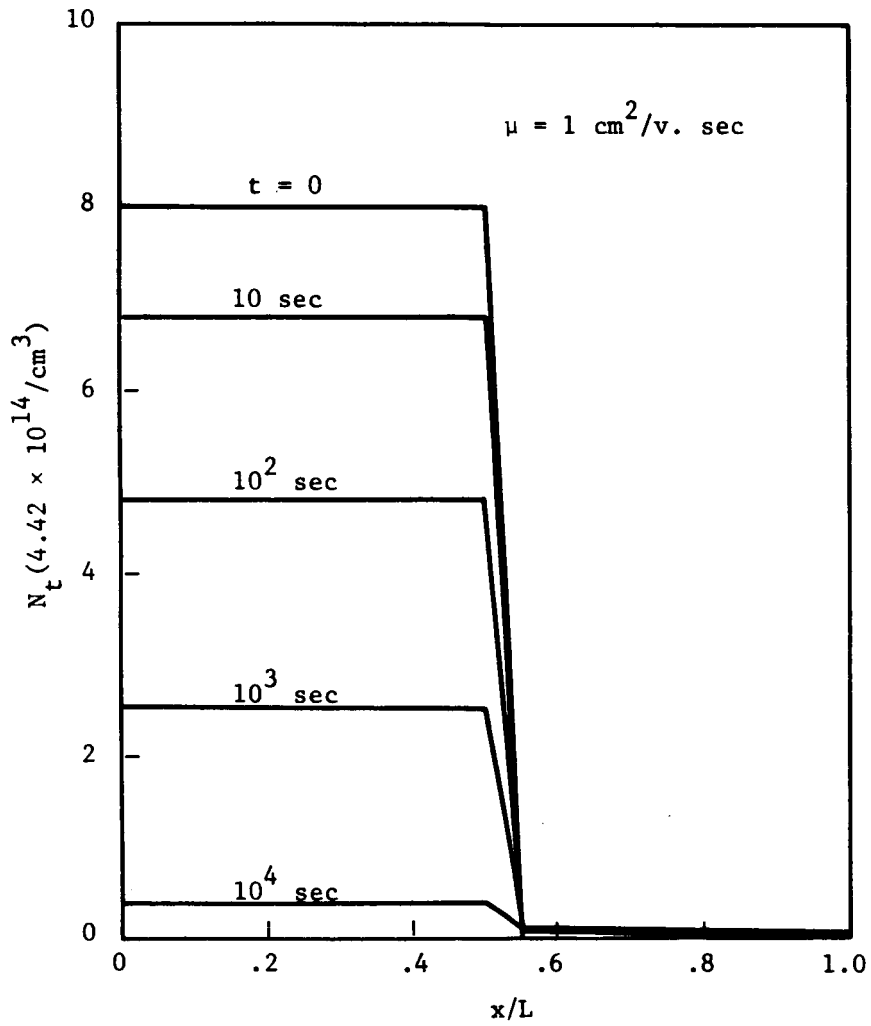
Figure 5. Spatial distribution of trapped charge at various times
during charge release for $\mu = 1$ cm^2/v-sec (uniform
initial distribution).
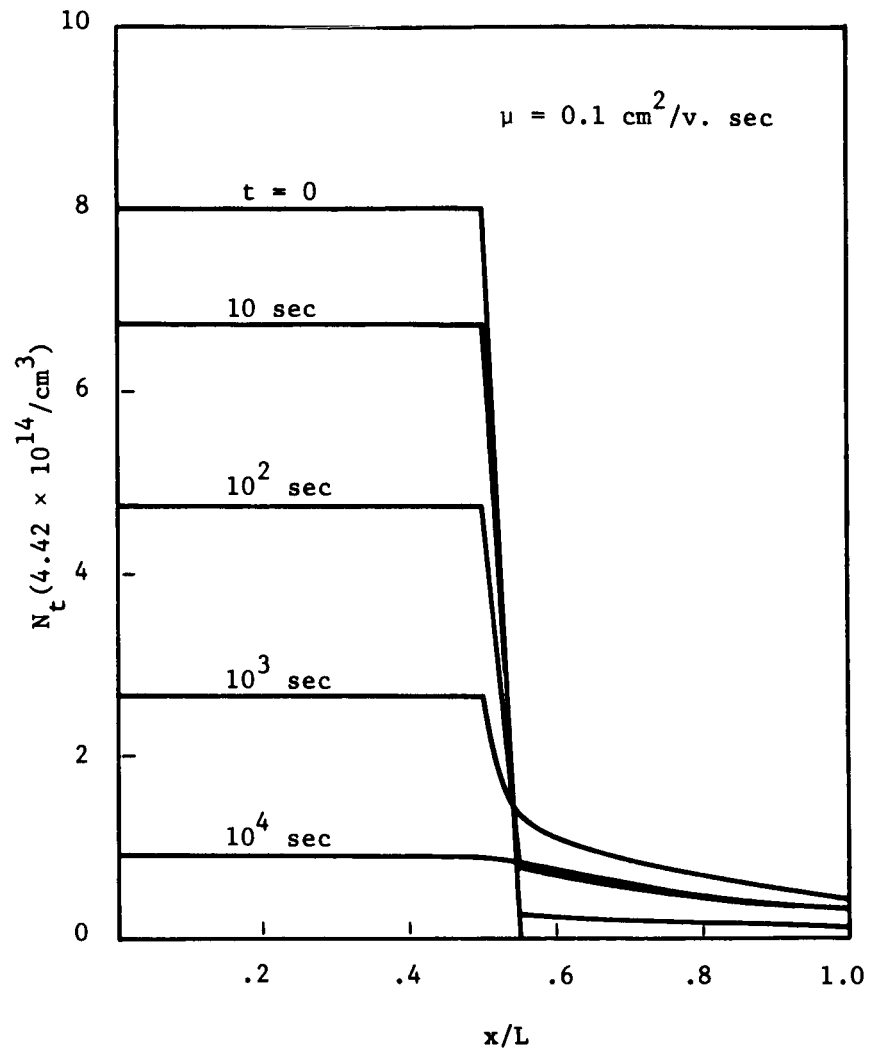
Figure 6. Spatial distribution of trapped charge at various times during charge release for $\mu = 0.1$ cm^2/v-sec (uniform initial distribution).
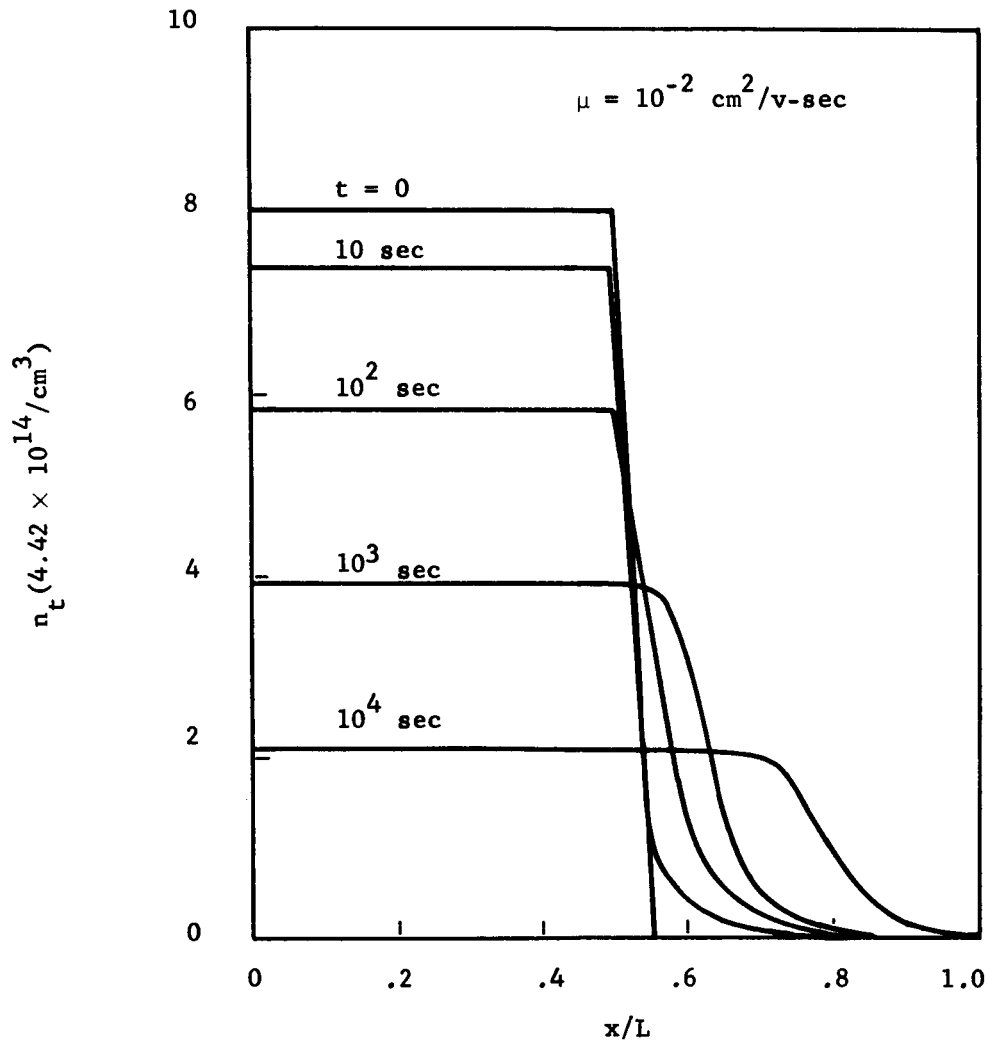
Figure 7. Spatial distribution of trapped charge at various times during charge release for $\mu = 0.01$ cm^2/v-sec (uniform initial distribution).
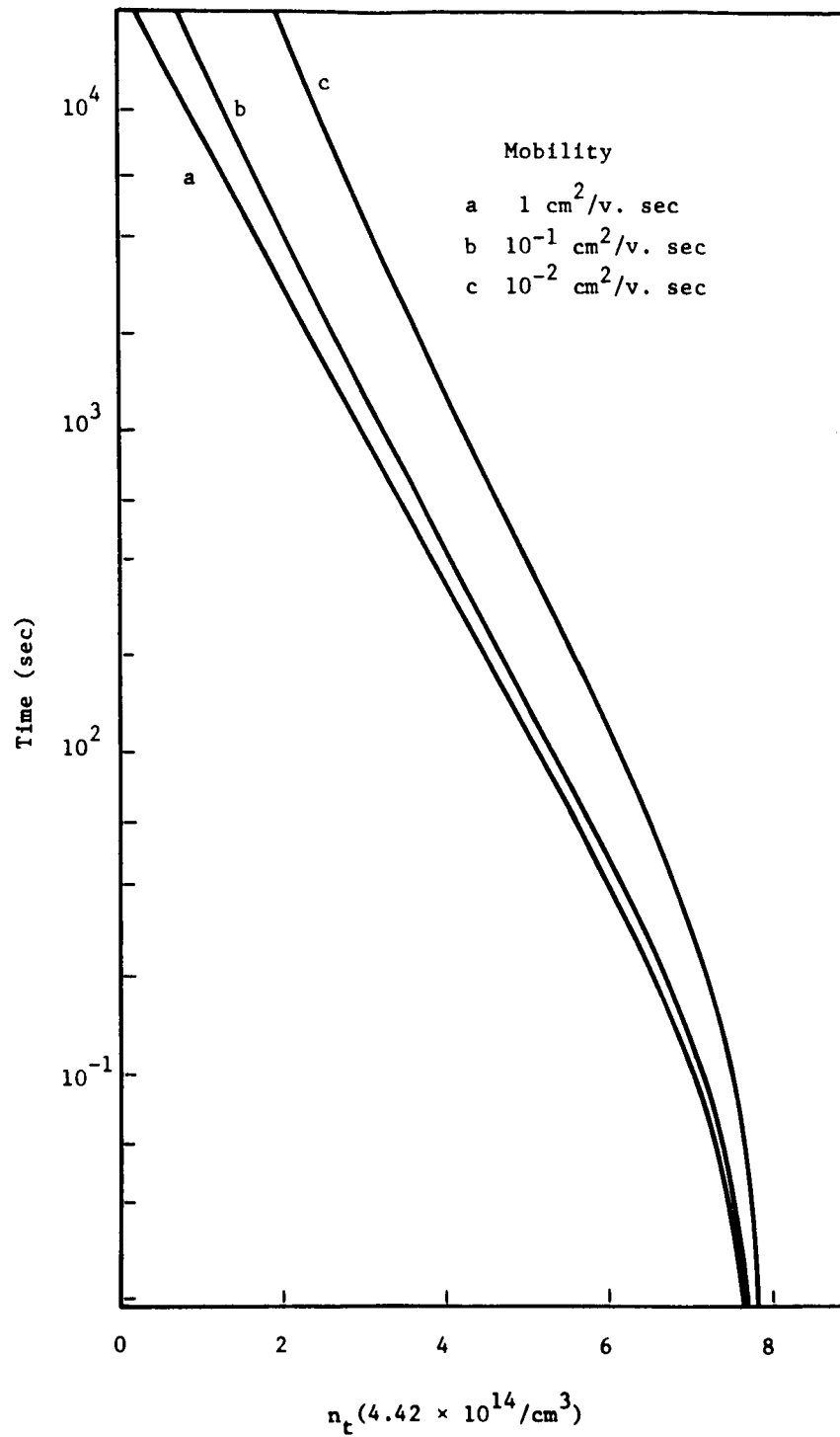
Figure 8. Trapped charge as a function of time for various mobility values.

The figure shows Time (sec) on the vertical axis with values 10^{-1}, 10^2, 10^3, 10^4, and the horizontal axis labeled $n_t(4.42 \times 10^{14}/cm^3)$ with values 0, 2, 4, 6, 8.

Mobility

a 1 cm^2/v. sec
b 10^{-1} cm^2/v. sec
c 10^{-2} cm^2/v. sec
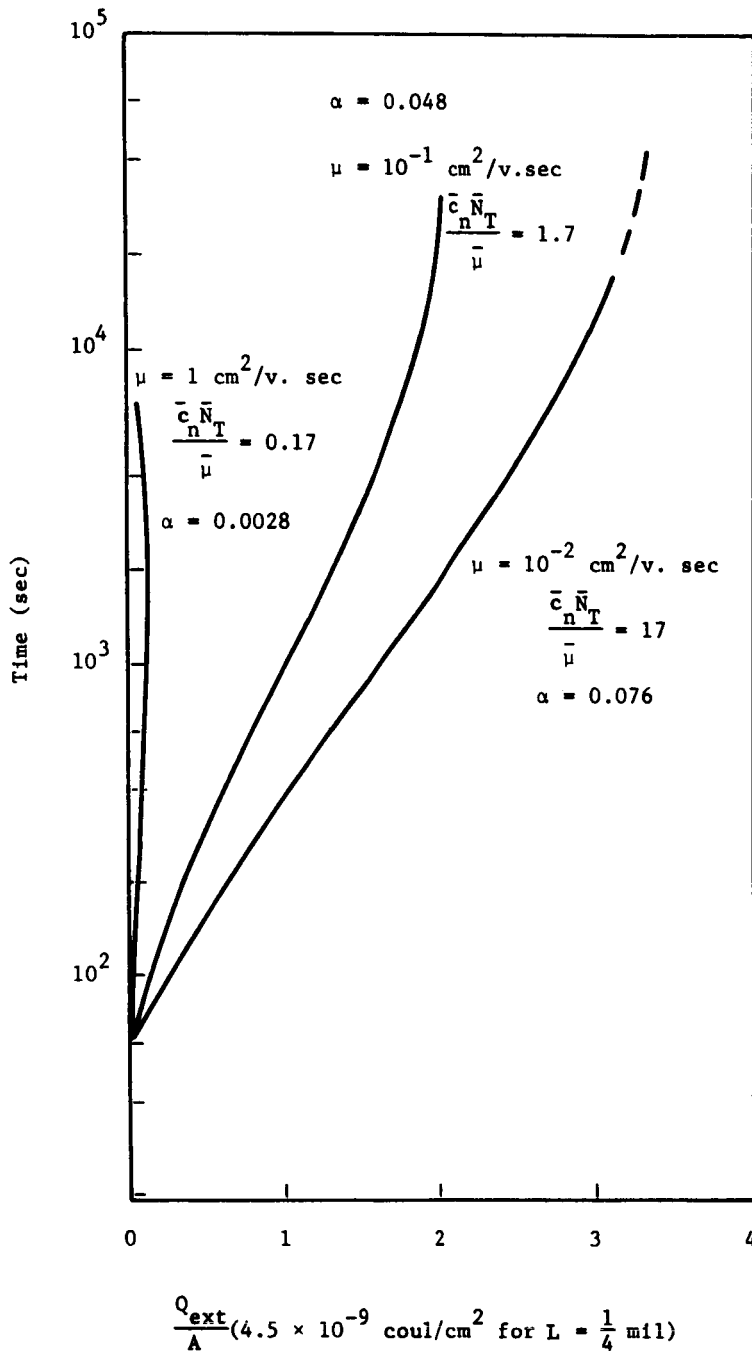
Figure 9. External charge transfer as a function of time for various mobility values and for the same spatial distribution of initial trapped charge.

from these results is that the space charge decay model is useful for interpreting experimental results only for those materials where $\bar{c}_n \bar{N}_T / \bar{\mu}_n > 1$.

SPATIAL DISTRIBUTIONS FOR TRAPPED CHARGE

A uniform distribution has been used in the above analyses. Other distributions have also been considered to investigate the effects of various distributions on the transfer of external charge. A distribution for the transmission of a monoenergetic electron flux in PET has been calculated by M. Berger (Ref. 4). From these results, a stopping distribution has been obtained as shown for the initial trapped charge (t = 0) in Fig. 10. The decay of space charge for this initial distribution has been calculated for $\mu_n = 0.1$ cm^2/v-sec and $\mu_n = 0.01$ cm^2/v-sec as shown in Figs. 10 and 11, respectively. A linear spatial distribution of trapped charge has also been considered as shown in Fig. 12. The main feature of these decay curves is the manner in which the space charge distribution approaches the uniformly distributed case. For the peaked distribution this effect is more notable for $\mu = 0.01$ cm^2/v-sec. This will also be true for any spatial distribution when $\bar{c}_n \bar{N}_T / \bar{\mu}_n > 10$. When this applies, the external charge transfer for an arbitrary spatial distribution is expected to have many of the characteristics of the uniform spatial distribution. A comparison of external charge transfer for two distributions is shown in Fig. 13. In this case, the external charge transfer curves have been normalized to the total initial trapped charge. Both curves exhibit approximately a ln t behavior for some portion of the decay, however, the peaked distribution results in a larger fraction of the total initial trapped charge transferred in the external circuit. The differences between these curves do not appear to be significant enough to permit an inference of the initial trapped charge spatial distribution from the charge transfer characteristics.

TRAPPED CHARGE BUILD-UP

In the previous sections, an initial trapped charge distribution has been assumed and the decay from this distribution has been investigated. In order to determine a realistic trapped charge distribution, one must first use the model to calculate the space charge build-up. Space charge build-up using a generating function G which is constant from the irradiated boundary to a depth of ½ the total thickness is shown in Fig. 14 for various irradiation times with a mobility $\mu_n = 0.1$ cm^2/v-sec and a flux rate $\phi = 3 \times 10^{11}$ e/cm^2-sec. The curve corresponding to an irradiation time of 38.6 sec. is close to the steady-state space charge distribution in the region x/L < .5. The steady-state condition results when the rate of charge release from traps and transport to the boundaries is equal to the rate at which carriers are added to the sample. Near x/L = 1, there will be an additional charge build-up for irradiation times greater than

16
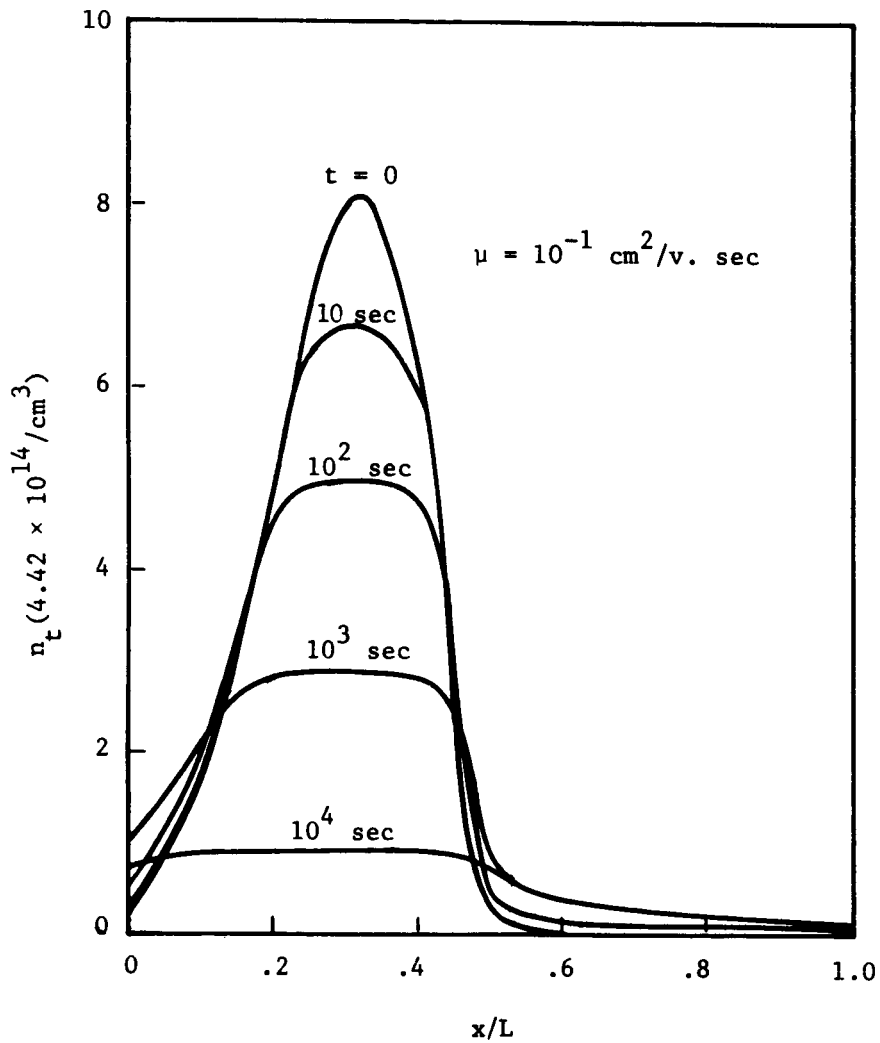
Figure 10. Spatial distribution of trapped charge at various times during charge release for peaked initial distribution and for $\mu = 10^{-1}$ cm^2/v-sec.
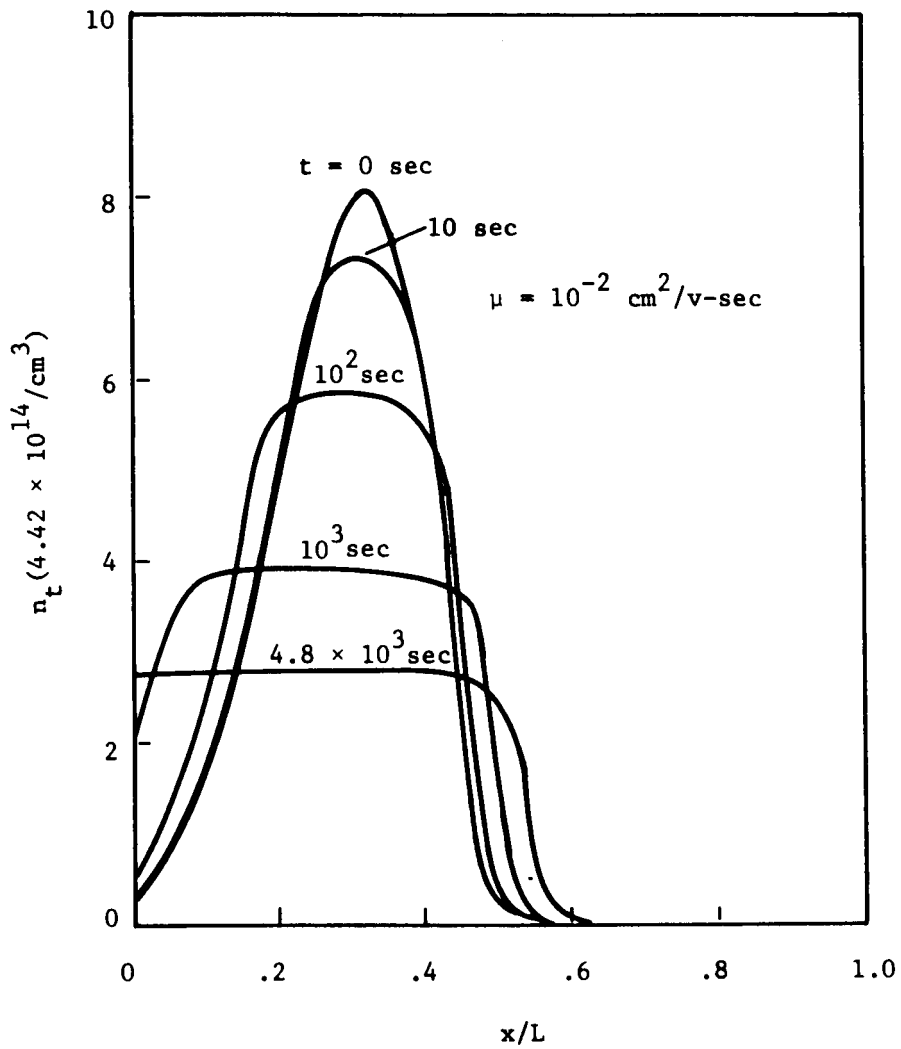
Figure 11. Spatial distribution of trapped charge at various times during charge release for peaked initial distribution and for $\mu = 10^{-2}$ cm^2/v-sec.
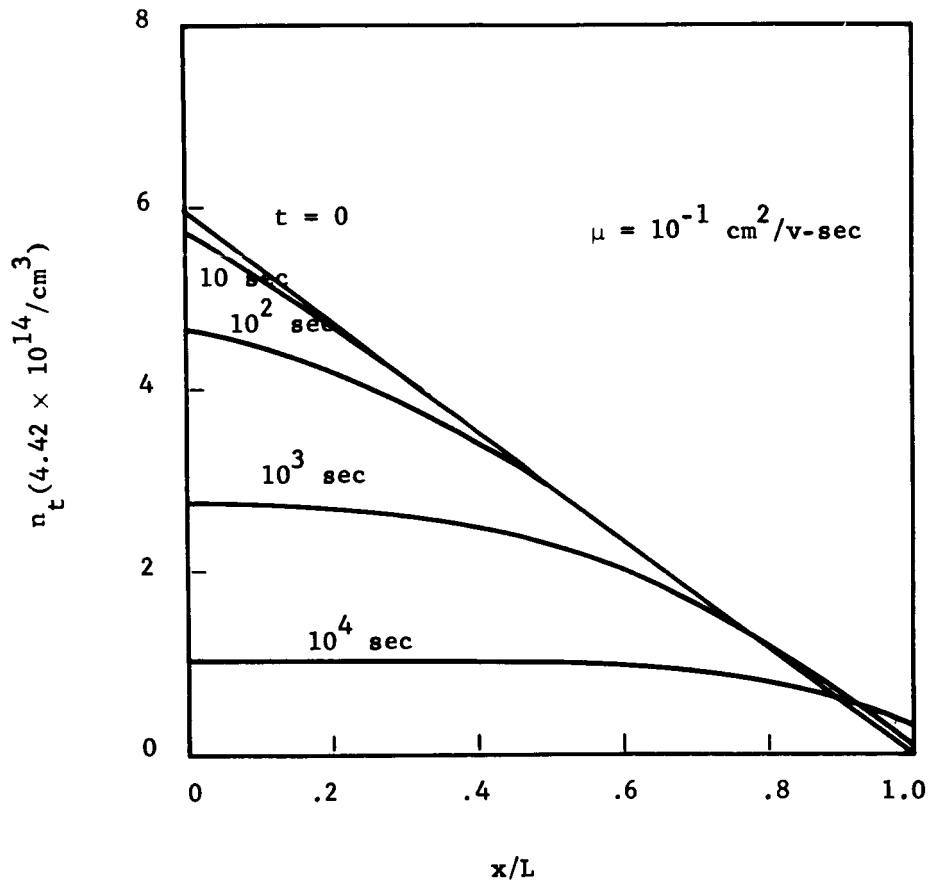
Figure 12. Spatial distribution of trapped charge at various times during charge release for linear initial distribution.

19
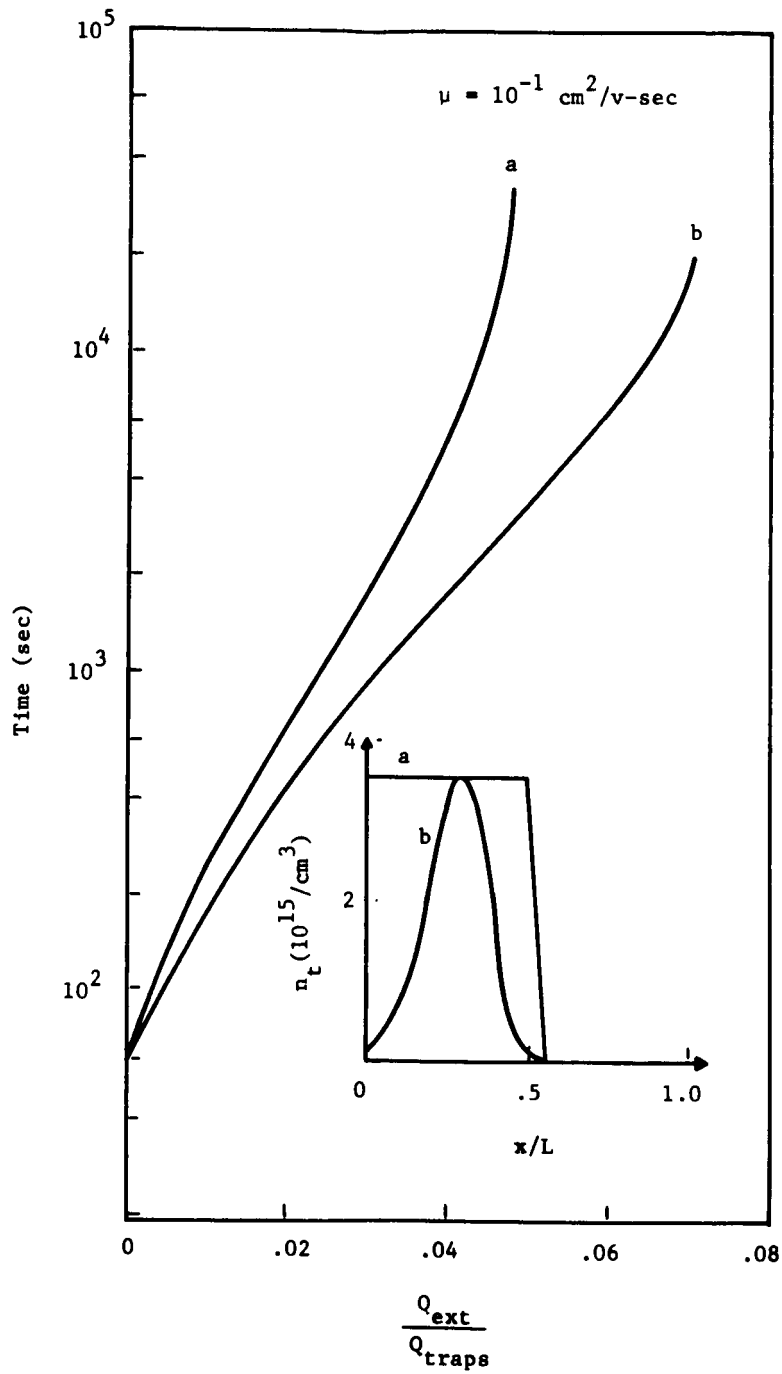
Figure 13. Ratio of external charge transferred to total trapped
charge as a function of time for two spatial distributions
of initial trapped charge.
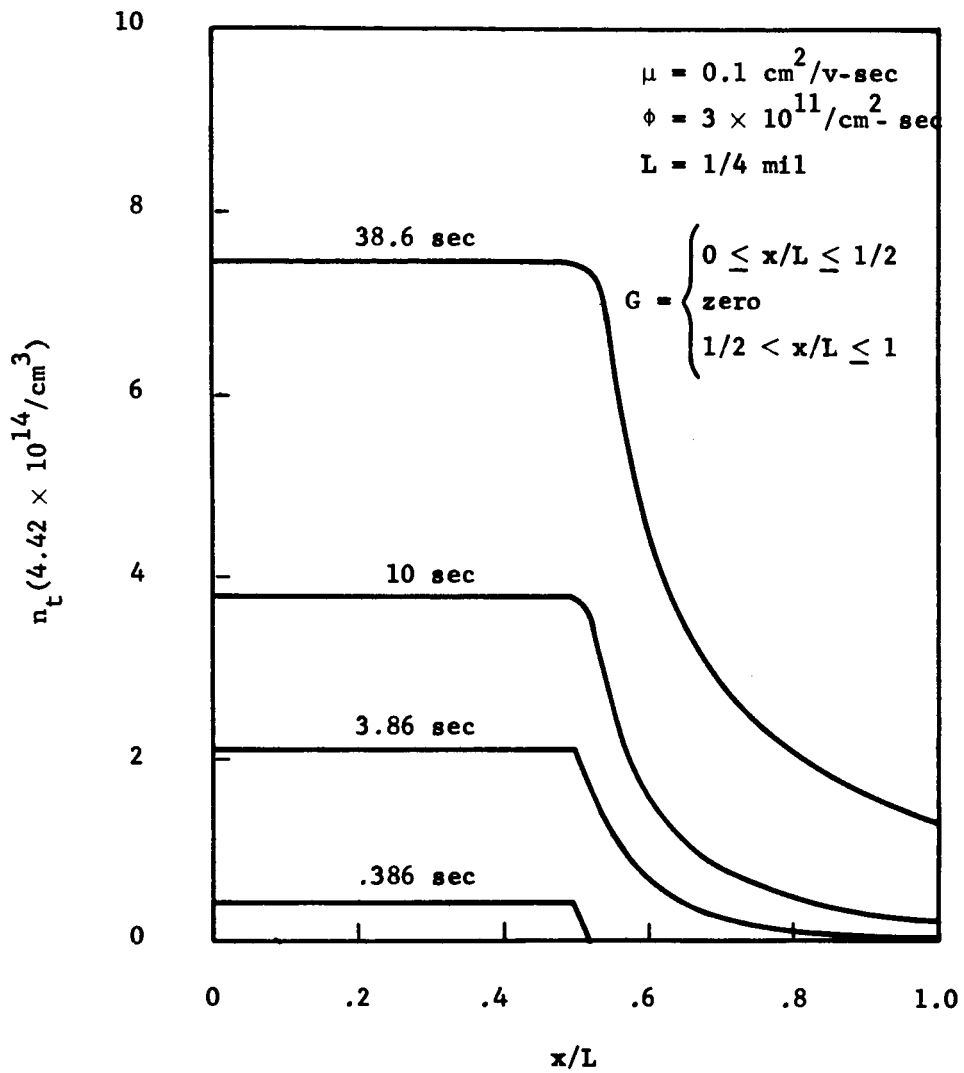
Figure 14. Trapped charge distribution at various times during charge build-up for uniform G function.

38.6 seconds. The main difference between this distribution and those assumed in previous sections is the tail for $x/L > .5$.

Using the G function corresponding to the stopping of electrons as shown in Fig. 15, the build-up of space charge shown in Fig. 16 has been calculated. The trapped charge distribution maintains some of the characteristics of the generating function until steady-state is approached. Near steady-state the space charge distribution is similar to that for the uniform generating function. After 100 seconds irradiation time, the space charge distribution is approaching steady-state.

The transfer of external charge which results from two of the build-up distributions in Fig. 14 have been calculated with the results shown in Fig. 17. To compare these results with those in Fig. 1, one must consider distributions which have approximately the same value of total trapped charge. Distribution b in Fig. 17 has approximately the same value of total trapped charge as distribution e in Fig. 1. The transfer of external charge for the two distributions is initially the same, however, the distribution in Fig. 17 results in an earlier saturation of external charge due primarily to the finite charge at $x/L = 1.0$ at the beginning of the decay period.

Another interesting quantity is the fraction of the total irradiation charge in traps Q_{traps}/Q_{flux} at any time. This is approximately the same for the two $\bar{G}$ functions used in the present calculations and the results are shown in Fig. 18. The total trapped charge becomes a smaller fraction of the total incident charge because of the approach to a steady-state condition. After about 100 sec. irradiation time, the charge in traps is only about 0.1 times the total incident charge. For longer times, the fraction decreases approximately an order of magnitude for each order of magnitude in time.

MAXIMUM INTERNAL ELECTRIC FIELD
RESULTING FROM TRAPPED CHARGE BUILD-UP

The maximum internal electric field as a function of irradiation time for space charge build-up shown in Figs. 14 and 16 has been calculated. The results are shown in Fig. 19. As the space charge distribution approaches steady-state, the maximum value of internal electric field is approximately 6×10^5 v/cm. This corresponds to approximately an order of magnitude less than quoted values of internal field strength for PET.

STEADY-STATE VALUES OF TRAPPED CHARGE

It is possible to obtain estimates of the steady-state values of trapped charge and of the time to reach steady-state conditions during charge build-up without the computer solutions. These are readily obtained at the zero field point, where the equations for $\bar{n}_t$ and $\bar{n}$ are
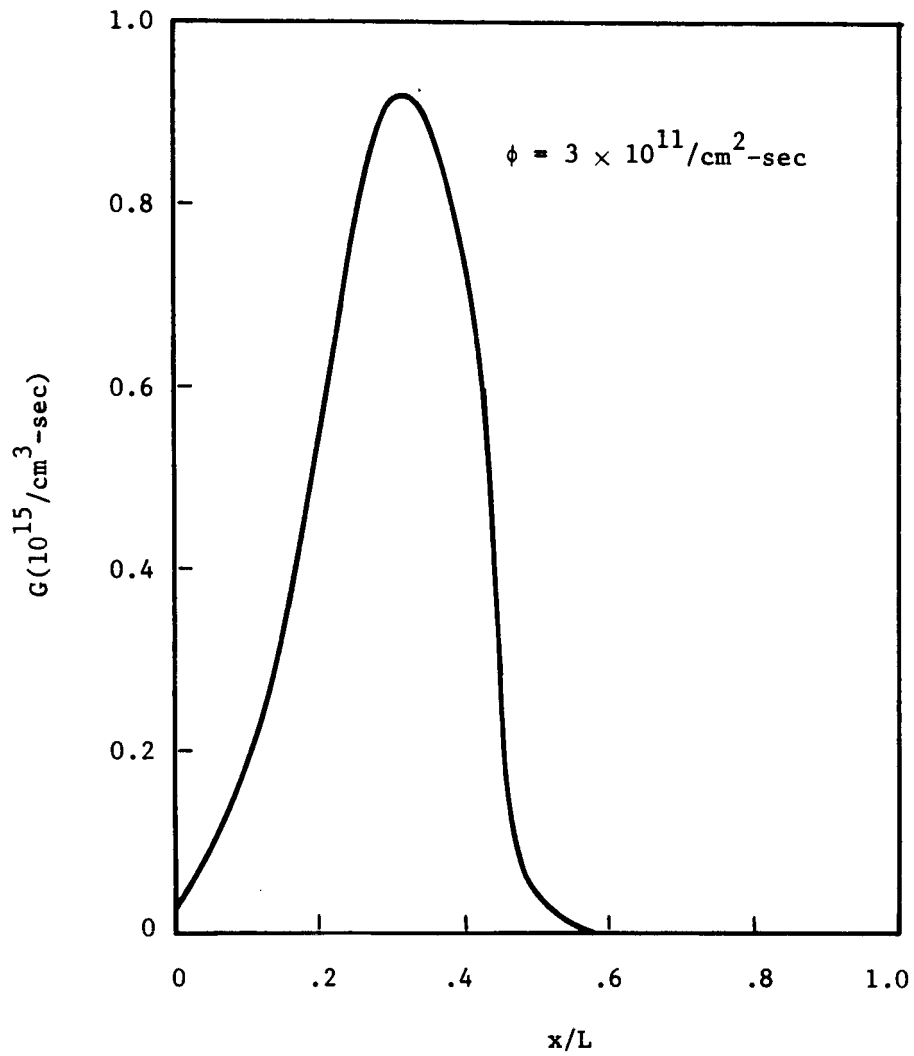
Figure 15. Charge generation function G as a function of distance
for stopping of electrons in mylar.
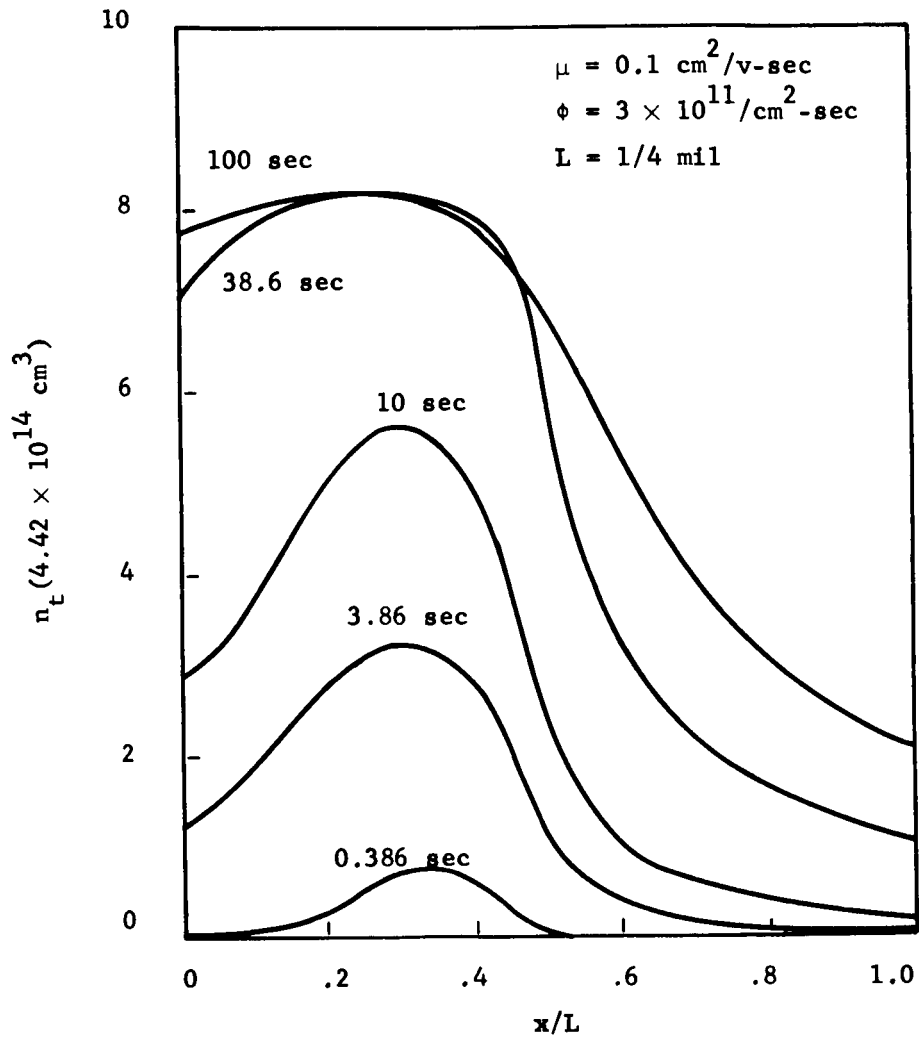
Figure 16. Trapped charge distribution at various times during charge build-up for the generation function of Figure 15.
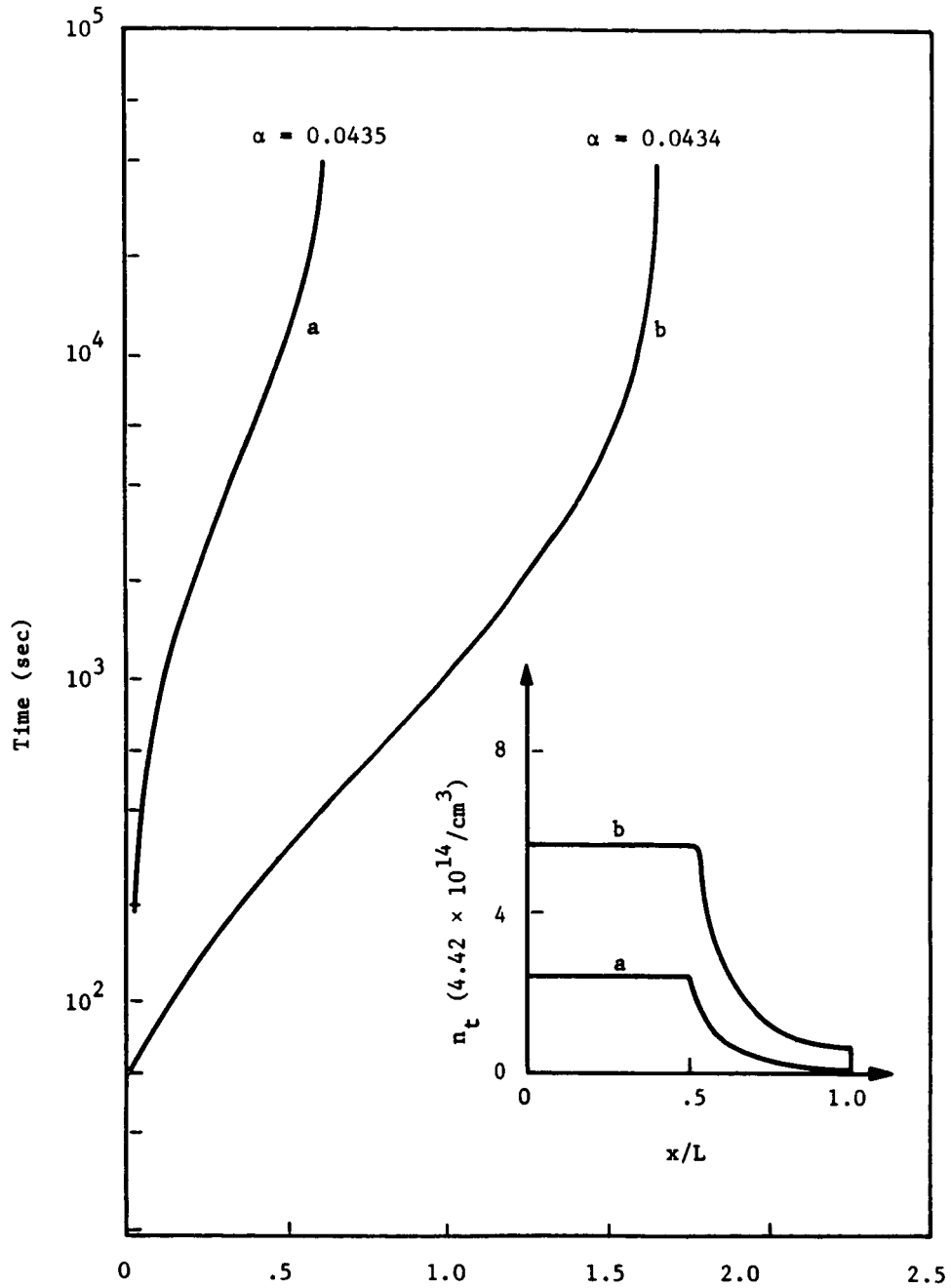
Figure 17. External charge transfer as a function of time following charge build-up.

25
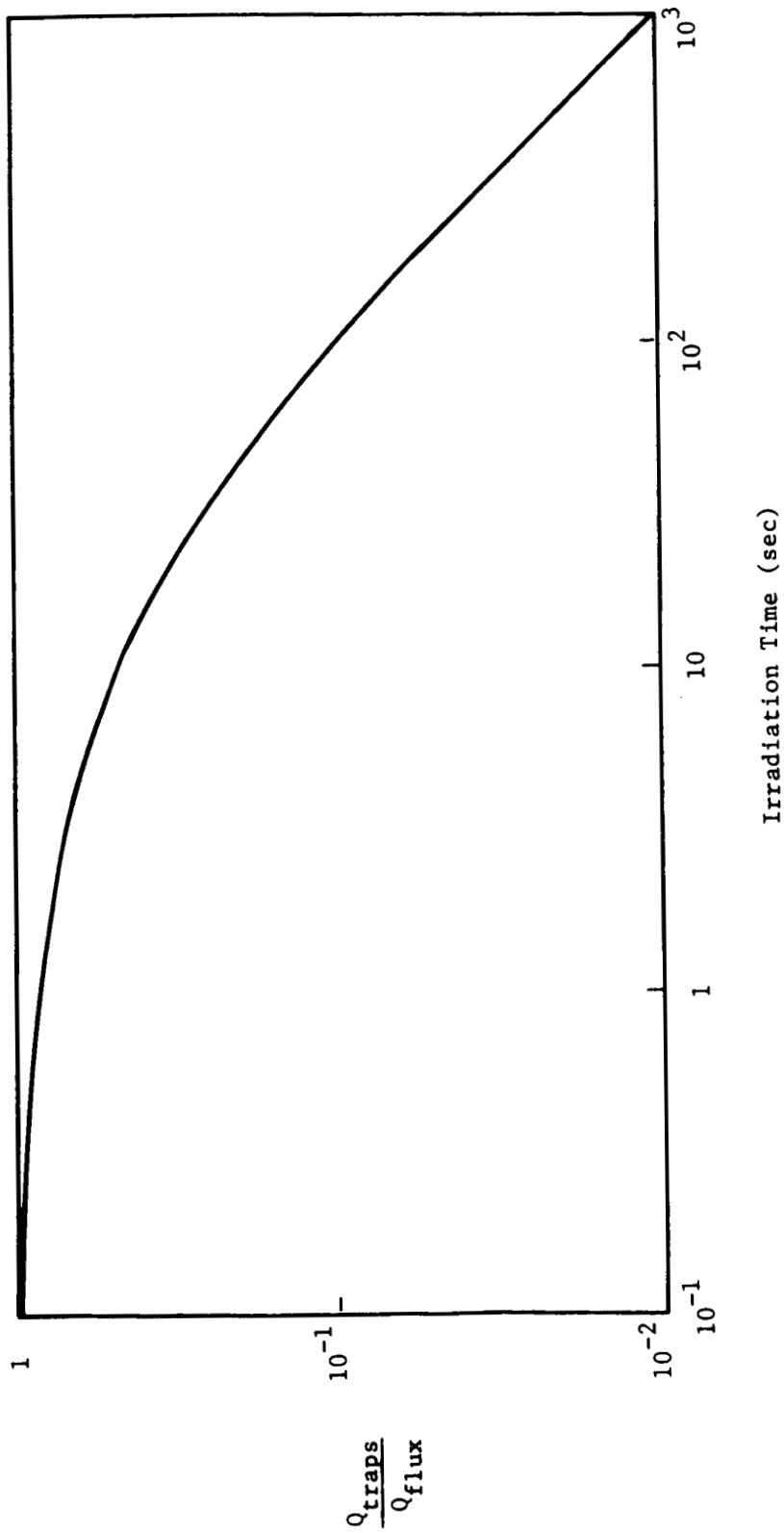
Figure 18. Ratio of total trapped charge to total incident charge as a function of irradiation time.
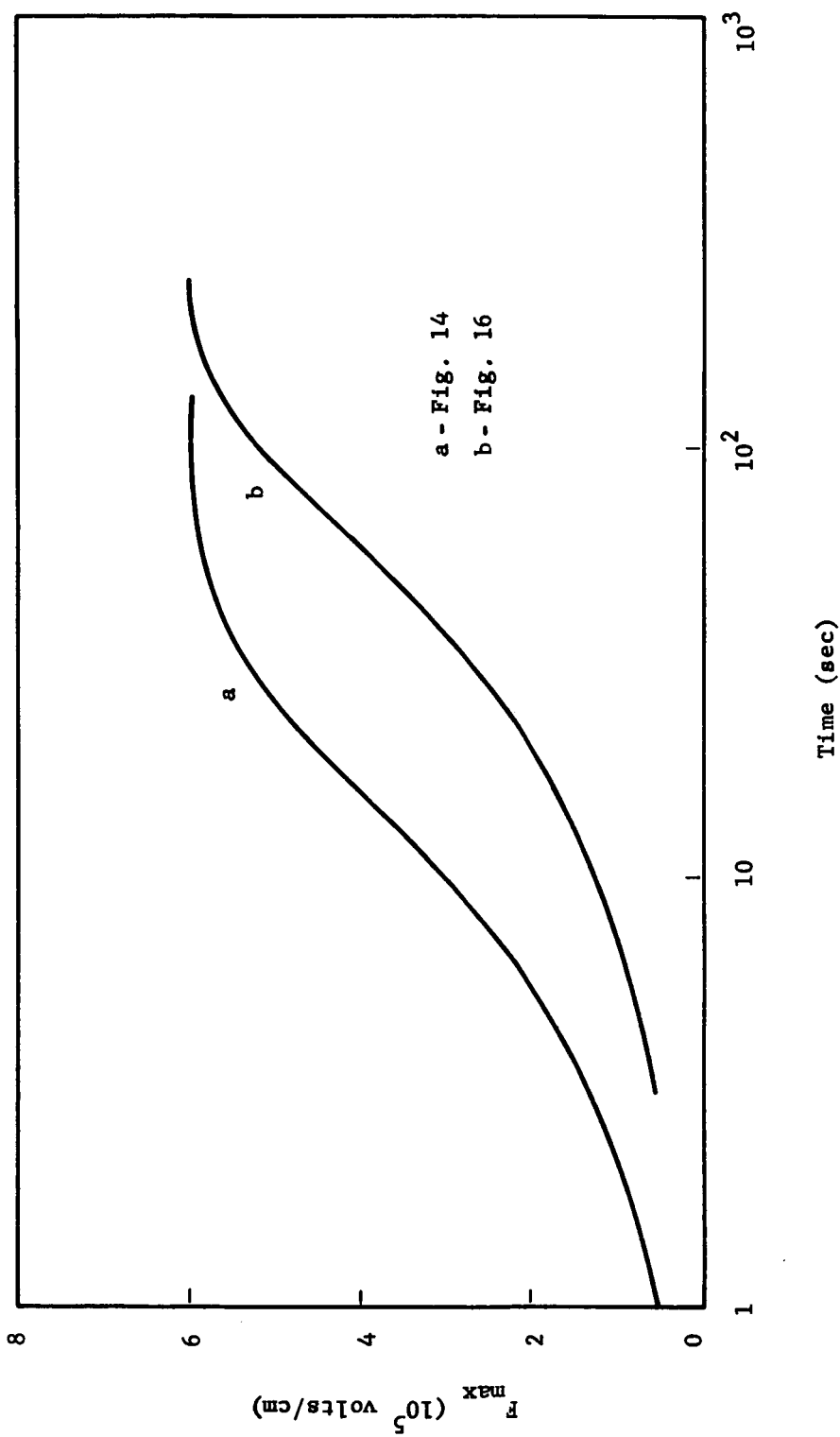
Figure 19. Maximum internal electric field during charge build-up as a function of irradiation time.

27

$$\frac{\partial n_t}{\partial \bar{t}} = \bar{c}_n \bar{n} (\bar{N}_T - \bar{n}_t) - \exp(\bar{n}_t) \; , \qquad (16)$$

$$\bar{n} [\bar{\mu}_n \bar{n}_t + \bar{c}_n (\bar{N}_T - \bar{n}_t)] = \bar{G} + \exp(\bar{n}_t) \; . \qquad (17)$$

In steady-state where $\partial \bar{n}_t / \partial \bar{t} = 0$, the steady-state value of $\bar{n}_t$ ($\bar{n}_{ts}$) is related to $\bar{G}$ from the above equations by

$$\left(\frac{\bar{c}_n \bar{N}_T}{\bar{\mu}_n} \right) \bar{G} = \left(1 + \frac{\bar{n}_{ts}}{\bar{N}_T} \right)^{-1} \bar{n}_{ts} \exp(\bar{n}_{ts}) \; . \qquad (18)$$

This equation leads directly to an estimate of the saturation value of trapped charge. The equation is exactly valid only at the zero field point. However, the zero field point will occur near the point at which $\bar{G}$ has its maximum value. Thus, reasonable estimates of the maximum trapped charge can be obtained from the above equation if the maximum value of $\bar{G}$ is known.

During the initial stages of charge build-up, $\exp(\bar{n}_t) \ll \bar{c}_n \bar{n}$ $(\bar{N}_T - \bar{N}_T)$, and from Eqs. (16) and (17) $\bar{n}_t$ is described by the equation:

$$\frac{\partial \bar{n}_t}{\partial \bar{t}} \left(1 + \frac{\bar{\mu}_n}{\bar{c}_n \bar{N}_T} \bar{n}_t \right) \simeq \bar{G} \; . \qquad (19)$$

This can be integrated to give

$$\bar{n}_t + \frac{\bar{\mu}_n}{2 \bar{c}_n \bar{N}_T} \bar{n}_t^2 \simeq \bar{G} \bar{t} \; . \qquad (20)$$

As steady-state is approached, $\bar{n}_t$ deviates from the value given by the above expression because of the release of carriers from traps. However, an estimate of the time required to reach steady-state can be obtained from the above equation by taking

$$\bar{t}_s \simeq 3 \; \frac{\bar{n}_{ts} + \bar{\mu}_n \bar{n}_{ts}^2 / 2 \bar{c}_n \bar{N}_T}{\bar{G}} \; , \qquad (21)$$

where $\bar{n}_{ts}$ is the saturation value of $\bar{n}_t$ as obtained from Eq. (18).

The steady-state values of trapped charge and time to reach steady-state are shown in Figs. 20 and 21 for various mobility values as a function of flux rate. In obtaining this data, it has been assumed that the electrons

28
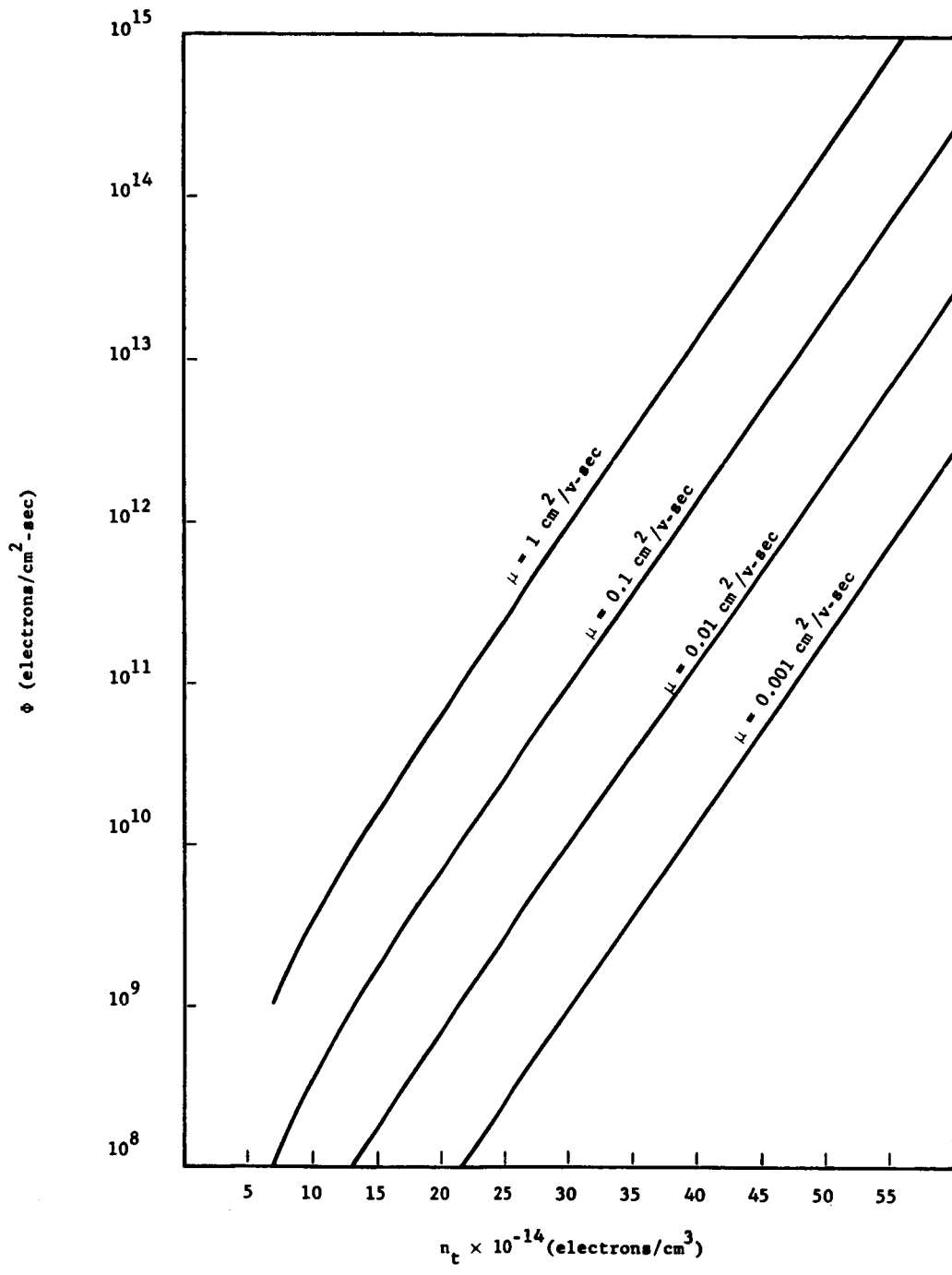
Figure 20. Steady-state trapped charge density as a function of thermalized
electron flux rate for various mobilities.
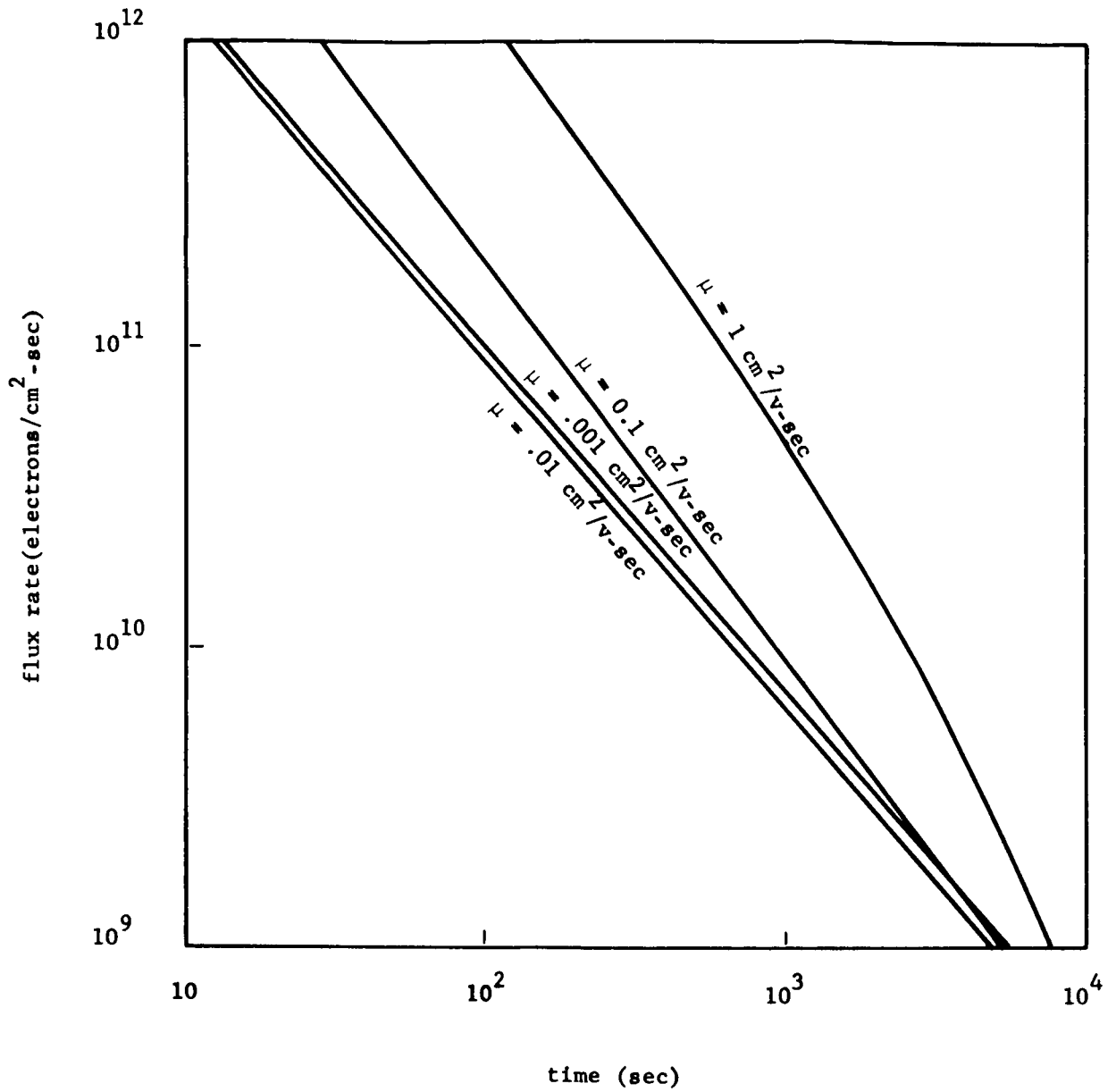
Figure 21. Irradiation time required to achieve steady-state space charge distribution as a function of thermalized electron flux rate for various mobilities.

are stopped uniformly throughout the sample thickness. Values on these graphs have also been found to be consistent with values obtained from the computer solutions. The saturation value of trapped charge is seen to be approximately logarithmically related to the flux rate.

EXPERIMENTAL

There has been no concerted effort to fit the model for space charge build-up and decay to the experimental results obtained to date. However, the external charge transfer curves shown in Figs. 1, 3, 9, 13 and 17 are in reasonable qualitative agreement with the experimental results reviewed in Appendix D. The dependence on irradiation time and primary electron energy exhibit the same general characteristics. To investigate in more detail the applicability of the model, experimental techniques outlined in Appendix D were employed to obtain external current during space charge decay as a function of various irradiation parameters. These results were then graphically integrated to obtain charge transfer.

Samples of 1/4 mil mylar with 6500 $\overset{\circ}{A}$ aluminum electrodes were irradiated with 14 kev electrons, which resulted in the maximum external charge transfer as a function of energy as shown in Appendix D. The current density was 5×10^{-8} amp/cm^2. This corresponds to a flux rate of 3.1×10^{11} e/cm^2sec. For these irradiation conditions, the primary electrons are thermalized in the mylar and Fig. 20 can be used to obtain an estimate for the trapped charge density of $n_t \simeq 3.4 \times 10^{15}$ e/cm^3. The results obtained in Figs. 1 and 2 should provide a reasonable estimate of the external current and charge transfer characteristics for the stated irradiation times as shown in Fig. 22. Also shown as a dotted curve is the external current for distribution e in Fig. 1. Two of the current measurements were graphically integrated and are plotted in Fig. 23. The accuracy in determining the charge transfer beyond 10^3 seconds limits the range of comparison, however, the model predicts a charge transfer as shown by the dotted curve. These results are the most straightforward to compare since the irradiation conditions can be controlled such that the initial conditions of the model are roughly approximated. The results in Figs. 1 and 2 are for a distribution which extends from the irradiated boundary to 1/2 the thickness of the sample and for various depths of trap filling. The range of 14 kev electrons is approximately 1/2 the thickness of 1/4 mil mylar and the irradiation will result in various depths of trap filling assuming a steady-state condition is not achieved for the times used. This aspect will be considered in more detail.

External current and charge transfer during space charge decay have also been computed for the spatial extend of the initial space charge region. However, the depth of trap filling was assumed to be the same for each initial distribution. Since the thermalized electron flux rate and the time required to reach steady-state were unknown, data with these initial conditions were not obtained. However, the
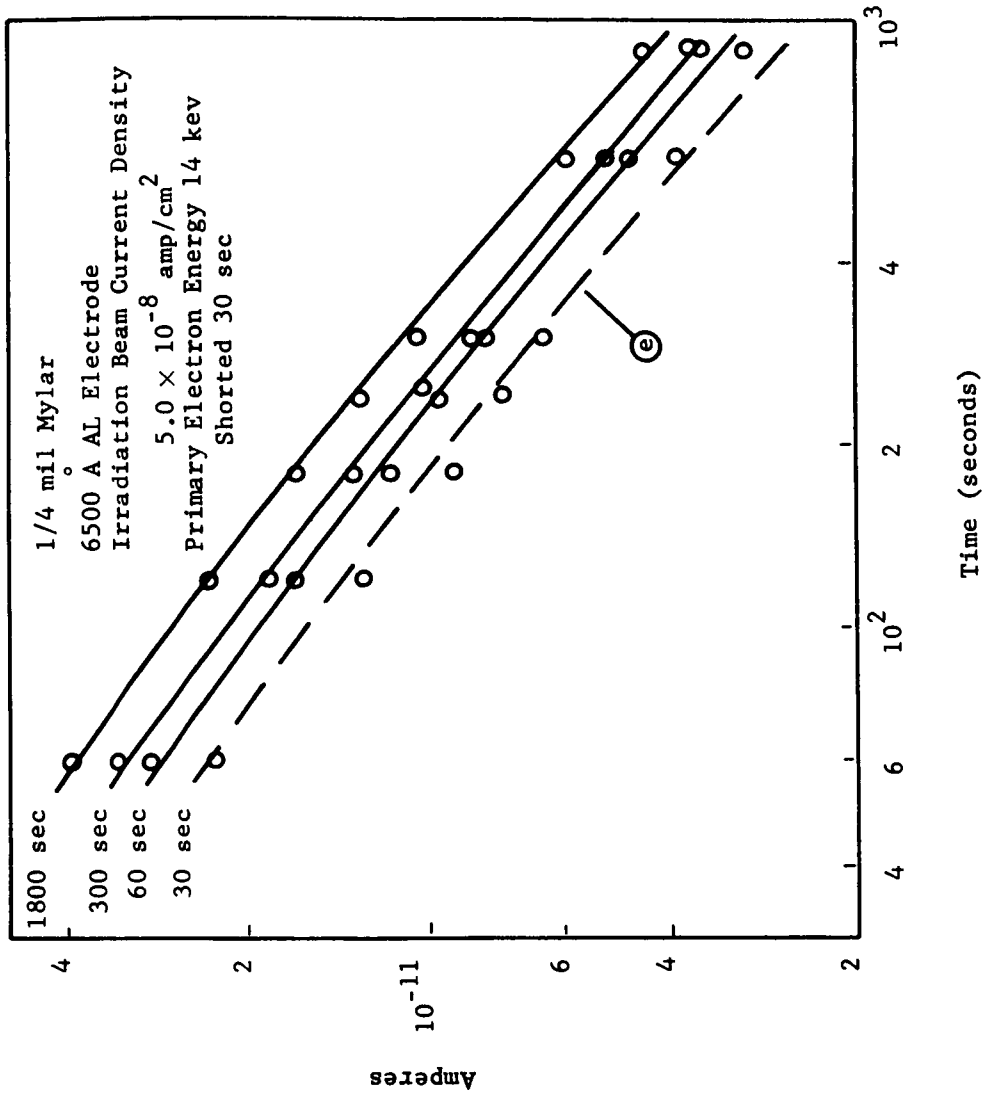
Figure 22. External current during space charge decay for various irradiation times at a constant primary electron energy and flux rate (1/4 mil mylar).
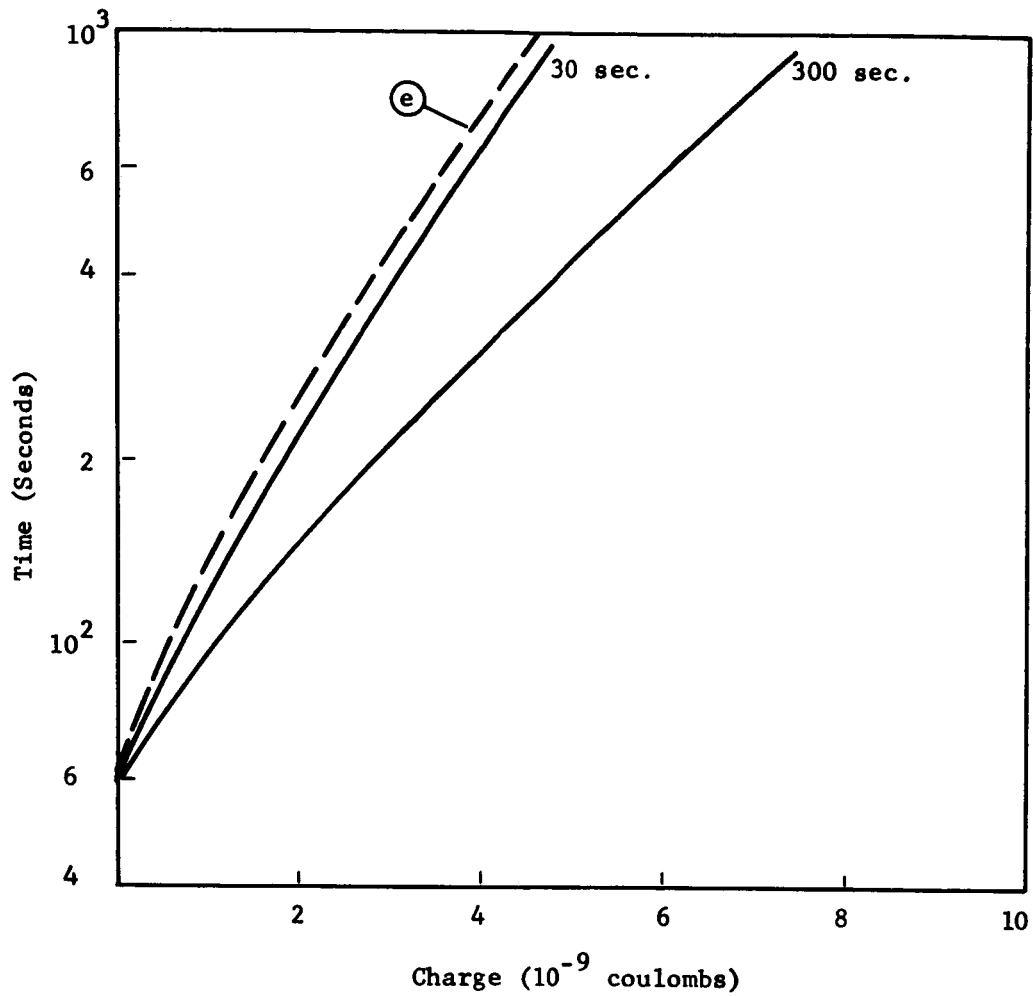
Figure 23. External charge transfer during space charge decay
obtained from Figure 22 by graphical integration.

results for a constant primary electron flux rate at 12 and 14 kev were obtained with the external current data shown in Fig. 24. The dotted curve corresponds to distribution b in Fig. 3. The external charge transfer resulting from these currents is shown in Fig. 25.

An important consideration when comparing the results of the model and experiments is the time required to reach steady-state condition in the irradiated volume. An estimate of this time can be obtained from the considerations used to obtain Fig. 18. The region where Q_{traps}/Q_{flux} has a slope of $1/t$ represents a steady-state condition. The charge in traps can only be inferred from the model, therefore, a more meaningful concept experimentally is the relationship of Q_{ext}/Q_{flux} as a function of irradiation time. Using a constant flux rate and observing external charge transfer for various irradiation times yielded the plot shown in Fig. 26. These results indicate an irradiation time greater than 600 seconds results in a steady-state condition in the irradiated volume. For the parameters used to obtain quantitative results from the model as outlined in Appendix C, the steady-state condition should occur in approximately 100 seconds.

Silicon monoxide films were investigated using charge build-up and release techniques discussed in Appendix D. The silicon monoxide was evaporated from an R. D. Mathis oven. The substrate was $.8$-1.2Ω cm p-type silicon wafer $.9$-1.1 inches in diameter and 15 to 20 mils thick. The substrate was rinsed in alcohol and deionized water before mounting in the vacuum chamber prior to evaporation. SiO was evaporated to various thicknesses from 0.1 to 5 microns and aluminum was evaporated over the SiO film to obtain a capacitor structure. For SiO film thicknesses less than 2 microns the low resistance of the sample (less than 10^7 ohms) precluded charge release measurements. Therefore, the thicker films ($\sim$ 4 microns) were used. The thickness was estimated using the crystal monitor technique and by an optical interferometer measurement.

Using a 4 micron SiO film, a silicon substrate and a 1000 $\overset{\text{o}}{\text{A}}$ aluminum electrode, irradiation techniques similar to those used for mylar were employed to investigate charge build-up and space charge decay. The external current and charge transfer depended upon primary electron energy as shown in Figs. 27, 28 and 29. The analytical results for distribution b in Figs. 4 and 5 are shown as dotted curves. Range energy data were not available for SiO, however, the maximum charge transfer at 20 kev as compared to 14 kev for 6 micron mylar is probably due to the fact that the density of SiO is approximately 4 times that of mylar.

External charge transfer data for various irradiation times are shown in Fig. 30. Using a constant primary electron flux rate and the results of Fig. 30, one can plot Q_{ext}/Q_{flux} as a function of irradiation time as shown in Fig. 31. These results indicate that steady-state in the irradiated volume is achieved after 10^3 seconds.

The concept of a steady-state distribution of trapped charge for a given flux rate was further investigated by irradiating various
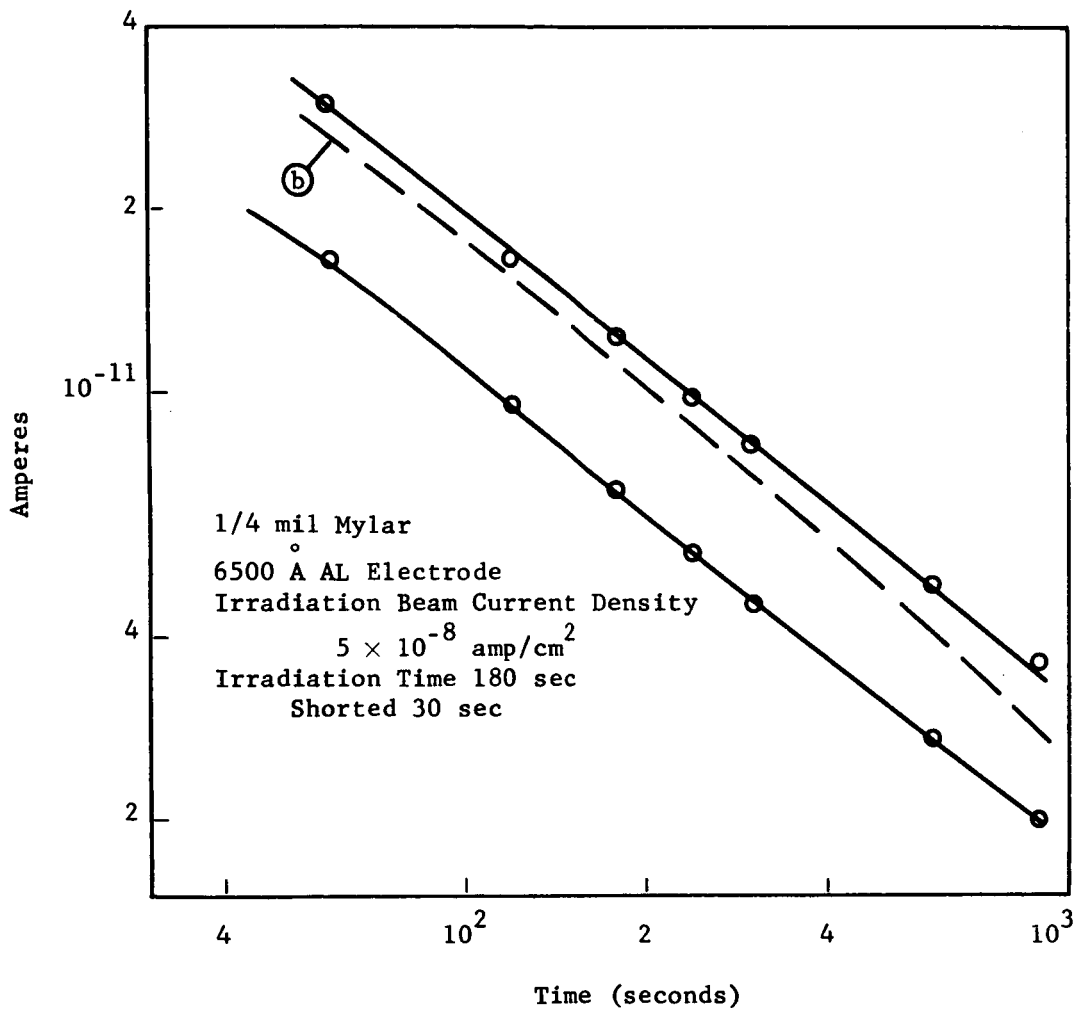
Figure 24. External current during space charge decay for 12 and 14 kev
            irradiation electron energies (1/4 mil mylar).

35
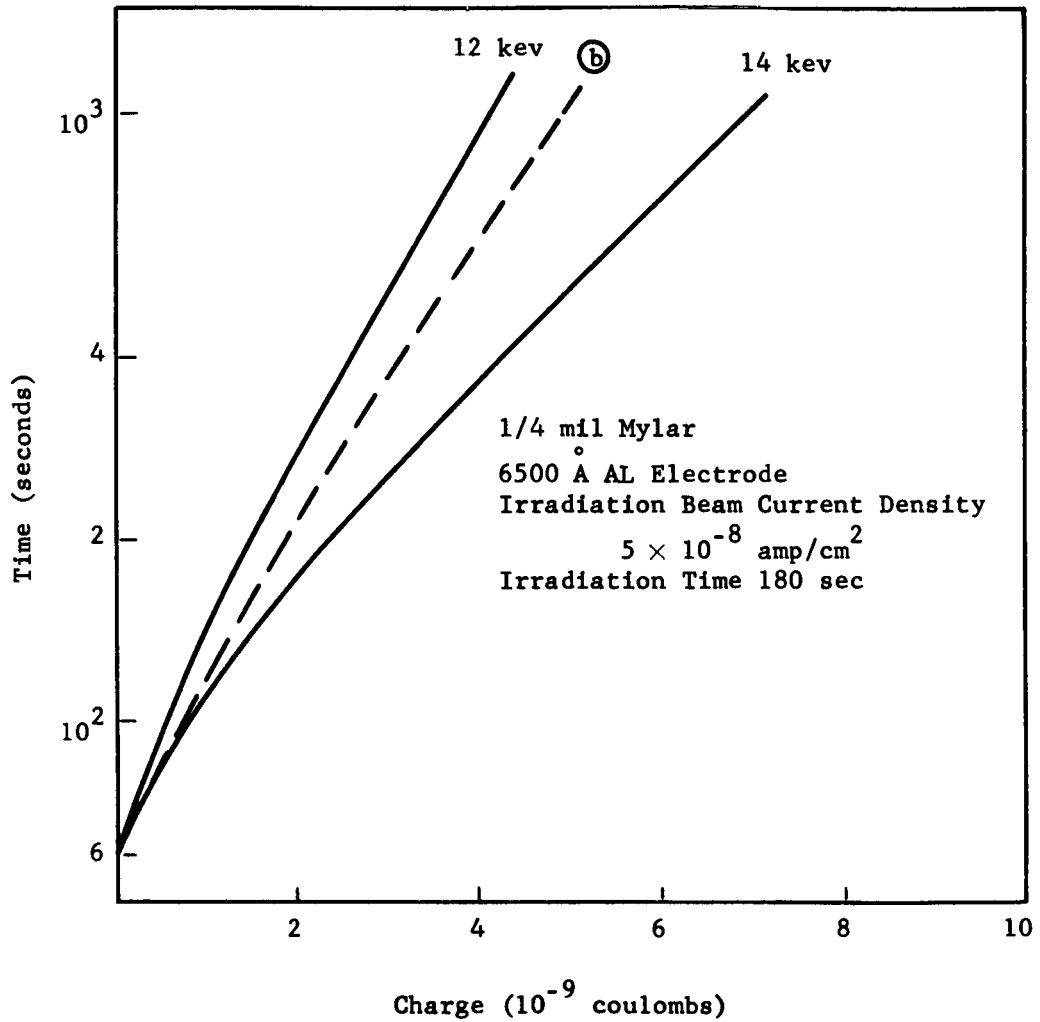
Figure 25. External charge transfer during space charge decay obtained from Figure 24 by graphical integration.
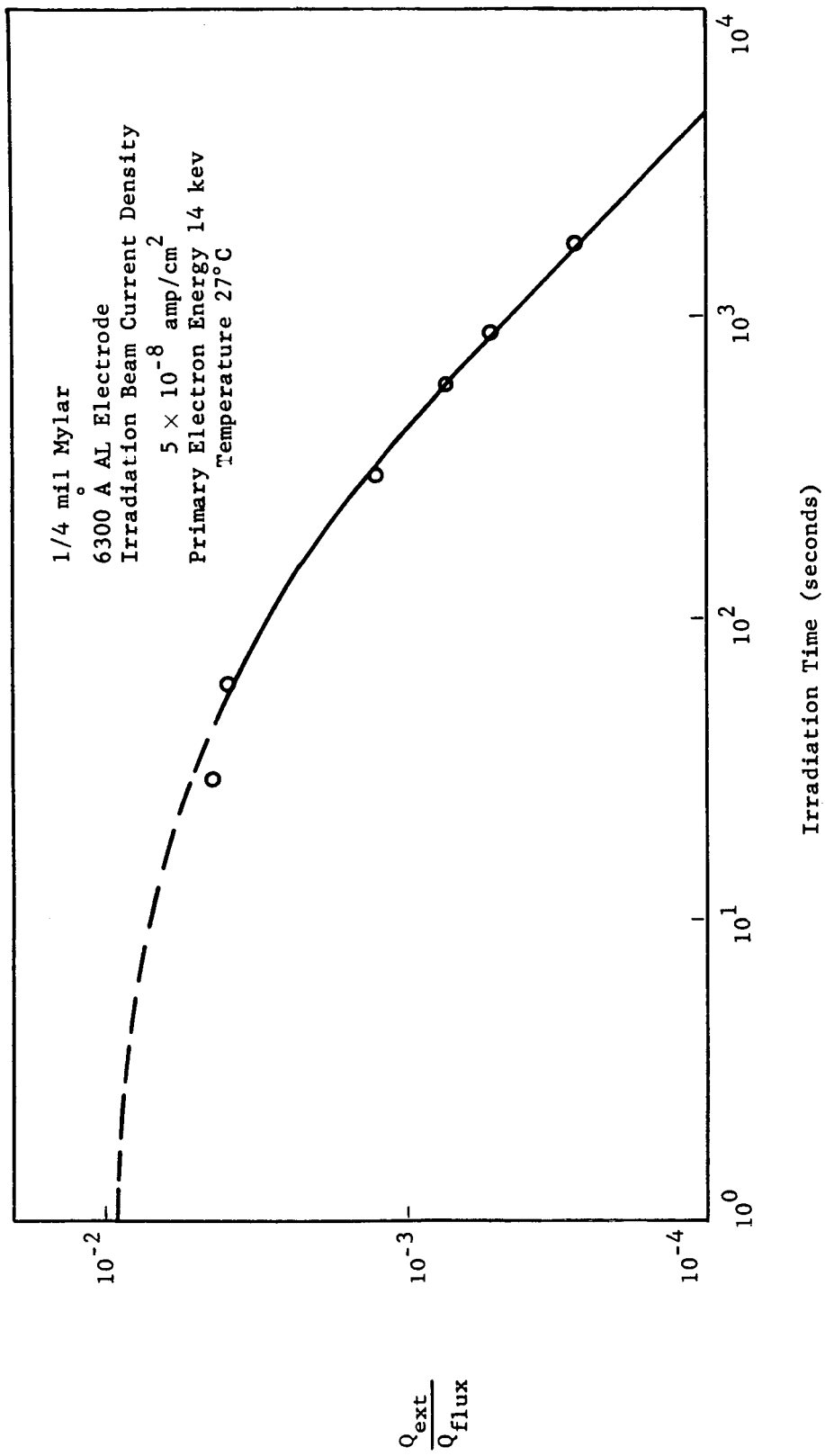
Figure 26. Ratio of external charge transfer to total incident charge vs irradiation time (1/4 mil mylar). (14 kev)

The figure plot contains the following labels:

1/4 mil Mylar
6300 Å AL Electrode
Irradiation Beam Current Density
5×10^{-8} amp/cm^2
Primary Electron Energy 14 kev
Temperature 27°C

Y-axis: $\dfrac{Q_{ext}}{Q_{flux}}$

X-axis: Irradiation Time (seconds)
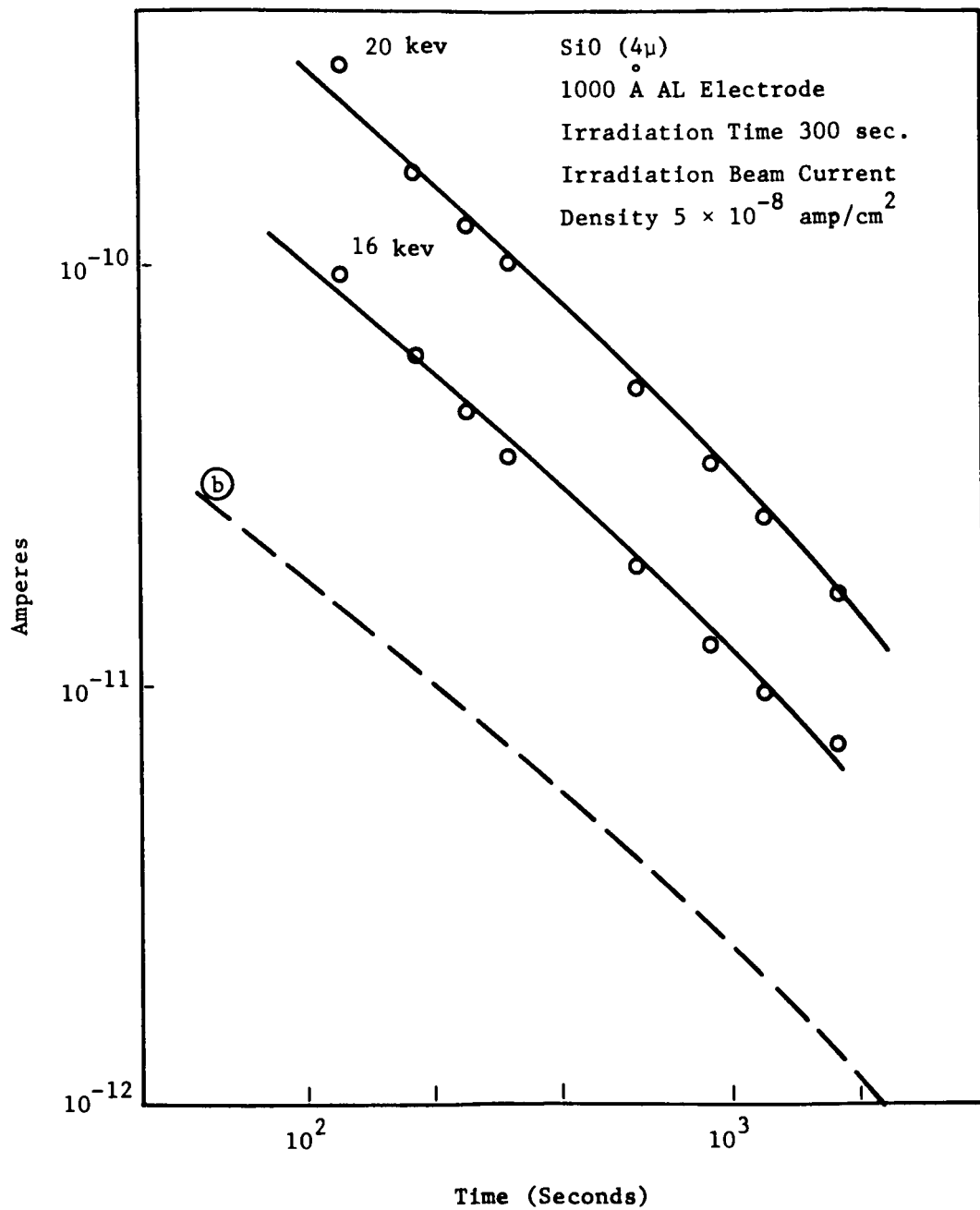
Figure 27. External Current During Space Charge Decay (4 micron SiO).
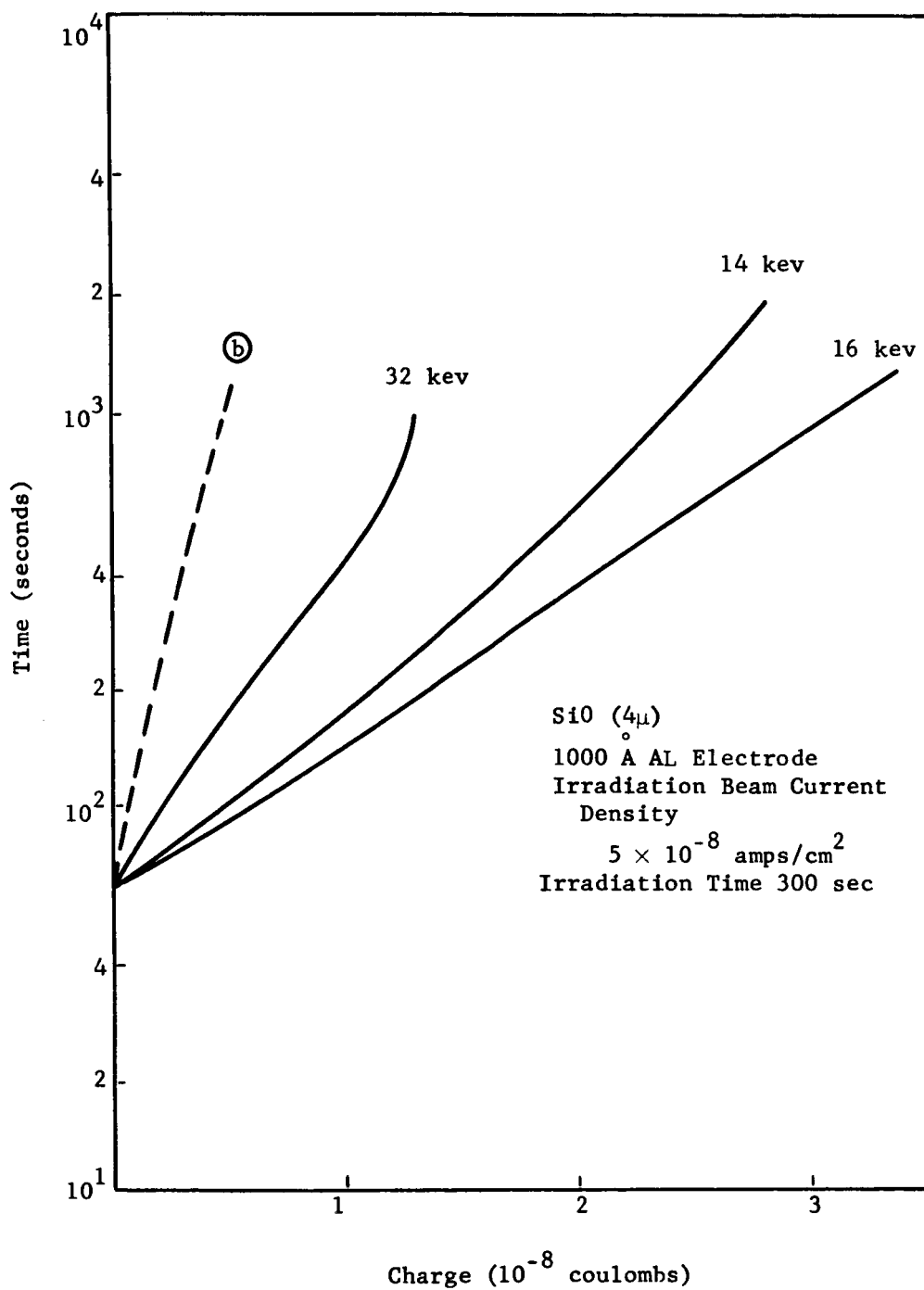
Figure 28. External charge transfer during space charge decay
            (4 micron SiO).
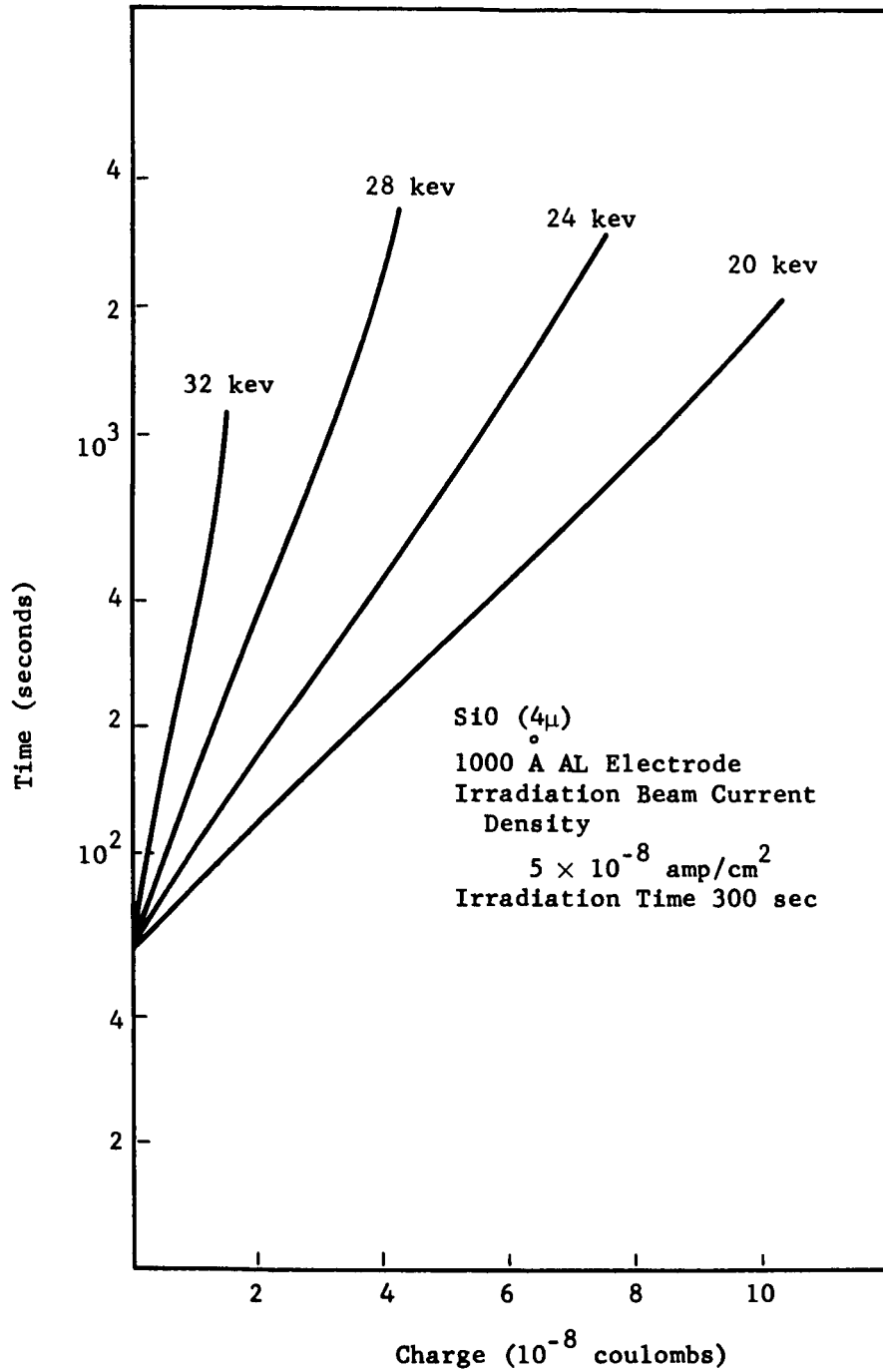
Figure 29. External charge transfer during space charge decay (4 micron SiO).
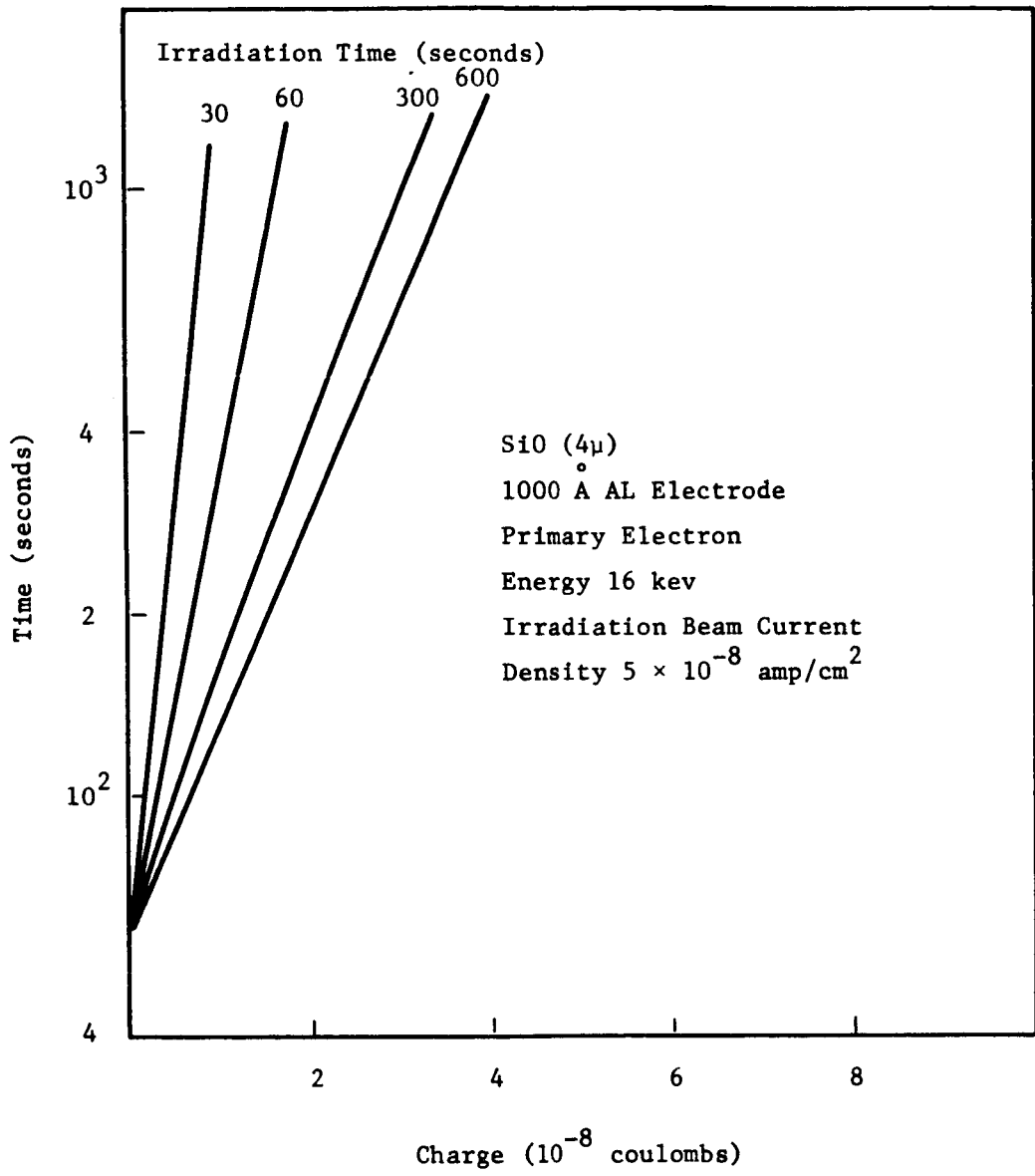
Figure 30. External charge transfer during space charge decay for various irradiation times (4 micron SiO);

41
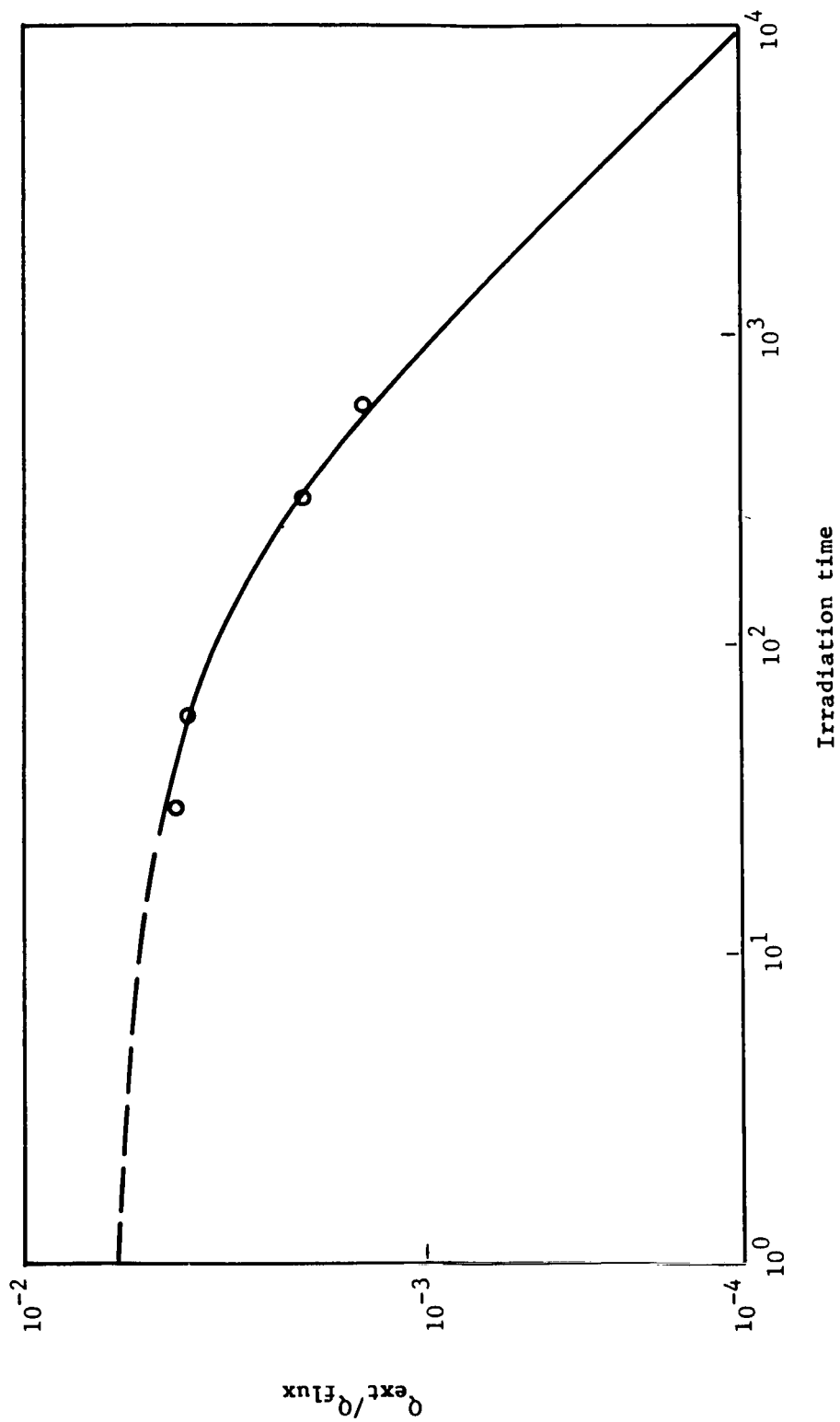
Figure 31. Ratio of external charge transfer to total incident vs irradiation time (4 micron SiO).

thicknesses of mylar with the Pm^{147} source. The thermalized electron flux rate during irradiation can be crudely approximated from

$$I/I_o = e^{-\mu x} \qquad (22)$$

where I/I_o is the fraction of the initial intensity after the β rays have passed through x cm of the absorbing material and μ (cm^{-1}) is the apparent absorption coefficient for the particular spectrum. The apparent absorption coefficient has been approximated by (Ref. 5)

$$\mu/\rho = \frac{17}{E_m^{1.14}} \qquad (23)$$

where ρ is the material density and E_m(Mev) is the maximum energy of the β-ray spectrum. For Pm^{147} $E_m \sim .223$ Mev and the density of mylar is 1.3 gm/cm^3 which results in $\mu \sim 121$ cm^{-1}. For mylar films with thin aluminum electrodes

$$I/I_o = e^{-0.3x} \qquad (24)$$

where x is in mils. For thick aluminum films, I_o must be adjusted for the stopping of betas in the electrodes. For 1/2 mil aluminum, I_o must be reduced by a factor of 2. However, for these experiments, 1000 Å thick aluminum electrodes were used and the primary electron flux is not greatly affected before interacting with the mylar. Measured flux rate values for the Pm^{147} source are approximately 10^9 e/cm^2sec.

The experimental arrangement for Pm^{147} irradiations is shown in Fig. 37. An added feature for the space charge decay measurements was a shutter to shield the sample from the beam. Leakage current due to incomplete shielding was less than 10^{-12} $amps/cm^2$.

For 1/4 and 1 mil mylar films and irradiation times from 30 to 7200 seconds, external charge transfer could not be detected after shielding the sample from the source. This indicates that either the trapped charge density is too small to result in an external charge transfer above the sensitivity of the measurement or the spatial distribution is approximately uniform throughout the sample. Using the apparent absorption coefficient $\mu \sim 121$ cm^{-1}, the latter explanation appears more reasonable. For a thermal electron flux rate determined by Eq. (24), the model predicts the spatial charge distribution shown in Fig. 32. There is negligible external charge transfer associated with the decay of these spatial distributions which is consistent with the experimental work.

43

$$\mu = 0.1 \ cm^2/v\text{-sec}$$
$$\phi = 10^9 \ e/cm^2\text{-sec}$$
$$L = 1/4 \ mil$$

3.86×10^4 sec

10^4 sec

3.86×10^3 sec

y-axis: $n_t (4.42 \times 10^{14}/cm^3)$

x-axis: x/L
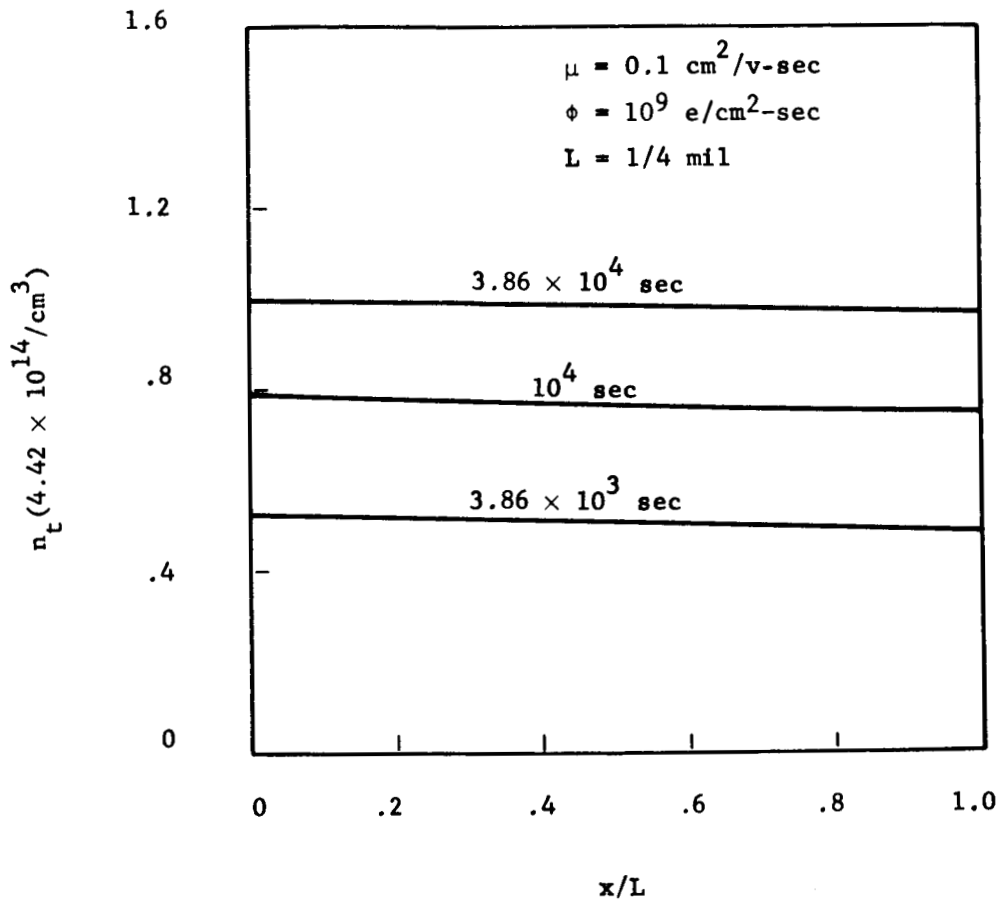
Figure 32. Trapped charge distribution resulting from generating function $I/I_o = e^{-\mu x}$ for 1/4 mil mylar.

For 10.0 mil mylar, various irradiation times resulted in the external currents shown in Fig. 33. The increasing current as the irradiation time is extended indicates that a steady-state space charge distribution was not obtained for irradiation times up to 7.2×10^3 seconds. Figure 21 indicates that steady-state should be achieved in approximately 10^4 seconds. Another aspect of the data in Fig. 33 should be noted. The current decays less rapidly than for the thinner samples of mylar irradiated at lower energies. This is interpreted as resulting from a predominance of retrapping of the charge carriers during space charge decay.

DISCUSSION

The transport model used to compute the build-up and decay of space charge resulting from electron irradiation agrees reasonably well with the experimental data for mylar. From the present comparisons between analytical and experimental results, it is anticipated that the parameters described in Appendix C should be adjusted in a manner to fit the model to the behavior observed experimentally. The major considerations must be the following:

(1) Using a value of $\bar{c}_n \bar{N}_T / \bar{\mu}_n = 1.7$, the model predicts an external current during the initial portion of space charge decay which is low by approximately a factor of 2 in Fig. 22.

(2) The irradiation time to achieve a steady-state condition in the irradiated volume inferred from Fig. 26 appears to take longer than the model predicts.

(3) The maximum ratio of the total external charge transfer to the total incident flux approaches a value of approximately 1 percent.

To provide a more reasonable fit for external current during initial space charge decay, the value of $\bar{c}_n \bar{N}_T / \bar{\mu}_n$ must be increased. Additional evidence is presented in Appendix C which indicates that $\bar{c}_n \bar{N}_T / \bar{\mu}_n \simeq 5.6$. However, this is in the wrong direction to bring (2) and (3) into better agreement. Since these aspects of the model result from complete decay of space charge, it is possible that the measurement of total external charge transfer was not obtained over a long enough time interval. An alternative explanation is that one should not use the abrupt distributions of trapped charge shown in Figs. 1 and 3. A more reasonable approach for fitting the model to the experimental data would be to compute the initial distribution of trapped charge using the space charge build-up from a generating function which best describes the thermal electron flux. From the results shown in Fig. 14, it is obvious that one would observe a smaller ratio for the total external charge transfer to the total incident flux.
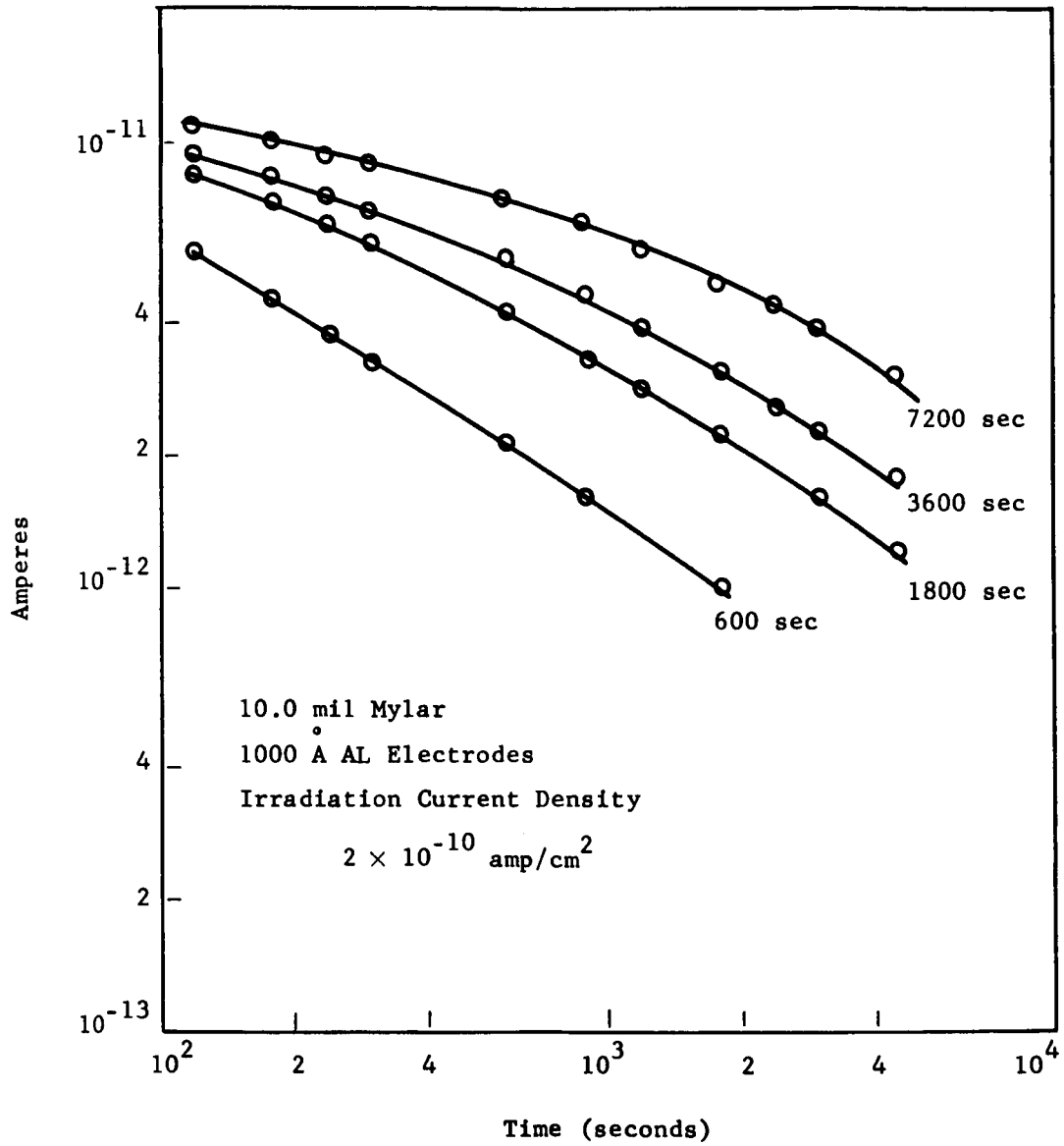
Figure 33. External current from 10.0 mil mylar during space charge decay after Pm[147] irradiation.

There is another important feature of the charge build-up which should be noted. It was recognized in Appendix D that a uniform distribution of space charge could logically explain the external charge transfer as a function of primary irradiation electron energy. The contribution from secondary electrons from the aluminum electrode was considered as a reasonable explanation as to how the uniform distribution might result from monoenergetic electron irradiations. However, the results shown in Fig. 16 indicate that the transport and trapping of charge during irradiation may also result in approximately a uniformly distributed space charge from the irradiated boundary to the practical range of the irradiation electrons. The external charge transfer during space charge decay will have many of the characteristics of those shown in Fig. 17. These results compliment the role of secondary electrons in space charge build-up when the primary electron flux rate constitutes the majority of the thermal electron flux rate.

The results of the analytical model do not agree either quantitative or qualitatively with the experimental results for SiO. This is not too surprising since there has been no effort to adjust the parameters to describe SiO. The main difficulty has been in determining the value of the parameters necessary to use in the transport model. The main feature of the experimental work is that for a given irradiation condition SiO results in more external charge transfer than mylar.

SECTION III

SPONTANEOUS DISCHARGE

The purpose of this investigation is to develop an understanding
of spontaneous discharge associated with electron irradiations and to
determine whether testing techniques are conducive to structure pulsing
for capacitor-type micrometeoroid detectors. The experiments were
centered around detection of spontaneous discharges from capacitor
structures irradiated with monoenergetic electrons and a Pm^{147} source.
The monoenergetic irradiations were performed at Ling-Temco-Vought (LTV)
and Langley Research Center (LRC) with emphasis on spontaneous discharge
rate with respect to the irradiating flux density, irradiated electrode
thickness, and capacitor temperature. The irradiations with the Pm^{147}
source were carried out at the Research Triangle Institute (RTI) with
a flux of approximately 2.2×10^9 e/cm^2-sec.

MEASUREMENT TECHNIQUES

The circuit used to detect the spontaneous discharge from the
capacitors irradiated in the electron accelerator is shown in Fig. 34.
The RC network was inserted to provide a dc path to ground and prevent
saturation of the electrometer. The values of the RC network were
selected so that the input impedance to the electrometer and the
capacitor detector determined the time constant of the discharge pulse.
The RC network was only used in the electron accelerator experiments.
To provide continuous monitoring the electrometer output was connected
to a strip chart recorder. The 200 cycle per second pass band of the
recorder placed a limitation on the time constant of the discharge
event with minimum distortion of the pulse characteristics. The capa-
citance of the irradiated capacitor was typically 10 nanofarads and the
input impedance to the electrometer 10^7 ohms which results in a time
constant of 0.1 seconds. The stray and lead capacitance was always less
than 100 picofarads. The accuracy of the measuring circuit was determined
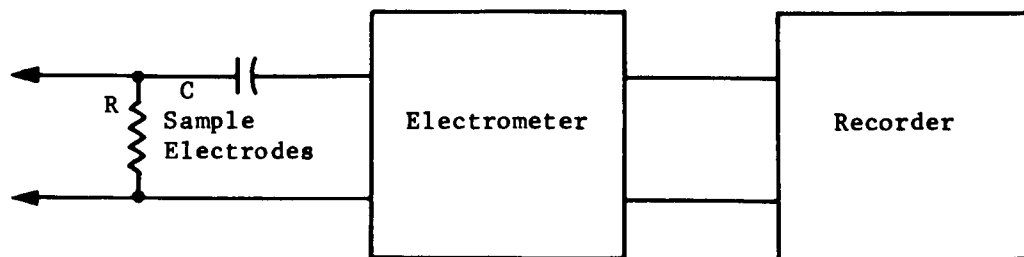
Figure 34. Block diagram for detecting spontaneous discharge.

using a commercial capacitor the same value as the capacitor structure to be irradiated. The commercial capacitor was charged with various voltages and discharged through the RC network and the input resistance of the electrometer. By adjusting the input resistance of the electrometer different values of the decay time constant for the recorded pulses were obtained. Using these various time constants and voltages, the amplitude of the recorded pulses were compared to the initial voltage across the capacitor. The difference was less than 5 percent. The characteristics of the discharge pulse obtained at the recorder output provides a discrimination technique whereby only those pulses with the proper decay time constant are counted. Other disturbances which may occur due to power line fluctuations, induction motor start-up or other sources typically result in shorter time constants and can be correlated with the sources indicated with one exception that being accelerator beam stability. Pulses greater than 50 millivolts can be easily detected using this technique. The lower limit was determined by the stability of the current supplied by the accelerator. Slowly varying fluctuations developed approximately 50 millivolts across the electrometer input impedance.

An alternate technique of pulse recording was attempted with a multichannel pulse height analyzer and appropriate amplifier circuits. An oscilloscope was used simultaneously to observe pulse characteristics. It was observed that small beam variations would be recorded in the multichannel analyzer. The small changes in the irradiation beam were found to occur due to power line fluctuations caused by welding equipment or other similar devices. Noise background necessitated a 100 millivolt discrimination level and prevented its use for detecting small amplitude pulses. Therefore, the electrometer and strip chart recorder were used for recording pulses from the irradiated sensors.

EXPERIMENTAL ARRANGEMENTS

LTV

The experimental arrangement at the accelerator facility is shown in Fig. 35. For this experiment, a homogeneous beam of electrons was desired. This was accomplished by allowing the primary electron beam from the accelerator to pass through a gold foil diffuser about six feet in front of the chamber aperture. A thin scattering foil must be used and the permissible thickness of the foil depends upon the primary electron energy one desires to use. A uniform beam was obtained for energies greater than 50 kev.

The intensity of the beam was measured with two Faraday cups connected to a pair of current integrators. For an irradiation flux rate of 10^{11} to 10^{13} e/cm^2-sec, the reproducibility in the measurement of the electron flux was about 2 percent. The outputs of the current integrators were connected to the alternate channel of the strip chart recorder used to detect the discharge events. Pulses from the capacitor structure created by variations in the electron flux attributed to extraneous effects could be observed simultaneously with those pulses from the Faraday cups.
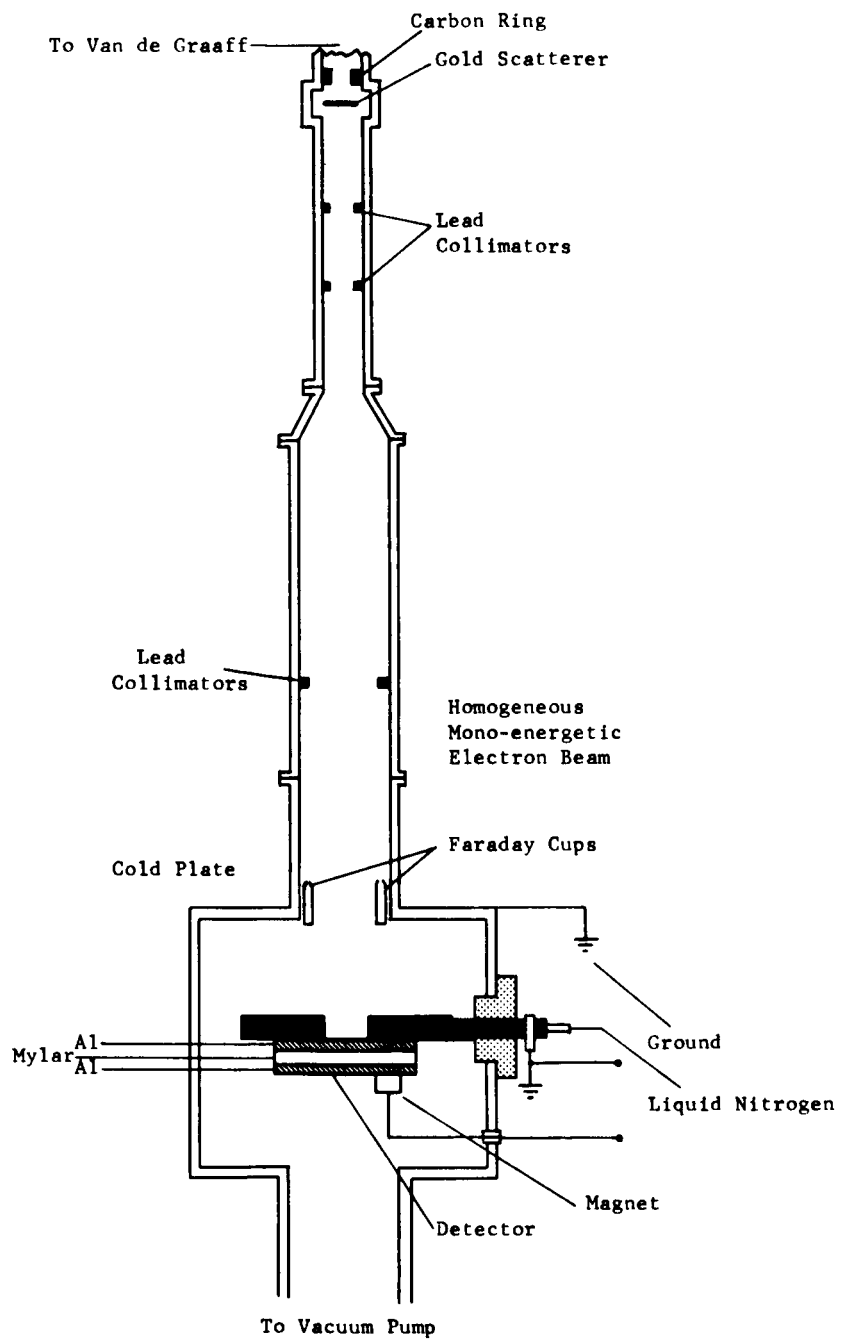
Figure 35. Accelerator irradiation test chamber.

The aluminum test chamber was approximately a 12 inch cube with ports entering four sides. The beam entrance port was approximately 4 inches in diameter, while the opposite cube face was about 8 inches in diameter and provided an access to the chamber for mounting the capacitor structures. The third port was connected to a 6 inch vacuum pump. During the irradiations, the vacuum was at least 10^{-5} torr. The fourth port shown in detail in Fig. 36 was used to provide cooling and act as a support for the capacitor structure. Since data were desired at temperatures colder than ambient temperature, a system for flowing liquid nitrogen through the detector support was used. This device constructed of brass and a phenolic thermal insulator with both neoprene and lead gaskets made it possible to cool the capacitor detector to about -160°C without affecting the seals of the vacuum system. The phenolic thermal insulator on the liquid nitrogen port was shielded by a sheet of lead to prevent scattered electrons from charging it. All other insulators such as feedthroughs were shielded very carefully to eliminate charging effects. No insulation was used on any leads in the chamber during irradiations. The beam tube was magnetically shielded from the gold diffuser to the entrance port to enhance reproducibility of the beam characteristics. A carbon ring with a 1/2 inch hole was placed before the gold diffuser to reduce the possibility of any electrons escaping between the wall and the diffuser. About three feet farther down the tube, a 3.5 inch inside diameter lead ring was used to reduce the electron flux that would be scattered from the tube wall.

During the irradiations, the desired temperature was obtained using a liquid nitrogen control system, based on maintaining a prescribed potential across a copper-constantan thermocouple which was used to measure the capacitor structure temperature. The temperature was monitored by reading the potential developed by two copper-constantan junctions. One junction was immersed in an ice water bath, while the other was thermally connected to the sensor support. The potential was read on a vacuum tube voltmeter placed in the copper line of the thermocouple leads. The liquid nitrogen control circuitry obtained its signal from the output of a vacuum tube voltmeter.

RTI

The apparatus associated with the detection of spontaneous discharge from the capacitor structures exposed to Pm^{147} source is shown in Fig. 37. The irradiation chamber was a 6 inch glass assembly with two ports. One was attached to an oil diffusion pump while the other was used for access to samples. The irradiated area of the sample was 9.6 cm^2. The irradiated samples were connected to the electrometer for monitoring. Only those pulses with the proper time constant were counted as a discharge event.
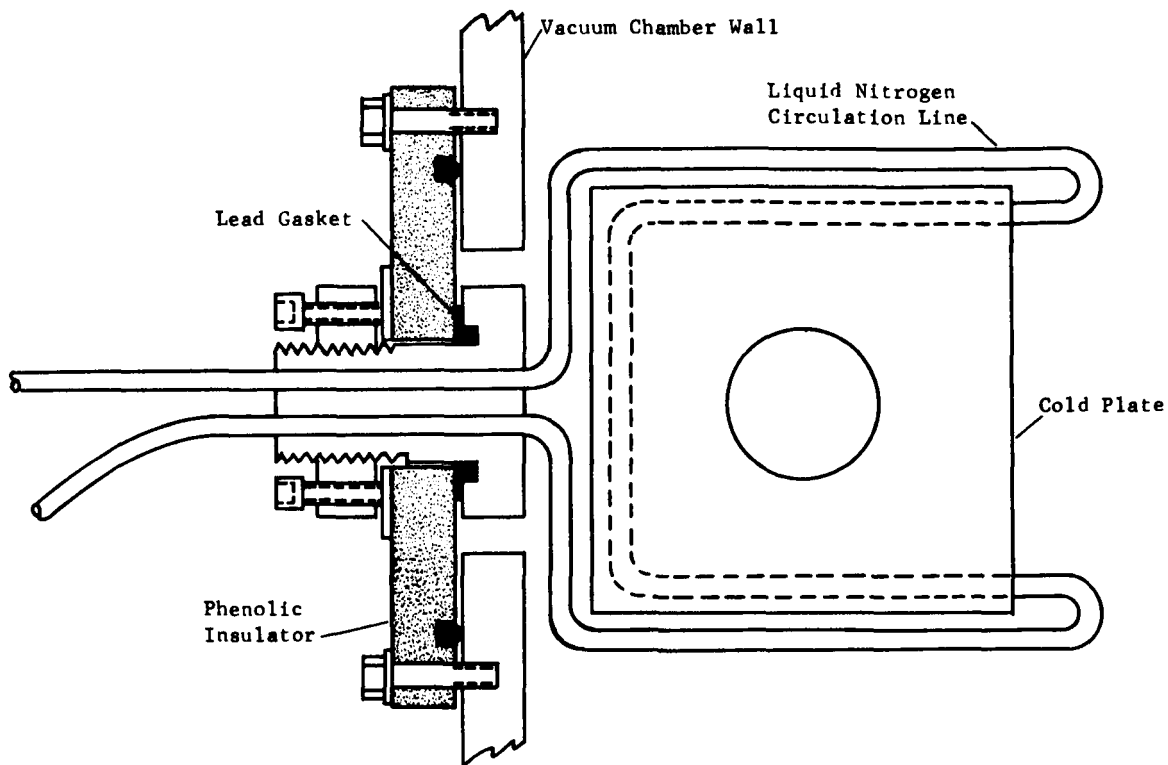
Figure 36. Sensor support and cooling apparatus.
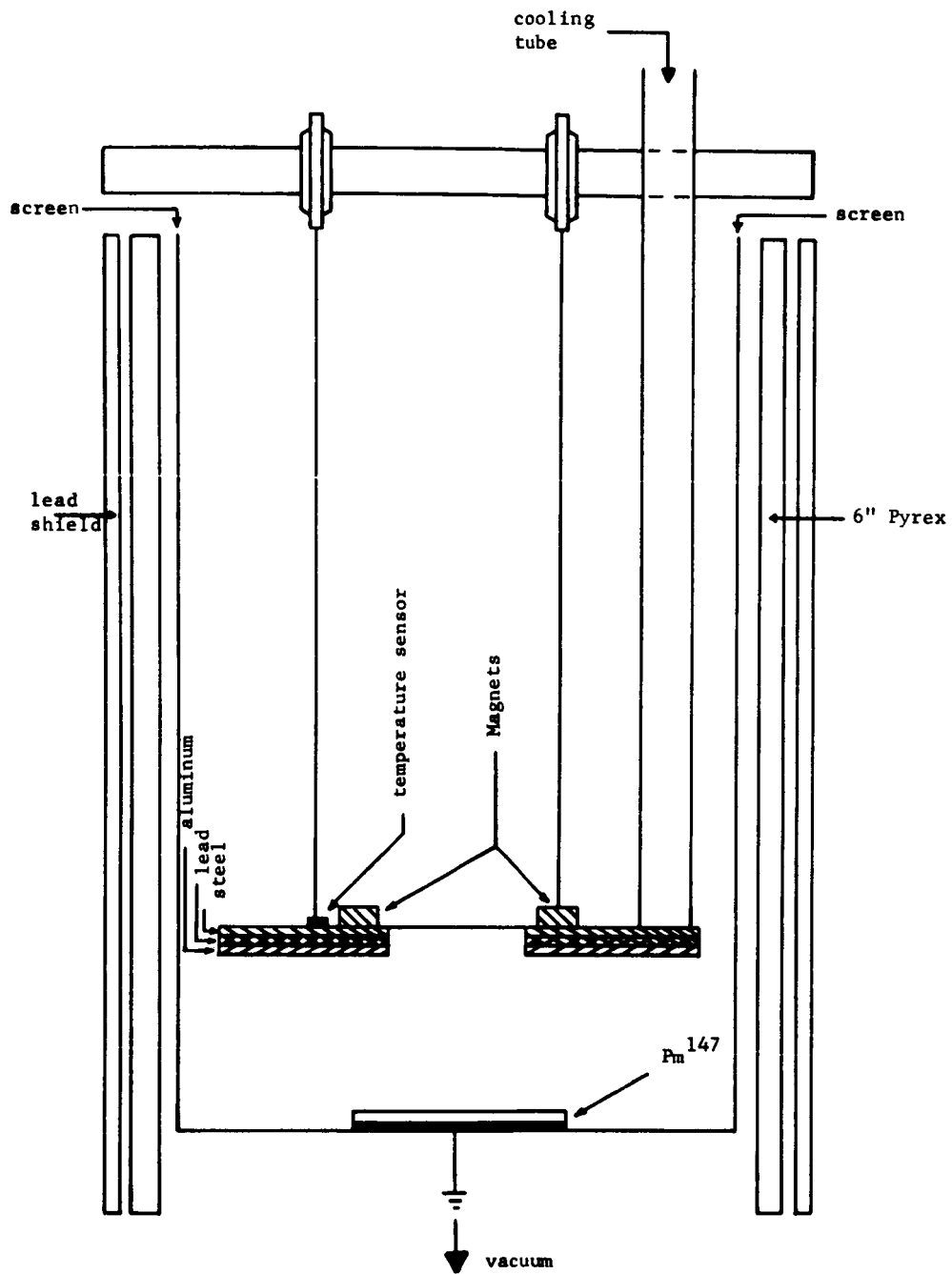
Figure 37. Assembly for Pm^{147} experiment.

The capacitor structures irradiated were mounted within a chamber 76 cm high, 7.6 cm wide, and 30 cm deep. The irradiation chamber was independently evacuated and contained a cold bucket which could be filled with liquid nitrogen to control the temperature of the samples being tested. During the tests, the irradiation chamber vacuum ranged between 10^{-5} torr and 10^{-7} torr depending upon the temperature of the cold bucket.

The electrons from the accelerator passed through an evacuated beam-handling tube to the irradiation chamber. Upon entering the beam-tube, the beam of electrons was widened horizontally to approximately the chamber width of 7.6 cm by a quadrupole magnetic lens. Next, the electrons traveled through the field of two electromagnets that were driven by a triangular wave. The beam was scanned vertically at the rate of approximately 10 cycles per second in a fan-shaped scan horn before entering the irradiation chamber. In order to reduce back scattering, an aluminum shield with a rectangular aperture 5 cm wide and 12 cm high was placed approximately 10 cm in front of the test sample. The shield greatly reduced scattering of electrons and current on the bare signal leads. The beam current density was monitored by an aluminum plate with a circular area of 1 square cm imbedded in a carbon block adjacent to the sample. A bare lead was used within the chamber to connect this plate to a shielded feedthrough. The current collected by this plate was fed to an integrating electrometer.

EXPERIMENTAL OBSERVATIONS

Capacitor structures supplied by Langley Research Center with 1/4 mil mylar dielectric; 0.1 mil, 0.5 mil and 1.0 mil aluminum front electrodes and evaporated back electrodes were irradiated with the Pm^{147} beta source. Irradiations in the Pm^{147} source were carried out at 27° C and -140° C with and without bias applied to the capacitor. Each irradiation period was for 48 hours yielding an integrated flux of approximately 10^{14} e/cm^2. A few pulses were observed, however none were greater than 0.01 volts. The discrimination level was always in excess of 0.001 volts. A total of six capacitors were irradiated for 2421 hours with the Pm^{147} beta source. Pulses of the order of 10 millivolts were detected with one exception. For one of the capacitors with 1.0 mil aluminum front electrode, regular pulsing was observed with a maximum amplitude of approximately 500 millivolts. The detector was cooled and the pulsing ceased. After removal from the irradiation chamber, it was noted that the back aluminum electrode had eroded under the contact area. This suggests that the pulsing was connected with the behavior of the contact region. This was the first observation of this particular behavior and reemphasizes the need for non-insulating contacts to the sensor.

A group of six sensors which were supplied by Langley Research Center were irradiated in the LTV accelerator after qualification tests in the

Pm^{147} beta source. The irradiations were carried out using energy increments of 25 kev from 50 kev to 300 kev with the sensor temperature 27°C and -140°C. Each irradiation period was 10^3 seconds with an electron flux rate of 9.4×10^{10} e/cm^2-sec yielding an integrated flux of approximately 10^{14} e/cm^2. The sensors with 0.1 mil front electrode were tested under the above conditions with two exceptions, the temperature of -140°C and energies greater than 150 kev were not used. Electron energy, electrode thickness, temperature, and electron flux rate was varied within the above limits and no pulsing was observed with amplitudes in excess of the discrimination level of 0.050 volts.

A 1/4 mil mylar sample with two evaporated electrodes was irradiated by the Pm^{147} beta source for a period of 166 hours through 0.5 mil aluminum scattering foil. Ten pulses were observed with a maximum amplitude of 80 millivolts at -140°C. For the pulsing time, the data yielded a value of 10^{12} e/cm^2-pulse. The sample was warmed to 27°C and the pulsing ceased. The same sample was irradiated with monoenergetic electrons from the LTV accelerator through a 0.5 mil aluminum foil with irradiation electron energies between 50 kev and 200 kev. Regular pulsing was observed at 27°C. The pulse height was typically 200 millivolts. The time interval between pulses depended upon energy as well as flux rate with the interval decreasing for increasing flux rate or energy. Pulsing disappeared as the sample was cooled. If the sample was warmed to 27°C in the evacuated chamber one could not obtain the regular pulsing again. If the sample was exposed to room ambients and then the chamber evacuated, the sample would resume pulsing. It was recognized early in the irradiations that when bare insulators were exposed to the electron flux, one could obtain a substantial surface charge which could result in a discharge. The exposed surface of the mylar was painted with silver paint within 1/16 inch of the edge and irradiated under a variety of conditions. The regular pulsing as previously observed could not be induced; however, approximately ten pulses with the largest about 0.1 volts were observed intermittently for 50 kev electrons and an electron flux of 3.7×10^{11} e/cm^2-sec which yielded a value of 3.3×10^{13} e/cm^2-pulse. The energy was increased to 75 kev at the same electron flux and five pulses less than 0.050 volts were recorded which yielded 4.4×10^{13} e/cm^2 pulse. One would interpret the regular pulsing observed before the painting of the exposed edges as a surface effect and the pulsing observed after painting the edges as spontaneous discharge events similar to those observed for the Pm^{147} irradiations.

A series of irradiations on the sensors were made with the flux rate in excess of 10^{12} e/cm^2-sec. For energies greater than 175 kev and temperatures ambient or cooler pulsing was induced for 1.0 mil aluminum electrodes. The pulse rate appeared to increase rapidly with increasing flux rate as shown in Fig. 38. The pulses observed were negative on the irradiated electrode with respect to the back electrode and
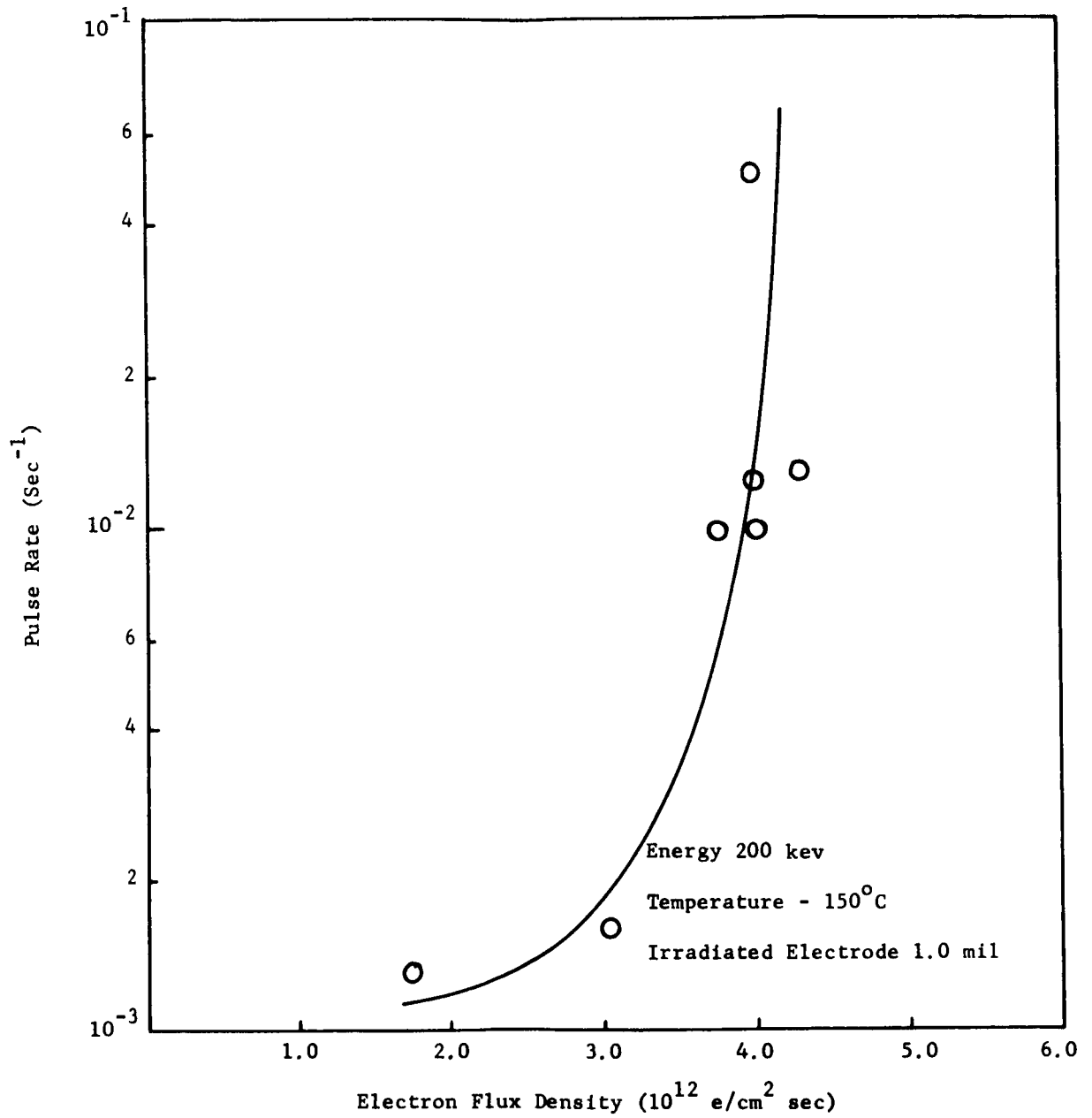
Figure 38. Pulse rate as a function of irradiating flux density.

appeared to have approximately the same amplitude. Upon irradiating the sensors at higher flux rates, the voltage across the capacitor would become very erratic after several irradiations and prevent further measurements. None of the capacitors tested exhibited these erratic behaviors until it had been irradiated for approximately 10^4 seconds. The capacitors exposed to the minimum flux required to induce pulsing showed no degradation upon completion of the irradiation periods.

The sensors were also irradiated at various temperatures from 40°C to -150°C and the interval between pulses decreased with decreasing temperature for each sample tested. Using an electron flux rate of 4.0×10^{12} e/cm^2-sec and 200 kev electrons, the pulse rate approximately doubled when going from 40°C to -150°C.

The pulse rate was also investigated as a function of irradiation electron energy for an electron flux rate of 4.0×10^{12} e/cm^2-sec. The pulse rate increased with increasing energy up to approximately 250 kev when the maximum pulse rate occurred and then decreased with increasing energy as shown in Fig. 39. No pulses greater than the discrimination level of 8.4 volts were observed for electron energies less than 175 kev.

For electron flux rates exceeding 2.0×10^{12} e/cm^2-sec, the pulse amplitude was investigated using electron energies in excess of 175 kev and temperatures from 40°C to -150°C. The average pulse amplitude was 90 volts with the exception of one sample which had an average pulse height of 120 volts under the same conditions. This pulse amplitude distribution is shown in Fig. 40 including the one sample that had the high pulse height average.

A few limited irradiations were made on capacitors utilizing silicon oxides as the dielectric. They were tested from 50 kev to 150 kev in approximately 25 kev increments and did not pulse. The flux rate was approximately 10^{11} e/cm^2-sec with an integrated flux of 10^{14} e/cm^2 for each of the 13 irradiations. Five of the runs were carried out for temperatures between -130°C and -160°C.

Monoenergetic irradiations were performed at Langley Research Center using an accelerator with a swept beam. A group of sensors which were supplied by Langley Research Center with 1/4 mil dielectric; 0.5 mil and 1.0 mil aluminum front electrodes and evaporated back electrodes were irradiated in the swept beam accelerator after previous testing at Ling-Temco-Vought with a monoenergetic stationary beam and at Research Triangle Institute using a Pm^{147} beta source. The swept beam irradiations were carried out using energy increments of 50 kev from 50 kev to 200 kev at 27°C and -140°C. Each irradiation period was 10^3 seconds with an electron flux rate of 9.4×10^{10} e/cm^2-sec yielding an integrated flux of approximately 10^{14} e/cm^2. Ten pulses
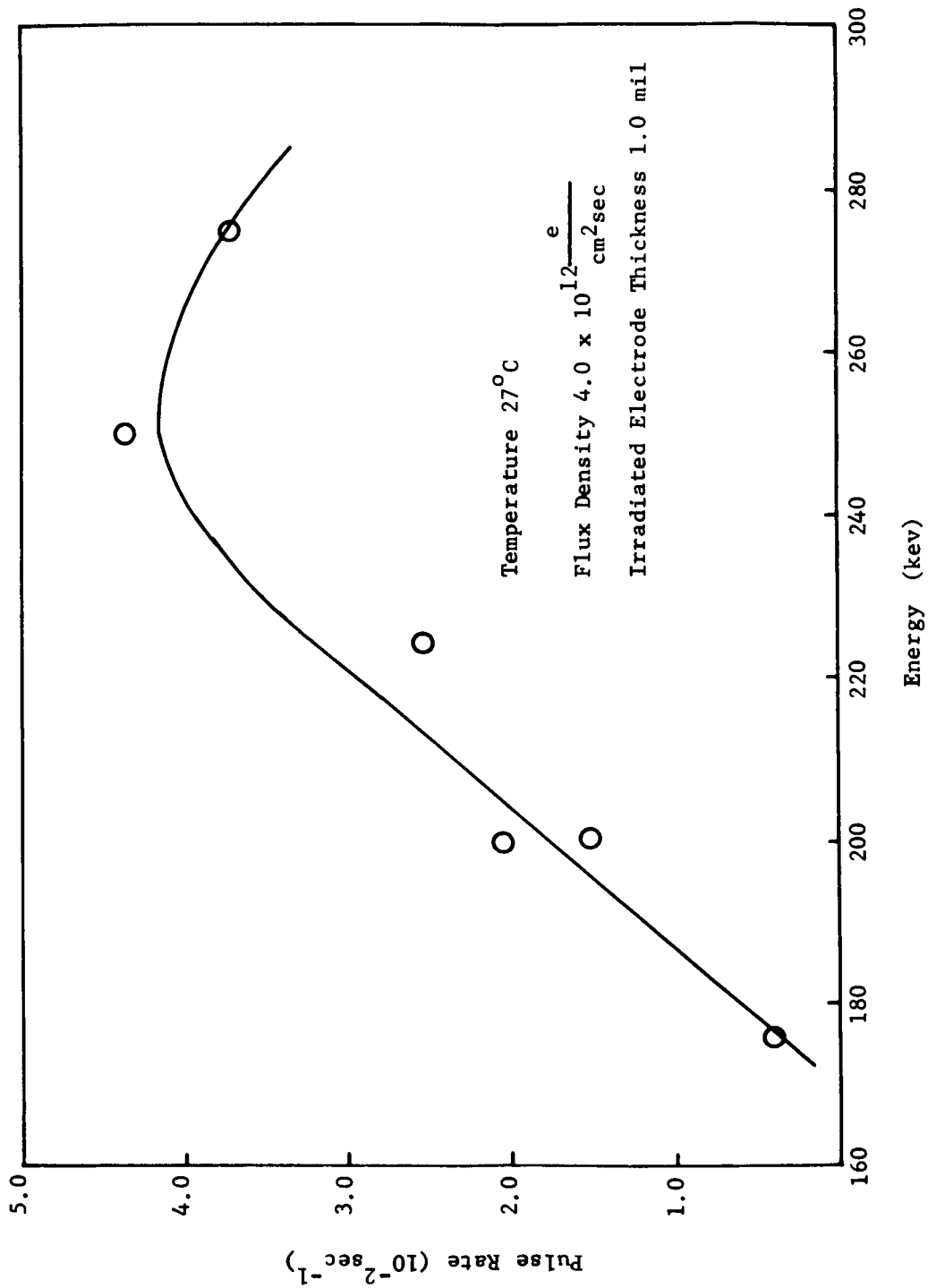
Figure 39. Pulse rate as a function of energy at 27°C.

The plot axes and labels read:

Pulse Rate (10^{-2} sec^{-1}) (vertical axis), with values 1.0, 2.0, 3.0, 4.0, 5.0

Energy (kev) (horizontal axis), with values 160, 180, 200, 220, 240, 260, 280, 300

Temperature 27°C

Flux Density $4.0 \times 10^{12} \dfrac{e}{cm^2 sec}$

Irradiated Electrode Thickness 1.0 mil

58
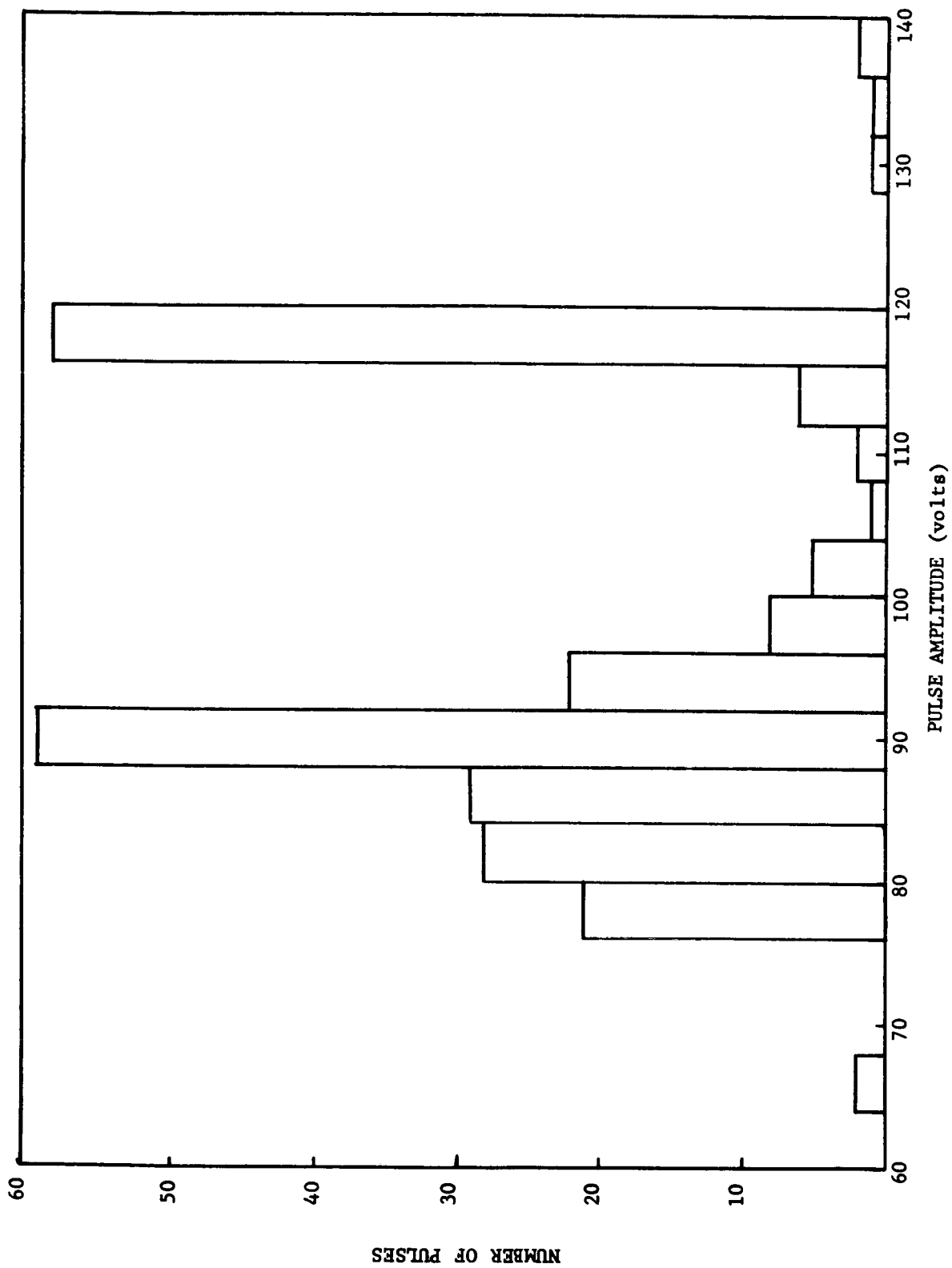
Figure 40. Pulse height distribution from spontaneous discharge of electron irradiated sensors.

were observed with amplitudes less than 350 millivolts with a discrimination level of 60 millivolts.

A sample of 1.0 mil GT-201 adhesive manufactured by G. T. Schjeldahl Company with two evaporated aluminum electrodes was irradiated by the Pm^{147} beta source for a period of 60 hours with 0.5 mil aluminum scattering foil. The sample was irradiated 45 hours at 27°C and 15 hours at -140°C and no pulsing was observed with a discrimination level of 50 millivolts. The same adhesive sample prepared with evaporated aluminum electrodes was irradiated with monoenergetic electrons from the LRC accelerator using a swept beam of electrons through a 0.5 mil aluminum scattering foil with energies between 50 kev and 200 kev using energy increments of 50 kev. The sample was irradiated at 27°C and -140°C with each irradiation period of 10^3 seconds and an electron flux rate of 9.4×10^{10} e/cm^2-sec yielding an integrated flux of approximately 10^{14} e/cm^2. No pulsing was observed from the adhesive sample with a discrimination level of 200 millivolts. The small capacitance of the 1.0 mil adhesive sample was responsible for the larger discrimination level because of the increased input impedance to the electrometer to obtain a time constant within 200 cycle bandwidth of the strip chart recorder.

The intensity effect observed at Ling-Temco-Vought using a stationary beam with an electron flux rate in excess of 10^{12} e/cm^2-sec was investigated using the accelerator with the swept beam. Sensitivity of the monitoring equipment was reduced because of the time varying voltage across the capacitor as a result of sweeping the beam. The voltage across the capacitor also increased with higher beam intensities and thereby increasing the discrimination level to 1.2 volts.

A series of irradiations were made on capacitor structures with 1.0 mil aluminum electrodes for energies of 150 kev to 225 kev in 25 kev increments of energy. The pulse rate was investigated at 27°C and -150°C for an electron flux rate of 4.0×10^{12} e/cm^2-sec. A few pulses were observed, however, the limited number of pulses does not permit one to infer a dependence on energy, temperature, and flux rate. The large amplitude pulses observed at Ling-Temco-Vought could not be induced in the structures tested with a swept beam, however, a few pulses with amplitudes less than 5 volts were observed at the high beam current intensities. In a further attempt to enhance pulsing a 16.0 mil aluminum back-up plate was installed directly behind the capacitor structure, however, the discrimination level increased to 2.0 volts and no pulsing was observed either at 27°C or -140°C.

DISCUSSION

The results obtained from the irradiation of capacitor structures at RTI, LTV and LRC indicate that the experimental techniques associated with the irradiation influences the characteristics of the spontaneous

discharge events. The results discussed have been either directly or
indirectly attributed to the rate of charge build-up in the mylar due
to the trapping of thermalized primary and secondary electrons. There-
fore, the spontaneous discharge characteristics should be related to the
charge storage model discussed in Section II. Using this model, one can
provide a phenomenological description as to how the rate of space
charge build-up influences the spontaneous discharge events. The per-
tinent aspects of the model are included in Figs. 20 and 21. For a
given flux rate of thermal electrons ϕ the steady-state value of
trapped charge assumed to be uniformly distributed throughout the ir-
radiated volume is shown in Fig. 20 for various mobility values. The
approximate irradiation time required to achieve steady-state is shown
in Fig. 21.

Although a flux rate dependence has been observed, the flux rates
in Figs. 20 and 21 pertain to thermalized electrons and a quantitative
relationship between the primary irradiation flux and the thermalized
flux is not available. To use the results of the model to interpret
spontaneous discharge characteristics requires an assumption as to this
relationship. The pulse rate dependence on energy correlates more
closely with secondary electron processes than with the stopping of

primaries. The secondary yield from 5.2 mg/cm^2 aluminum target elec-
trodes is approximately 4 percent in this energy range (Ref. 7).
Secondary yield from thinner aluminum films at lower energies range up
to 50 percent (Ref. 8). Therefore, a reasonable assumption for a thermal
electron flux rate appears to be approximately 10 percent of the primary
flux rate.

For the samples irradiated by all three methods, the integrated
flux for each irradiation period was at least 10^{14} e/cm^2, however, the
flux rates were 2.2×10^9 e/cm^2-sec at RTI and 9.4×10^{10} e/cm^2-sec at
LTV and LRC. The Pm^{147} irradiations at RTI resulted in a few pulses
the order of 10 mv. Using the diffused beam technique at LTV, no pulses
in excess of the discrimination level of 50 mv were detected. For the
swept beam irradiations at LRC, 10 pulses were detected with an average
pulse height of approximately 100 mv and a maximum pulse height of 350 mv.
The discrimination level was 60 mv. Since the discrimination levels at
LTV and LRC were too high to detect 10 mv pulses, the data at RTI must
be disregarded when attempting to compare the results of the three
techniques. Therefore, the major difference noted for the low intensity
irradiations was the pulses obtained at LRC.

For a thermal electron flux rate of 9.4×10^9 e/cm^2-sec the steady-
state trapped electron density is $n_t \sim 2.2 \times 10^{15}$ e/cm^3 for mobility of
0.1 cm^2/v-sec and the irradiation time required to achieve steady-state
is $t_s \sim 10^3$ sec. Therefore, the maximum value of internal electric
field occurs only after 10^3 sec irradiation time. The average spontan-
eous discharge pulse height of .1 volt represents a liberated charge of

10^{-9} coulombs. The charge in traps for the assumptions used to obtain Fig. 20 is 3×10^{-6} coulombs. Therefore, the observed charge is only a small fraction of the charge in traps.

The average flux rate for the diffused beam and swept beam techniques were the same resulting in approximately the same steady-state conditions. However, the instantaneous flux rate for the swept beam technique must be higher. For a constant sweep rate across a 1 cm pick-up used to monitor the beam current, the instantaneous flux rate (ϕ) is related to the average flux rate ($\bar{\phi}$) by

$$\phi \simeq \bar{\phi} \, \frac{L'}{\Delta x} \qquad (25)$$

where Δx is the beam dimension in the direction of beam displacement and L' is the displacement amplitude. The actual value of $L'/\Delta x$ depends upon the energy of the irradiation electrons, however $L'/\Delta x > 10$ is not uncommon. Therefore, the instantaneous flux rate of electrons which interact with the capacitor structure is at least an order of magnitude larger for the work at LRC as compared to the LTV irradiations. Another factor to consider is the percent of charge released from traps for approximately one-half cycle of the swept beam. From Eq. (A-14) the release rate is $\exp(\bar{n}_t)$ and

$$\frac{\Delta \bar{n}_t}{\Delta \bar{t}} \leq \exp(\bar{n}_t) \ . \qquad (26)$$

Therefore, the percent released in Δt is

$$\frac{\Delta n_t}{n_t} \leq \frac{e^{\bar{n}_t}}{\bar{n}_t} \; 9 \times 10^{-3} \; \Delta t \text{ percent} , \qquad (27)$$

after introducing the normalization constant. For a flux rate $\phi = 4 \times 10^{12}$ e/cm^2-sec, $\bar{n}_t = 10$ and $\Delta n_t / n_t \leq 2.2 \, \Delta \tau$ percent where $\Delta \tau$ is the time for 1/2 cycle of the beam sweep. Therefore, for each sweep of the beam, very few trapped electrons will be released before the next sweep and the initial rate of trapped charge build-up will depend upon the instantaneous flux rate rather than the average flux rate.

For the low intensity work at LTV and LRC, one should note the irradiation time required to reach steady-state hence the maximum value of internal electric field. Each irradiation period was typically 10^3 seconds. The use of the charge storage model indicates that steady-state may not be achieved for the low intensity irradiations while the high intensity irradiations may result in a steady-state value early in the irradiation period. This factor could account for the pulsing characteristics observed.

The intensity effect was investigated in some detail at LTV. For a flux rate in excess of 10^{12} e/cm^2-sec discharge pulses on the order of 100 volts were detected. The pulse height observations at various flux rates and energies were approximately the same value for a given sample. However, the pulse rate was strongly influenced by both the flux rate and the irradiation electron energy. The energy dependence is consistent with the work reported in Appendix D and can be interpreted in terms of charge storage resulting from secondary electrons injected from the aluminum electrode into the mylar as well as the stopping of primaries in the mylar. However, in this instance, only a small fraction of the primaries are stopped in the mylar (Ref. 6).

The high intensity effect was investigated in less detail at LRC with the major results being that an intensity effect was noted, however, the pulse height was only the order of 5 volts. This corresponds to liberated charge of 5×10^{-8} coulombs.

When the primary electron flux rate was increased above 10^{12} e/cm^2-sec at LTV, the charge liberated in the discharge event was approximately 10^{-6} coulombs. The steady-state charge in traps should reach approximately 5×10^{-6} coulombs for a thermal electron flux rate of 4×10^{11} e/cm^2-sec in approximately 60 sec irradiation time. The model of Section II indicates that approximately 1/5 the trapped charge density is detected in each discharge event. It is just as likely that the liberated charge is essentially all the charge. The main point is that for the higher flux rates the discharge events result in an appreciable portion of the stored charge being liberated while the lower flux rates yield only a small fraction of the stored charge.

The mechanism which responds to the rate of charge build-up has not been identified. However, the data presented indicates that there are two types of spontaneous discharge. Irregular pulsing with pulse heights the order of a volt or less can be logically interpreted as discharges occurring either due to excessive charge build-up in a localized region or due to the ionization of a localized region where the field strength is less than that for most of the irradiated volume. Full discharge events are those for which most of the space charge is liberated.

Data indicates that the localized discharges are more likely for irradiation flux rates comparable to those expected in the Van Allen belts. Full discharges were only observed at primary electron flux rates in excess of 10^{12} e/cm^2-sec and at energies which correlate more closely with the expected secondary electron processes than with the stopping of primary electrons. For the flux rates employed where charge storage can reach a steady-state condition, excessive charge build-up in a localized region is unlikely if the trap density remains constant with time. In this case, previous results obtained under NASA Contract NAS1-3183 could be related to the discharge mechanism (Ref. 9). It has

been determined that significant gas products result from irradiation of PET. A low field strength could be associated with localized gas concentrations in the PET which lead to a subsequent ionization and a discharge over the volume. The full discharge event could then be interpreted as a critical gas concentration resulting from the high flux rates.

Although excessive charge build-up in localized regions appears unlikely using the model in Section II to infer a steady-state condition, it must be realized that the analytical work is based upon a constant trap distribution with time. Although the model is in reasonable agreement with charge release experiments, there is evidence that suggests the traps may also be radiation induced (see Appendix D). Radiation induced traps could play a predominant role in determining the spontaneous discharge characteristics.

SECTION IV

CONCLUSIONS AND RECOMMENDATIONS

Charge storage in insulating materials is well documented in terms of phenomenological models derived from the kinetics of space charge build-up and decay. During NASA Contract NAS1-3892, charge storage in mylar was observed resulting from irradiation with energetic electrons. A phenomenological model which agreed with the kinetics of the observed space charge decay was developed. Under the present contract, the model has been extended to include space charge build-up, transport of charge during irradiation and the decay of space charge after ceasing irradiation. The observed external charge transfer characteristics indicate that no-retrapping in the space charge region is a fair approximation during the initial decay period. Therefore, the mean range of an electron liberated from a trap is approximately the sample thickness. From Fig. 19, the maximum internal electric field for most cases considered is approximately 6×10^5 volts/cm and the average electric field is 3×10^5 volts/cm for a uniform spatial distribution of charge. This results in a mean range per unit field $(\mu\tau) \sim 2 \times 10^{-9}$ cm^2/volt. It has also been possible to account for the release of charge from traps and the resulting changes in the trapped charge asymmetry. The spatial symmetry of the trapped charge does not strongly influence the external charge transfer during space charge decay. The depth of trap filling and the spatial extent of trapped charge are the major factors in determining the external charge transfer characteristics. The model has been shown to be in reasonable agreement with the experimental observations obtained to date. However, from the results, it has not been possible to determine if the traps are radiation induced or an intrinsic material property. This question can best be answered through an intensive fundamental investigation of radiation effects in mylar. Much of the information pertaining to the radiation chemistry of mylar was obtained under NASA Contract NAS-3183 (Ref. 9).

There has also been evidence obtained from many sources which demonstrates that the charge storage associated with electron irradiation can result in spontaneous discharge events. Data obtained under this contract indicate that the method for obtaining a given flux rate across the irradiated sample can influence the spontaneous discharge characteristics. Considering the results obtained at RTI, LTV and LRC on identical samples, the swept beam irradiations are more likely to result in a spontaneous discharge event. This conclusion is based in part on the results of Section II and the concept of a steady-state space charge distribution for a given flux rate. In addition, data indicate that there are two operative mechanisms associated with spontaneous discharge. Irregular pulse rates and pulse heights the order of a volt or less can be logically interpreted as discharges occurring either due to excessive charge build-up in a localized region or due to the ionization of a localized region where the field strength is less than that for most of the irradiated volume. Full discharge events are those for which most of the space charge is liberated. Data indicate

that the localized discharges are more likely at least for irradiation flux rates comparable to those expected in the Van Allen belts.

From this discussion, it becomes obvious that one should determine whether these phenomena are peculiar to the organic polymers. Present data indicate that inorganics such as SiO, SiO_2 and Al_2O_3 do store charge and in some instances more charge than mylar for a given irradiation condition. However, this space charge does not result in the discharge characteristics noted for mylar and similar polymers. The gas concentration concept introduced in Section III represents a reasonable explanation; however, there is the possibility that the lack of spontaneous discharge for inorganic films is due to a volume effect. Usually, the inorganic films are the order of 1 micron in thickness while mylar is greater than 6 microns.

From the tests conducted at RTI, LTV and LRC, limitations and advantages of the various techniques employed became apparent. The relative stability of the electron flux from the Pm^{147} source was a definite advantage when long irradiation periods were desirable. However, 1/2 mil aluminum is approximately one half thickness for the Pm^{147} source and limits the electrode thickness one can use without appreciably decreasing the flux rate. A source with a maximum energy near 1 Mev would provide more flexibility in the testing program and provide a distribution of electron energies which approximates the Van Allen flux over a wider energy range. In addition, a flux rate approaching 10^{11} e/cm^2-sec would offer a better comparison to the data obtained in the accelerator facilities.

The variation of energy and flux rate available with the particle accelerators can be used to advantage in many instances, however, there are two aspects of this technique which must be examined carefully. The spontaneous discharge characteristics of the capacitor structure have been shown to depend upon the energy of the irradiation electrons. Relating these behavior to that expected in the Van Allen belts in a convincing manner is at best a difficult task. Also, fluctuations of the electron beam can result in ambiguous signal generation. For this latter consideration, the diffused beam technique appears to be superior to the swept beam. This conclusion is based primarily upon the existence of current variations in the external circuit resulting from the stopping of electrons in the electrodes each sweep of the beam.

Solid State Laboratory
  Research Triangle Institute
    Research Triangle Park, North Carolina, August 22, 1966

APPENDIX A

DERIVATION OF TRAPPING AND TRANSPORT EQUATIONS

For distributed traps, the equation describing a small increment Δn_t of the trapped charge is

$$\frac{\partial \Delta n_t}{\partial t} = c_n n (\Delta N_T - \Delta n_t) - s \Delta n_t e^{-E/kT} . \qquad \text{(A-1)}$$

In the general case, c_n and s can both depend upon the trap energy. To obtain an equation for the total density of trapped electrons, the above equation is integrated over the trap energies. If E is measured as positive downward from the conduction band,

$$\frac{\partial}{\partial t} \int_0^\infty \frac{\Delta n_t}{\Delta E} \, dE = n \int_0^\infty c_n \left(\frac{\Delta N_t}{\Delta E} - \frac{\Delta n_t}{\Delta E} \right) dE$$

$$\qquad \text{(A-2)}$$

$$- \int_0^\infty s \frac{\Delta n_t}{\Delta E} e^{-E/kT} \, dE .$$

At any instant of time, the traps below some energy E_{fn} will be essentially all filled while the traps above E_{fn} will be essentially empty. Then, as an approximation,

$$\frac{\Delta N_t}{\Delta E} - \frac{\Delta n_t}{\Delta E} = \begin{cases} \frac{\partial N_t}{\partial E} & 0 \leq E < E_{fn} \\ \\ 0 & E_{fn} < E \end{cases} \qquad \text{(A-3)}$$

$$\frac{\Delta n_t}{\Delta E} = \begin{cases} 0 & 0 \leq E < E_{fn} \\ \\ \frac{\partial N_t}{\partial E} & E_{fn} < E \end{cases} \qquad \text{(A-4)}$$

The above equation then becomes

$$\frac{\partial n_t}{\partial t} = n \int_0^{E_{fn}} c_n \frac{\partial N_t}{\partial E} \, dE - \int_{E_{fn}}^\infty s \frac{\partial N_t}{\partial E} e^{-E/kT} dE , \qquad \text{(A-5)}$$

Appendix A

where

$$n_t = \int_{E_{fn}}^{\infty} \frac{\partial N_t}{\partial E} \, dE \; . \qquad (A-6)$$

To carry the development further requires a specific model for the trap distribution as a function of energy. The distributions of most interest are:

(a) Uniform trap density

$$\frac{\partial N_t}{\partial E} = \frac{B}{kT_c} \qquad (A-7)$$

(b) Exponential trap density

$$\frac{\partial N_t}{\partial E} = \frac{B}{kT_c} \exp(-E/kT_c) \; . \qquad (A-8)$$

B and T_c are constants characterizing the trap distributions. Assuming that c_n and s are independent of energy, the following equations are obtained for the rate of change of trapped electrons:

(a)

$$\frac{\partial n_t}{\partial t} = c_n n \, (N_T - n_t) - sB \, \frac{T}{T_c} \exp \left[- \frac{T_c}{T} \frac{(N_T - n_t)}{B} \right] \, , \qquad (A-9)$$

(b)

$$\frac{\partial n_t}{\partial t} = c_n n \, (N_T - n_t) - sN_T \, (1 + \frac{T_c}{T})^{-1} \, (\frac{n_t}{N_T})^{(1 + \frac{T}{T_c})} \, , \qquad (A-10)$$

where N_T is the total trap density in both cases ($N_T = B$ for the exponential trap case). If c_n and s depend upon energy in the initial equation, then the factors c_n and s in the above equations must be considered as functions of n_t. Since they are probably weakly dependent upon the energy and since the traps are normally filled to only a small

Appendix A

fraction of the total trap density, the use of constant c_n and s is not a severe restriction.

For the purpose of numerically solving the equations, it is convenient to write the equations in terms of normalized variables. For the three cases, the normalized equations are:

(a) Single trap level

$$\frac{\partial \bar{n}_t}{\partial \bar{t}} = \bar{c}_n \, \bar{n} \, (1 - \bar{n}_t) - \bar{n}_t \tag{A-11}$$

$$\frac{\partial \bar{n}}{\partial \bar{t}} = - \frac{\partial \bar{n}_t}{\partial \bar{t}} + \bar{G} + \frac{\partial}{\partial \bar{x}} (\bar{\mu}_n \, \bar{n} \, \bar{F}) \tag{A-12}$$

$$\frac{\partial \bar{F}}{\partial \bar{x}} = - (\bar{n} - \bar{n}_o + \bar{n}_t - \bar{n}_{to}) \, , \tag{A-13}$$

where

$$\bar{n} = \frac{n}{N_T} \qquad\qquad\qquad \bar{n}_o = \frac{n_o}{N_T}$$

$$\bar{n}_t = \frac{n_t}{N_T} \qquad\qquad\qquad \bar{n}_{to} = \frac{n_{to}}{N_T}$$

$$\bar{c}_n = \frac{c_n N_T}{s} \exp(E_t/kT) \qquad\qquad \bar{x} = x/L$$

$$\bar{t} = t \, s \, \exp(-E_t/kT) \qquad\qquad \bar{F} = \frac{\epsilon F}{qLN_T}$$

$$\bar{\mu}_n = \mu_n \frac{1}{s} \frac{qN_t}{\epsilon} \exp(E_t/kT) \qquad\qquad \bar{G} = G \frac{1}{N_T s} \exp(E_t/kT)$$

(b) Uniform trap density

$$\frac{\partial \bar{n}_t}{\partial \bar{t}} = \bar{c}_n \, \bar{n} \, (\bar{N}_T - \bar{n}_t) - \exp(\bar{n}_t) \tag{A-14}$$

$$\frac{\partial \bar{n}}{\partial \bar{t}} = \frac{\partial \bar{n}_t}{\partial \bar{t}} + \bar{G} + \frac{\partial}{\partial \bar{x}} \, (\bar{\mu}_n \, \bar{n} \, \bar{F}) \tag{A-15}$$

$$\frac{\partial \bar{F}}{\partial \bar{x}} = - \, (\bar{n} - \bar{n}_o + \bar{n}_t) \tag{A-16}$$

where

$$\bar{n} = \frac{T_c n}{TB} \qquad\qquad\qquad \bar{n}_o = \frac{T_c n_o}{TB}$$

$$\bar{n}_t = \frac{T_c (n_t - n_{to})}{TB} \qquad\qquad \bar{N}_T = \frac{T_c (N_T - n_{to})}{TB}$$

$$\bar{c}_n = c_n \frac{1}{s} \left(\frac{TB}{T_c}\right) \exp \, (\bar{N}_T) \qquad\qquad \bar{F} = \frac{\epsilon T_c F}{qLBT}$$

$$\bar{t} = s \, \exp \, (-\bar{N}_T) \, t \qquad\qquad\qquad \bar{x} = x/L$$

$$\bar{\mu}_n = \mu_n \frac{1}{s} \frac{qBT}{\epsilon T_c} \exp \, (\bar{N}_T) \qquad\qquad \bar{G} = \frac{T_c}{TBS} \exp \, (\bar{N}_T) \, G$$

(c) Exponential trap density

$$\frac{\partial \bar{n}_t}{\partial \bar{t}} = \bar{c}_n \, \bar{n} \, (1 - \bar{n}_t) - (\bar{n}_t)^m \tag{A-17}$$

$$\frac{\partial \bar{n}}{\partial \bar{t}} = -\frac{\partial \bar{n}_t}{\partial \bar{t}} + \bar{G} + \frac{\partial}{\partial \bar{x}} (\bar{\mu}_n \, \bar{n} \, \bar{F}) \qquad \text{(A-18)}$$

$$\frac{\partial \bar{F}}{\partial \bar{x}} = -(\bar{n} - \bar{n}_o + \bar{n}_t - \bar{n}_{to}) \qquad \text{(A-19)}$$

where

$$\bar{n} = \frac{n}{N_T} \qquad\qquad\qquad \bar{n}_o = \frac{n_o}{N_T}$$

$$\bar{n}_t = \frac{n_t}{N_T} \qquad\qquad\qquad \bar{n}_{to} = \frac{n_{to}}{N_T}$$

$$\bar{c}_n = c_n \frac{N_T m}{s} \qquad\qquad\qquad m = (1 + \frac{T_c}{T})$$

$$\bar{t} = \frac{s}{m} t \qquad\qquad\qquad \bar{F} = \frac{\epsilon}{qLN_T} F$$

$$\bar{\mu}_n = \mu_n \frac{mqNt}{s\epsilon} \qquad\qquad\qquad \bar{x} = x/L$$

$$\bar{G} = \frac{m}{N_T s} G$$

71

APPENDIX B

DISCUSSION OF COMPUTER SOLUTIONS

This appendix discusses some of the techniques used and difficulties encountered in the computer solutions for $\bar{n}$ and $\bar{n}_t$. The equations which were solved are

$$\frac{\partial \bar{n}_t}{\partial t} = \bar{c}_n \bar{n} (\bar{N}_T - \bar{n}_t) - \exp (\bar{n}_t) , \qquad \text{(B-1)}$$

$$\bar{\mu}_n \bar{F} \frac{\partial \bar{n}}{\partial \bar{x}} - [\bar{\mu}_n \bar{n}_t + \bar{c}_n (\bar{N}_T - \bar{n}_t)]\bar{n} + \bar{G} + \exp (\bar{n}_t) = 0 , \qquad \text{(B-2)}$$

$$\frac{\partial \bar{F}}{\partial \bar{x}} = - \bar{n}_t ; \int_o^1 \bar{F} d\bar{x} = 0 . \qquad \text{(B-3)}$$

It is assumed that $\bar{n}_t \gg \bar{n}$.

To obtain solutions for these equations, a boundary condition on $\bar{n}$ is required. This can be obtained from Eq. (B-2) by noting that if $\partial \bar{n}/\partial \bar{x}$ is to remain finite at the zero field point (i.e., at $\bar{F} = 0$), the electron concentration at the zero field point must be given by

$$\bar{n}\Big|_{\bar{x}_o} = \frac{\bar{G} + \exp (\bar{n}_t)}{\bar{\mu}_n \bar{n}_t + \bar{c}_n (\bar{N}_T - \bar{n}_t)}\Bigg|_{\bar{x}_o} . \qquad \text{(B-4)}$$

The zero field point $\bar{x}_o$ is the value of $\bar{x}$ which satisfies the equation

$$\int_o^1 (\int_{\bar{x}_o}^{\bar{x}} \bar{n}_t d\bar{x}') d\bar{x} = 0 , \qquad \text{(B-5)}$$

or it is the point at which $\bar{F} = 0$. Since $\bar{n}_t \geq 0$, it is obvious that $0 \leq \bar{x}_o \leq 1$. For given $\bar{n}_t$, the numerical solution of Eqs. (B-2) and (B-3) for $\bar{n}$ with the boundary conditions as expressed by Eqs. (B-4) and (B-5) is fairly straightforward. The only difficulty is in evaluating $\partial \bar{n}/\partial \bar{x}$ from Eq. (B-2) near $\bar{x}_o$ because of the singularity at $\bar{x}_o$. This is overcome by taking a derivative of Eq. (B-2) from which it is found that

Appendix B

$$\left. \frac{\partial \bar{n}}{\partial \bar{x}} \right|_{\bar{x}_o} = \left[\frac{\exp (\bar{n}_t) - \bar{n} (\bar{\mu}_n - \bar{c}_n)}{2\bar{\mu}_n \bar{n}_t + \bar{c}_n (\bar{N}_T - \bar{n}_t)} \frac{\partial \bar{n}_t}{\partial \bar{x}} \right]_{\bar{x}_o} . \qquad (B-6)$$

This equation was used to evaluate $\bar{n}$ near $\bar{x}_o$.

The only difficulty encountered in the numerical solution of Eq. (B-1) for $\bar{n}_t$ is the large time interval over which the solution must be carried. This can be seen by considering only charge release (i.e., by setting $\bar{n} = 0$) which shows that $\bar{n}_t \propto - \ln \bar{t}$. The solution must then be carried over many orders of magnitude in time. For typical solutions about four orders of magnitude in time are required. This problem was handled by taking longer time intervals as the solution progressed. The time intervals were chosen to give equally spaced values on a $\ln \bar{t}$ scale with either ten or twenty points taken per order of magnitude in time.

The integrations on both $\bar{x}$ and $\bar{t}$ were done by a predictor-corrector method with the solutions iterated until consistent values were obtained at each value of $\bar{x}$ and $\bar{t}$.

APPENDIX C

DISCUSSION OF PARAMETERS USED IN
THE TRAPPING AND TRANSPORT MODEL

In Section II, a dynamic model for build-up and decay of irradiation induced space charge is introduced. The basic equations depend upon a combination of parameters which must be determined before quantitative aspects of the model can be pursued. Initially, these parameters were estimated either from the results of NASA Contract NAS1-3892 or from the literature.

The initial estimate of these parameters was obtained using:

(a) the attempt to escape frequency from the work of Fowler (Ref. 10) ($s \sim 9 \times 10^{10}$ sec^{-1}),

(b) the dielectric constant ϵ was determined by capacitance measurements at 1 kc for 1/4 mil mylar to $\pm$ 20 percent accuracy ($\epsilon \sim 3\epsilon_o = 2.65 \times 10^{-13}$);

(c) the trap density per unit energy for the uniformly distributed trap model (B/kTc) was inferred as a minimum value under NASA Contract NAS1-3892 (B/kTc $\geq 1.7 \times 10^{16}$ cm^{-3} ev^{-1}), and from the same works, a value of $N_T > 1.53 \times 10^{16}$/cm^3 was obtained (Ref. 1),

(d) the mobility was unknown, however, Fowler (Ref. 10) used a value of 10^{-3} cm^2/v-sec. Preliminary investigations of the photo response of PET indicated that the mobility was of the order of 0.1 cm^2/v-sec

(e) the free carrier concentration n_o was estimated from dark conductivity measurements to be discussed at a later point in this appendix ($n_o \sim 7.9 \times 10^2$ cm^{-3}).

With the values given above, $\bar{c}_n \bar{N}_T / \bar{\mu}_n = 1.7$ was calculated. This was the principal value used throughout the computer computations. However, a number of solutions for the model in Section II were obtained for $\bar{c}_n \bar{N}_T / \bar{\mu}_n = 0.17$ and $\bar{c}_n \bar{N}_T / \bar{\mu}_n = 17$. These results can be interpreted in terms of a mobility change for the problem. Therefore, solutions have been obtained for mobilities of 1, 0.1 and 0.01 cm^2/v-sec.

During the course of the contract, the parameters listed above for PET have been investigated by various methods. In addition, pertinent data have appeared in the recent literature. Using Eq. (C-1) and estimating the free carrier concentration from dark conductivity measurements the combination of parameters reduces to

Appendix C

$$\frac{\bar{c}_n \tilde{N}_T}{\bar{\mu}_n} = \rho \epsilon s \exp\left(-E_{fo}/kT\right) . \qquad \text{(C-1)}$$

The dielectric constant has been measured by Lengyel (Ref. 11) for
1.1 mil PET yielding a value of 3.4. In addition, PET samples with
aluminum electrodes were shown to display the Schottky type voltage-
current-temperature characteristic. The barrier height was 0.88 ev
as compared to the 0.87 ev obtained under NASA Contract NAS1-3892
(Ref. 1). A value for volume resistivity of 10^{18} ohm-cm has been
reported for PET (Ref. 12). Volume resistivity for dielectric films
in this range is difficult to obtain in a straightforward manner.
Using dark conductivity measurements to obtain a value for resistivity
requires ohmic contacts. In an attempt to obtain ohmic contacts to
PET, an electrolytic cell depicted in Fig. C-1 was employed with 0.1
mole NaCl solution in contact with the PET film. The results for
several measurements are shown in Fig. C-2. If one interprets these
results in a manner similar to the space charge limit current model
by Rose (Ref. 13) the near linear characteristic in the low voltage
region can be used to obtain an estimate of the resistivity. Using
the current-voltage data at 50 volts for 1/4 mil thick PET with elec-
trode areas of 1.25 cm^2, a value of 10^{17} ohm-cm is obtained. When
the full spectrum of the H_g lamp illuminates the PET through the NaCl
electrodes steady-state current increases. If the space charge limited
current model applies, this increase from the absorption of the light
near the illuminated surface can be interpreted as the creation of a
source of electrons within the PET which behaves as a contact. This
effectively reduces the thickness of PET. Unfortunately, there is
another interpretation which cannot be overlooked. The increase in
current can be due to a reduction of a barrier between the PET and the
electrodes.

The space charge limited model proposed by Rose for uniformly
distributed traps is of the form (Ref. 13)

$$J = c_1 V e^{\gamma V} . \qquad \text{(C-2)}$$

The value of γ is related to the trap density per unit energy, where

$$\frac{B}{kT_c} = \frac{\epsilon}{qkT\gamma L^2} = 4.53 \times 10^{16} \ cm^{-3} ev^{-1} . \qquad \text{(C-3)}$$

This result compares favorably with the minimum value of $1.7 \times 10^{16} cm^{-3} ev^{-1}$
obtained under NASA Contract NAS1-3892 (Ref. 1). This result lends support
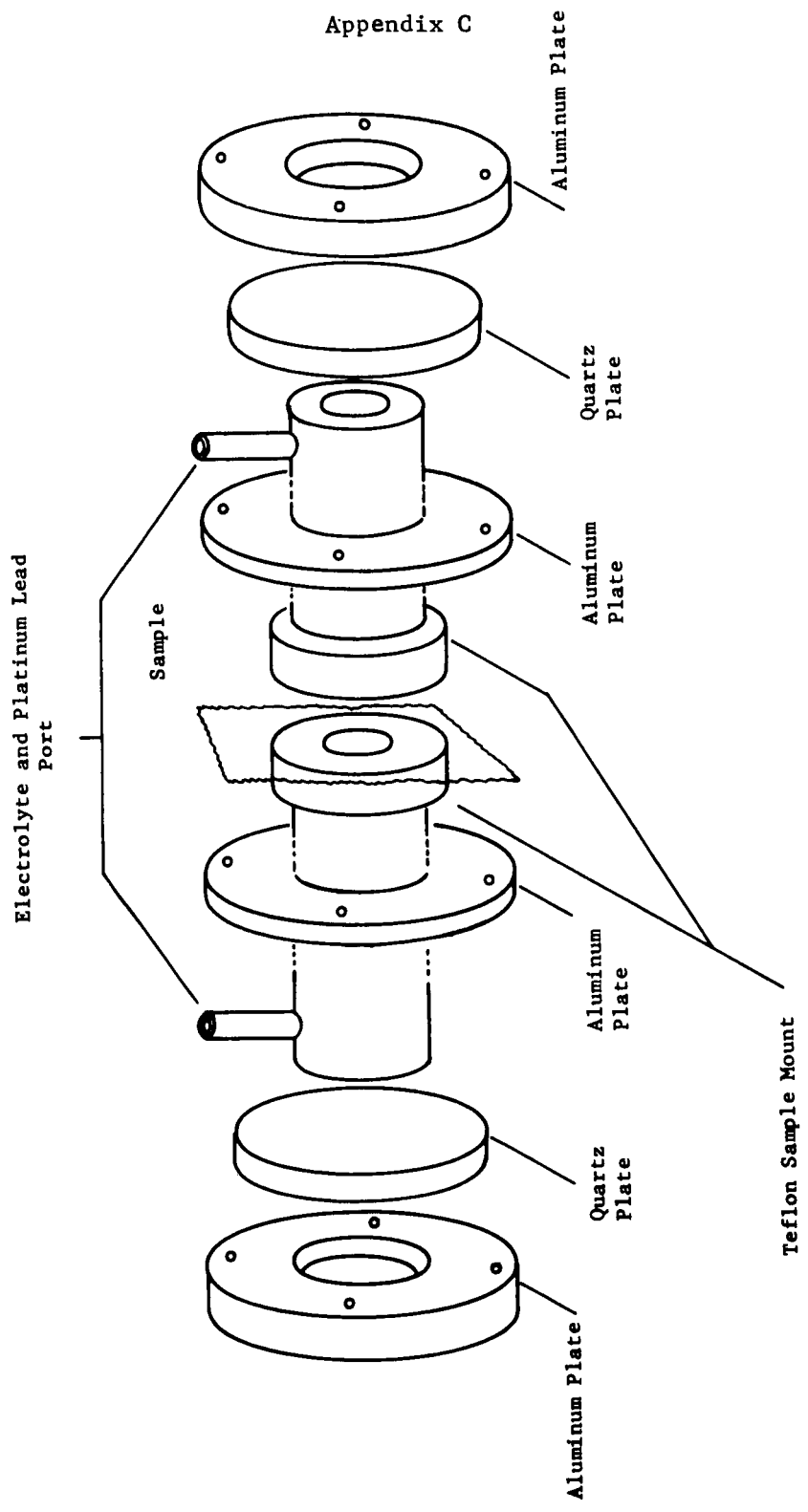
Figure C-1. Conductivity cell.

$$J = C_1 V e^{\gamma V}$$
$$C_1 = 2.9 \times 10^{-14}$$
$$\gamma = 3.6 \times 10^{-3}$$

$$J = C_1 V e^{\gamma V}$$
$$C_1 = 4.56 \times 10^{-14}$$
$$\gamma = 6.34 \times 10^{-3}$$

O □ Sample A

X Sample B

▲ Sample B illuminate
   $\lambda = 3000$ Å

1/4 Mil Mylar

Dupont Type C

NaCl Electrodes 0.1 Mole

CURRENT

Applied Voltage
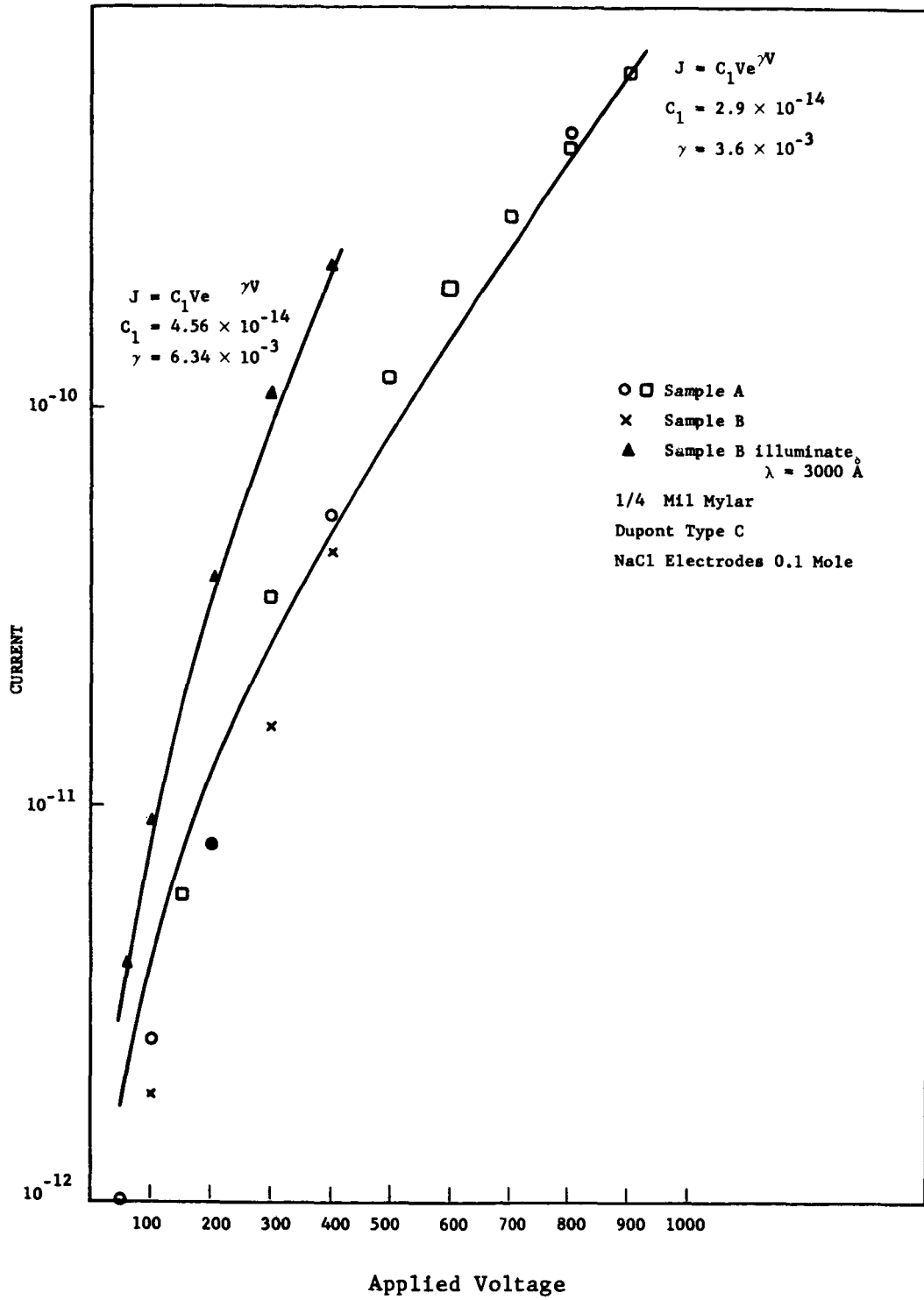
Figure C-2. Current-voltage characteristics for 1/4 mil mylar obtained using the electrolytic conductivity cell.

to the interpretation of the data using the space charge limited current model. However, it is recognized that the value for the volume resistivity of 10^{17} ohm-cm is tentative until more conclusive experimental data is obtained.

Using the more recent values of the parameters in Eq. (C-1) yields $\bar{c}_n \bar{N}_T / \bar{\mu}_n = 5.6$.

Solutions for the model in Section II have been obtained such that the predicted behavior for build-up and decay of irradiation induced space charge for a range of values of these parameters which are characteristic of PET can be compared to the experimental results.

APPENDIX D

PREVIOUS WORK RELATED TO

SPACE CHARGE EFFECTS IN MYLAR

The following work has been reported elsewhere (Ref. 14), however, the experimental techniques and the simplified model are pertinent to the material presented in this report.

EXPERIMENTAL TECHNIQUE

A heated tungsten filament was used as the electron source. The electrons were accelerated through a potential supplied by a regulated dc supply. The power supply ripple was less than 0.5 percent RMS with an output voltage resolution of 2 percent. Pressure in the working chamber measured at the diffusion pump port was maintained below 10^{-5} torr during all irradiations.

The samples were mounted on the fixture shown in Fig. D-1. The films were held in place by magnets. The irradiated electrode made electrical contact with the steel plate which was system ground and the contact to the back electrode was provided by the magnet which was in electrical contact through bare copper wire with a vacuum feed-through in the mounting plate. The aluminum front plate provided a shield against the electrons outside the irradiation area and specifically at the sample edges while the lead provided attenuation by any bremstrahlung created in the aluminum.

The beam current was measured by rotating a shutter so the electron beam was striking the aluminum portion of the shutter and by passing the collected electrons through a meter to the high voltage power supply. In the energy range from 10 kev to 50 kev, backscattered electrons are approximately 15 percent of the primary beam current (Ref. 15). The secondary yield is approximately the same value (Ref. 8). Therefore, the current measured by this technique can be in error as much as 30 percent with respect to the current actually striking the shutter. When the shutter was removed, the electron beam was incident on the aluminum electrode of the test sample. The secondary electrons from the irradiated surface will be approximately the same as for the shutter, however, the backscattered electrons will depend upon the thickness of the aluminum electrode (Ref. 16). The backscattering coefficient is smaller for aluminum films of interest, approximately 1000 Å thick, than for bulk aluminum. Therefore, the number of primary electrons which were able to provide secondary electrons at the aluminum-polyethylene terephthalate boundary or which were able to penetrate into the polyethylene terephthalate was larger than the value measured by the shutter current. The error involved was estimated to be approximately 20 percent.

The irradiated samples were prepared from commercially available polyethylene terephthalate. Films 6.3×10^{-4} cm thick and 5 cm in
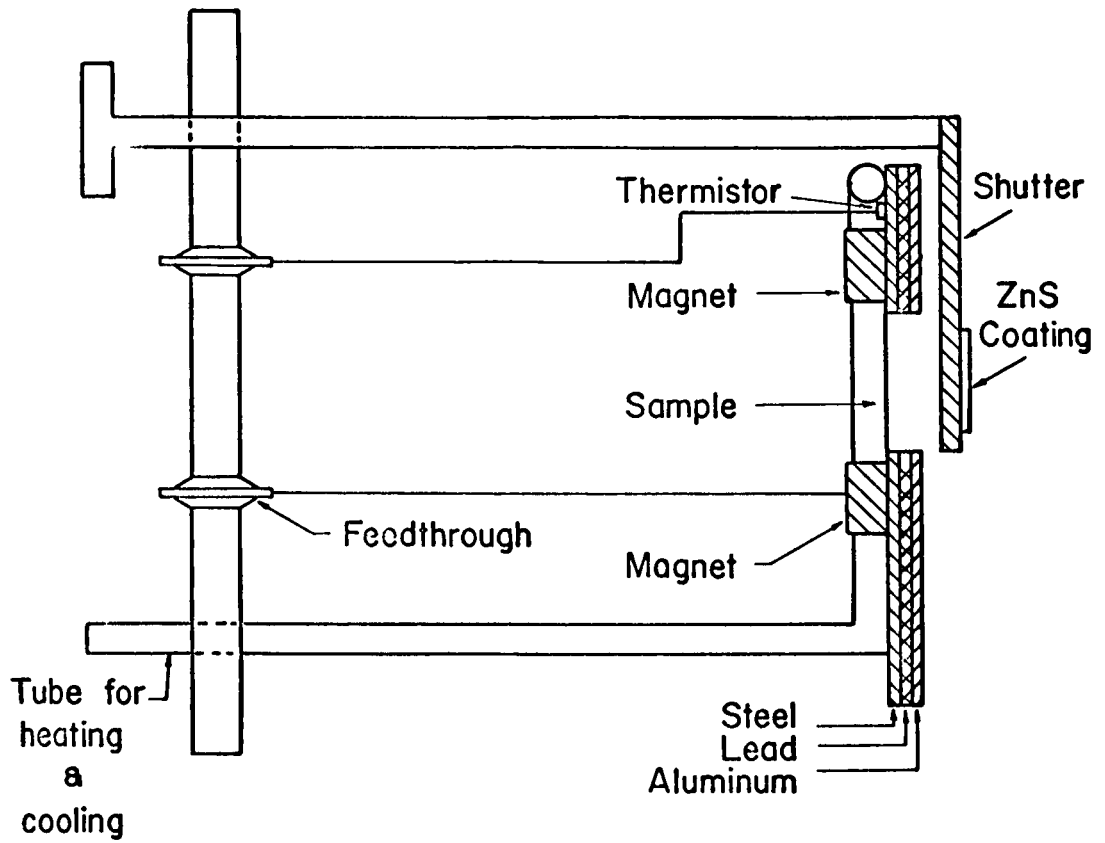
Figure D-1. Fixture for mounting sample in electron gun assembly.

diameter were cleaned twice in a detergent solution and rinsed after each wash in deionized water. Following a wash in hydrofluoric acid, and a deionized water rinse, the films were stored in methanol prior to electrode evaporation. After placing the films in the evaporator, and outgassing for approximately 30 minutes, aluminum electrodes were evaporated to the desired thickness. Simultaneously, the aluminum was evaporated onto the quartz crystal of a crystal controlled oscillator. The resulting frequency change of the oscillator was used to obtain an estimate of the evaporated aluminum thickness. Using the crystal monitoring technique, the uncertainty in electrode thickness has been estimated to be $\pm$ 250° A.

After evaporating the electrodes, the capacitance and dissipation factor of the samples were measured at 1 kc with typical values of 6 nanofarads and 0.005, respectively. The dc leakage resistance was measured and values at least an order of magnitude greater than the resistance of the external circuit were acceptable.

Asymmetrical decay of the trapped electrons resulted in a transfer of charge through an external circuit (Ref. 17). The circuit used to detect this charge was an RC network which integrates the current in the external circuit with a time constant of 10^5 seconds. The voltage across the capacitor was measured by an electrometer whose input resistance of 10^{11} ohms was a portion of the RC integrator. The output of the electrometer was fed into a strip-chart recorder. The minimum voltage across the integrator capacitor which could be measured was 1 millivolt.

After placing the sample in the irradiation chamber, an electron beam with a current density of 5×10^{-8} amperes/cm^2 was focused on the shutter. The shutter was then opened for the desired irradiation time. The energy of the electrons for each irradiation was in the range from 10 kev to 20 kev. Upon terminating the irradiation, the electrodes of the sample were shorted for a period of one minute. This allowed any transients due to turning off the electron beam to decay and provided ample time to connect the measuring circuit across the sample. Due to the high impedance levels encountered in the measurement, it was impractical to achieve the transition from the electron beam measurement to the trapped charge decay measurement with a switching device.

EXPERIMENTAL RESULTS

The trapped charge decay was observed from 60 seconds to approximately 2400 seconds after turning off the electron beam. The transfer of external charge as a function of time under these conditions is shown in Fig. D-2 for a typical sample. For integration times approaching 10^4 seconds, the error due to leakage through the RC integrator was
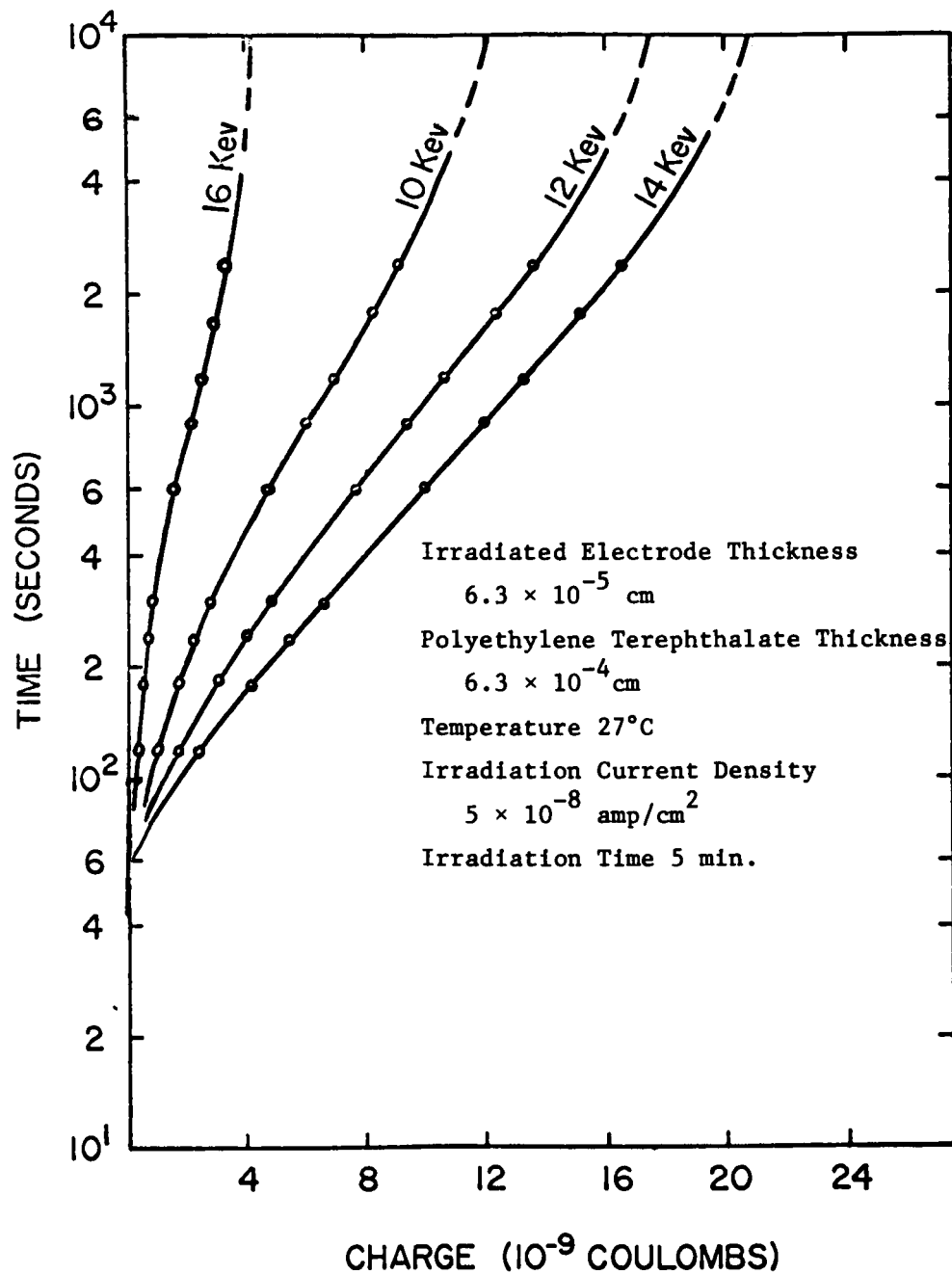
Figure D-2.   External charge transfer from thermal release of trapped
irradiation electrons for the indicated primary electron
energies.

comparable to the rate of external charge transfer. The dotted portion
of the curves drawn through the data represents estimates of the external
charge transfer which have been corrected for the error introduced by the
integrator. From this data, one aspect of the external charge transfer
is quite obvious. Using range-energy data for water (Ref. 18) which is
approximately the same as that for polyethylene terephthalate one readily
finds the range of the primary electrons at the energy which yields the
maximum external charge transfer is approximately one-half the thickness
of the polyethylene terephthalate film. Also, the energy at which the
external charge transfer is reduced below the sensitivity of the measure-
ment corresponds to a practical range approximately equal to the film
thickness.

For the latter observation, one may conclude that within the sensi-
tivity of the measurement, the trapped-charge decay is symmetrical.
The simplest trapped charge distribution which could yield such a result
is one that is uniform throughout the irradiated volume. Obviously, there
are other distributions which could yield a symmetrical decay; however,
when one considers the transmission of electrons in this energy range
through the comparable thicknesses of other materials, the linear decrease
in the number of transmitted electrons with depth appears to be a
reasonable assumption (Ref. 19). In general, one finds a somewhat less
than linear decrease near the irradiated surface. The possibility of
secondaries from the electrode being injected into the polyethylene
terephthalate could increase the number of electrons trapped near the
irradiated surface such that the overall distribution is more uniform
than one might expect based upon the transmission of primary electrons
alone.

The contribution of secondary electrons from the irradiated electrode
to the net charge distribution in the polyethylene terephthalate film was
further identified by the results shown in Fig. D-3. A sample was pre-
pared in the usual manner with 500 Å electrodes and irradiated with 16 kev
electrons. The beam current density was 5×10^{-8} amperes/cm^2. After ob-
serving the trapped charge decay, the irradiated electrode thickness was 1000 Å
2000 Å, 5000 Å, 7000 Å, and 10,000 Å and the sample irradiated with 16 kev
electrons and a beam current density of 5×10^{-8} amperes/cm^2 at each
thickness. The measurement was repeated at each thickness and the repro-
ducibility was well within the sensitivity of the measuring technique.
The results indicate that while the number of primaries entering the
polyethylene terephthalate decreased due to the increased aluminum
electrode thickness, the transfer of external charge initially increased
and subsequently decreased with increasing electrode thickness. This
initial increase can be explained in terms of the secondary yield from
the exit side of the irradiated aluminum electrode. Secondary yield has
been correlated with the energy dissipation density at the exit surface
(Ref. 8). For electrons in the energy range of interest, the energy
dissipation function in aluminum has a maximum at approximately one-fourth
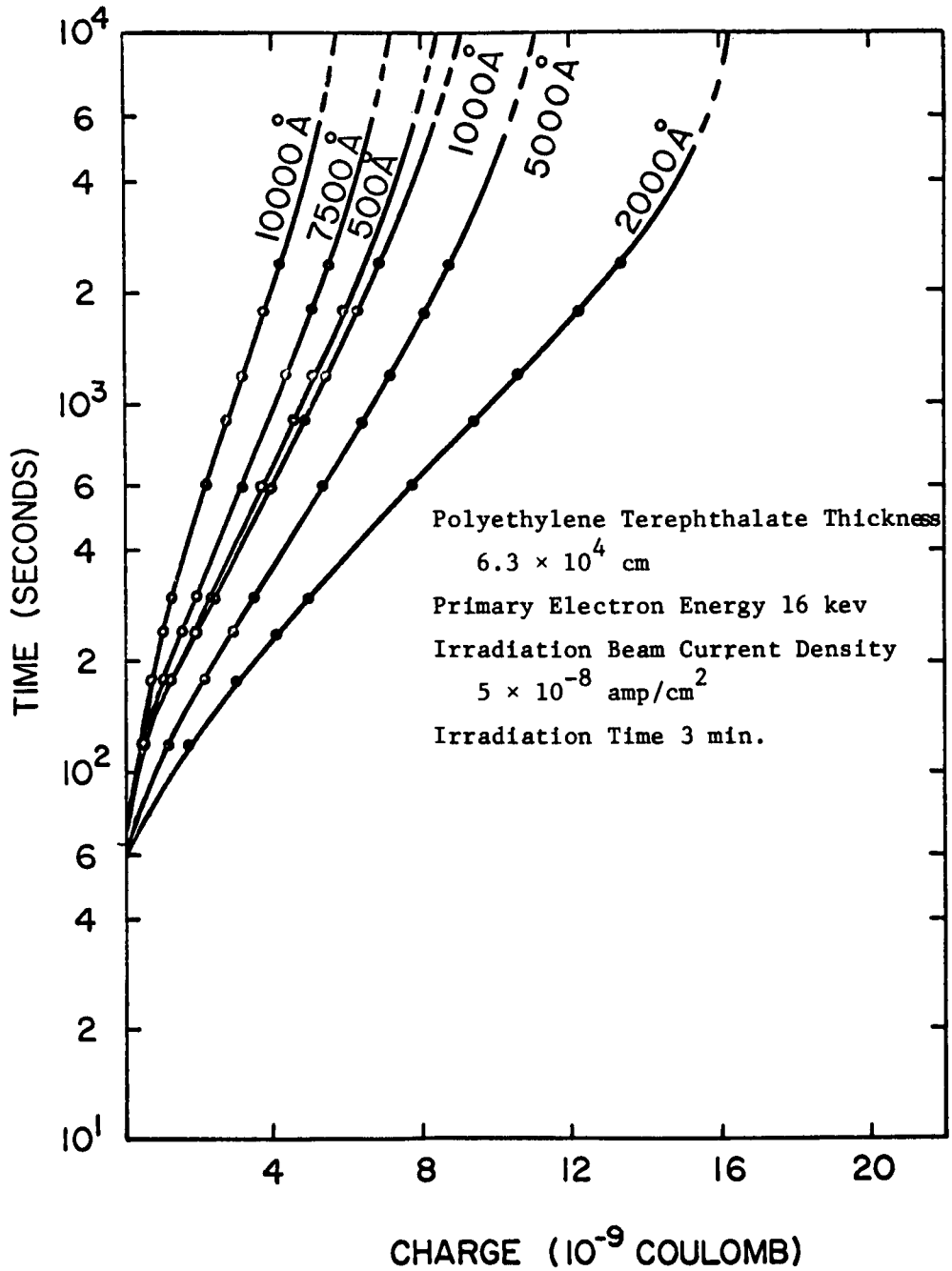the practical range of primary electron (Ref. 20). For a 16 kev electron

Figure D-3. External charge transfer as a function of time for irradiated aluminum electrode thickness indicated.

Polyethylene Terephthalate Thickness
6.3×10^4 cm

Primary Electron Energy 16 kev

Irradiation Beam Current Density
5×10^{-8} amp/cm^2

Irradiation Time 3 min.

Appendix D

in aluminum, this maximum occurs at approximately 7000 Å. The increased
secondary yield is at the expense of the number of primary electrons
transmitted through the aluminum electrode; therefore, the electrode
thickness which will yield the maximum number of electrons injected into
the polyethylene terephthalate will be less than or equal to 7000 Å de-
pending upon the rate of increase in the number of secondaries and the
rate of decrease of the number of primaries with increasing electrode
thickness. Other factors which can affect the net charge distribution
are the secondary electron yield from the irradiated polyethylene
terephthalate and the diffused energy spectra of the electron beam
transmitted through the electrode. These effects would decrease the
external charge transfer with increasing electrode thickness. Therefore,
the results of Fig. D-3 are consistent with the expected behavior when
one considers the net charge in the polyethylene terephthalate due to
primary and secondary electrons.

The dependence of the external charge transfer on the energy of
the primary electron in Fig. D-2 can be interpreted in terms of the
practical range corresponding to the various energies and the change
in the number of primary and secondary electrons injected into the
polyethylene terephthalate. To indicate this dependency, consider
the net charge distribution to be uniform from the irradiated surface
to the practical range. Furthermore, for primary electron energies less
than the energy corresponding to the maximum transfer of external charge,
assume that all the electrons thermally released from traps arrive at
the irradiated electrode without being retrapped. Since all the surface
charge on the unirradiated electrode must be transferred through the
external circuit, the limiting value of the external charge is

$$Q_{ext} = qA \, n_t \frac{r^2}{2\ell} \qquad (D-1)$$

where A is the irradiated area, r is the practical range of the primary
electrons, ℓ is the thickness of the polyethylene film and n_t is the
electrons per cm^3 in traps. Since the trapped electron distribution
extends through approximately one-half the thickness of the polyethylene
terephthalate for the maximum external charge transfer, some of the
thermally released electrons should reach the unirradiated electrode.
Therefore, Eq. (D-1) will only provide an estimate of the minimum value
of trapped charge for the uniform distribution. Using Eq. (D-1), the
minimum value for the total space charge for the 10, 12, and 14 kev
irradiations is approximately 7.5×10^{-8} coulomb. The irradiation ·
charge for each run was 1.5×10^{-5} coulomb.

External charge transfer during the thermal release of trapped
electrons was investigated at 14 kev using irradiation times from 30
seconds to 30 minutes at a fixed beam current of 5×10^{-8} amperes/cm^2.

85

Appendix D

The results are shown in Fig. D-4. The salient feature of these results is that $Q_{ext}(t) \alpha \log_e t$ for some portion of each measurement. The time interval over which the relationship holds increases as the irradiation time is increased. One can attempt to explain these observations by (1) asymmetry changes in the charge distribution, (2) the release of electrons from traps or (3) a combination of trap release and asymmetry changes.

For a distribution of trapped electrons which varies with distance through the media and is uniform over the irradiated area, a one dimensional solution of Poisson's equation

$$\frac{\partial E(x,t)}{\partial x} = -\frac{q}{\epsilon} \bar{n}(x,t) \qquad (D-2)$$

describes the electrical field within the material where $\bar{n}(x,t)$ is the excess charge concentration. For a thickness ℓ and the electrodes grounded, the zero field point x* can be determined for a given distribution $\bar{n}(x,t)$ by

$$\int_{o}^{\ell} \int_{x^*(t)}^{x} \bar{n}(\tilde{x},t) d\tilde{x} dx = 0 \ . \qquad (D-3)$$

The surface charge density at the electrode can be expressed as

$$\sigma(x',t) = D(x',t) = -\epsilon E(x',t) = -q \int_{x^*(t)}^{x'} \bar{n}(x,t) dx \qquad (D-4)$$

where the upper limit corresponds to the electrode of interest. As the space charge decays, a change in surface charge can result in a charge transfer through the external circuit. If the space charge on both sides of the zero-field point decays symmetrically in time, there will be no external transfer of charge between the electrodes. However, if the decay results in net charge pairs on the electrodes, external charge transfer will occur and can be expressed in terms of the moving zero-field point. The transfer of external charge can be expressed as (Ref. 17)

$$dQ_{ext}(t) = qA\bar{n}(x^*,t) dx^* \ . \qquad (D-5)$$

The difficulty in applying Eq. (D-5) involves the distribution $\bar{n}(x^*,t)$.

The release of electrons from traps can result in an external charge transfer which has the time dependence shown in Fig. D-4. For
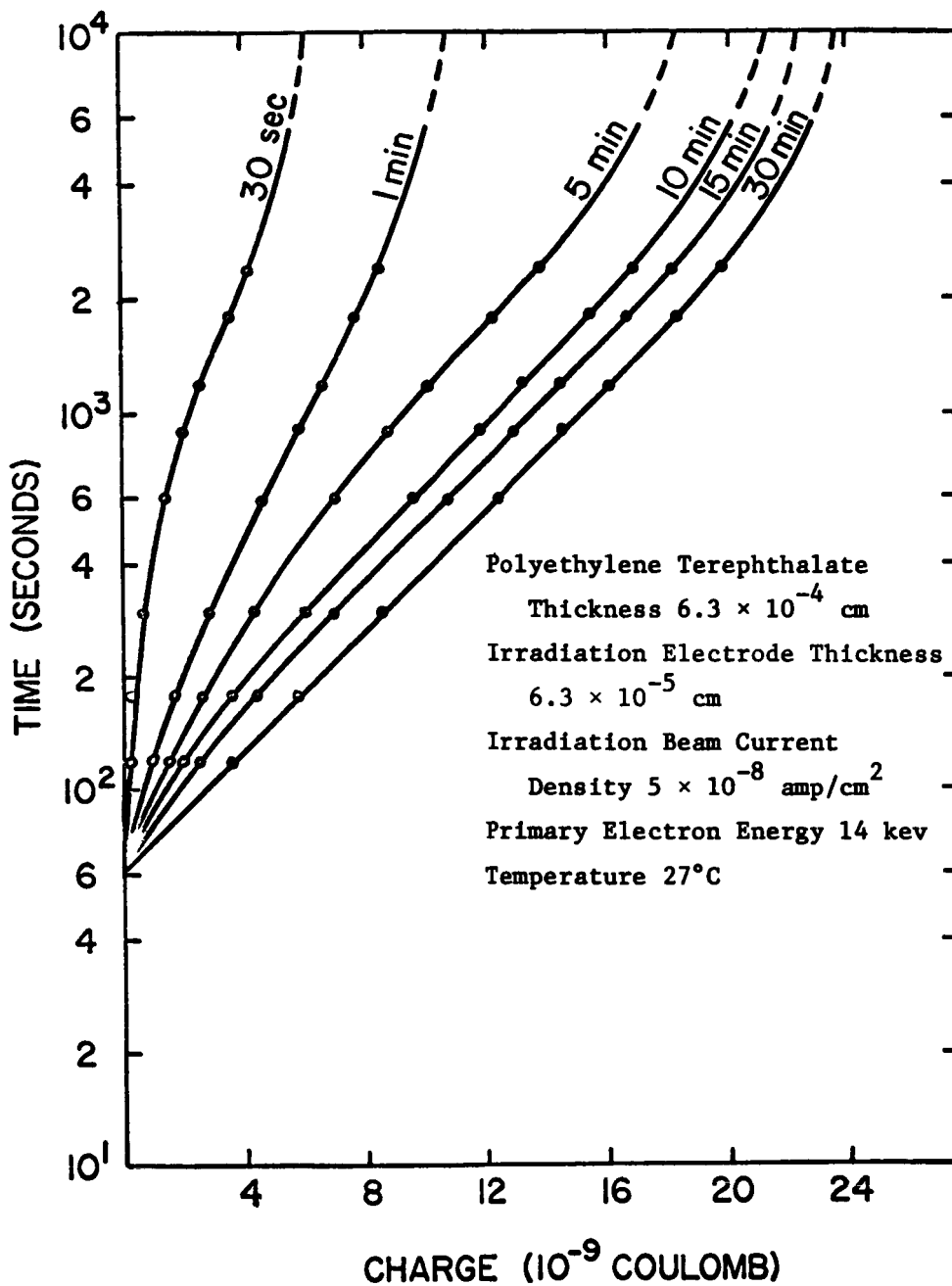
Figure D-4. External charge transfer as a function of time for the indicated irradiation period.

trapping sites which are distributed in energy such that a continuous function can be used to denote the number per cm^3 per electron volt below the conduction levels, it has been shown that the total charge in traps will decay at a rate which is inversely proportional to the elapsed time if one excludes very short and very long times (Refs. 17 and 21). This assumes that retrapping is a second order effect during space charge decay. If the time dependence of external charge transfer is to be the same as that for the trapped electron distribution, the space charge symmetry during decay must respond such that

$$n_t(x, t) \propto \int \bar{n}(x^*, t) dx^* . \qquad \text{(D-6)}$$

However, one cannot readily justify an assumption based upon Eq. (D-6) that will apply during the entire space charge decay.

The model for space charge decay can be extended to include the movement of the zero field point as the space charge redistributes. Assuming that the initial distribution of trapped electrons is uniformly distributed from the irradiated electrode to the practical range of the primary electrons, the space charge decay can be represented to a first approximation as shown in Fig. D-5. In the space charge region where the trapped electron concentration predominates in Eq. (D-2), the change in the free electron concentration is determined by the drift of free carriers as well as the emptying and retrapping of the electrons. If the charge in traps is much greater than the free carrier concentration and the rate of trap emptying is much greater than the rate of retrapping, the net charge distribution will remain essentially independent of distance during space charge decay.

In the region beyond the practical range, the electric field is initially constant and the transport of electrons depends upon the excess carrier concentration. The space charge redistribution in this region will occur through the thermal release of electrons in the space charge region between the zero field point and the practical range and retrapping beyond the practical range. If the rate of trapping is much greater than the rate of emptying for deep traps in the region where the electric field is essentially constant, the space charge redistribution will be primarily trap controlled. The space charge is not expected to redistribute with the abrupt front. However, the present analysis will assume that the trapping occurs such that the space charge distribution is independent of distance in this region throughout space charge decay. This is a good approximation if the mean distance traveled by the thermally released electrons is small compared to the extent of the space charge region. If all the thermally released electrons in the region between the zero field point x^* and the extent of the space charge region r are retrapped within $\triangle r$ one obtains

$$\frac{d\bar{n}(x^*)}{dr} = - \frac{\bar{n}(x^*)}{r - x^*} . \qquad \text{(D-7)}$$
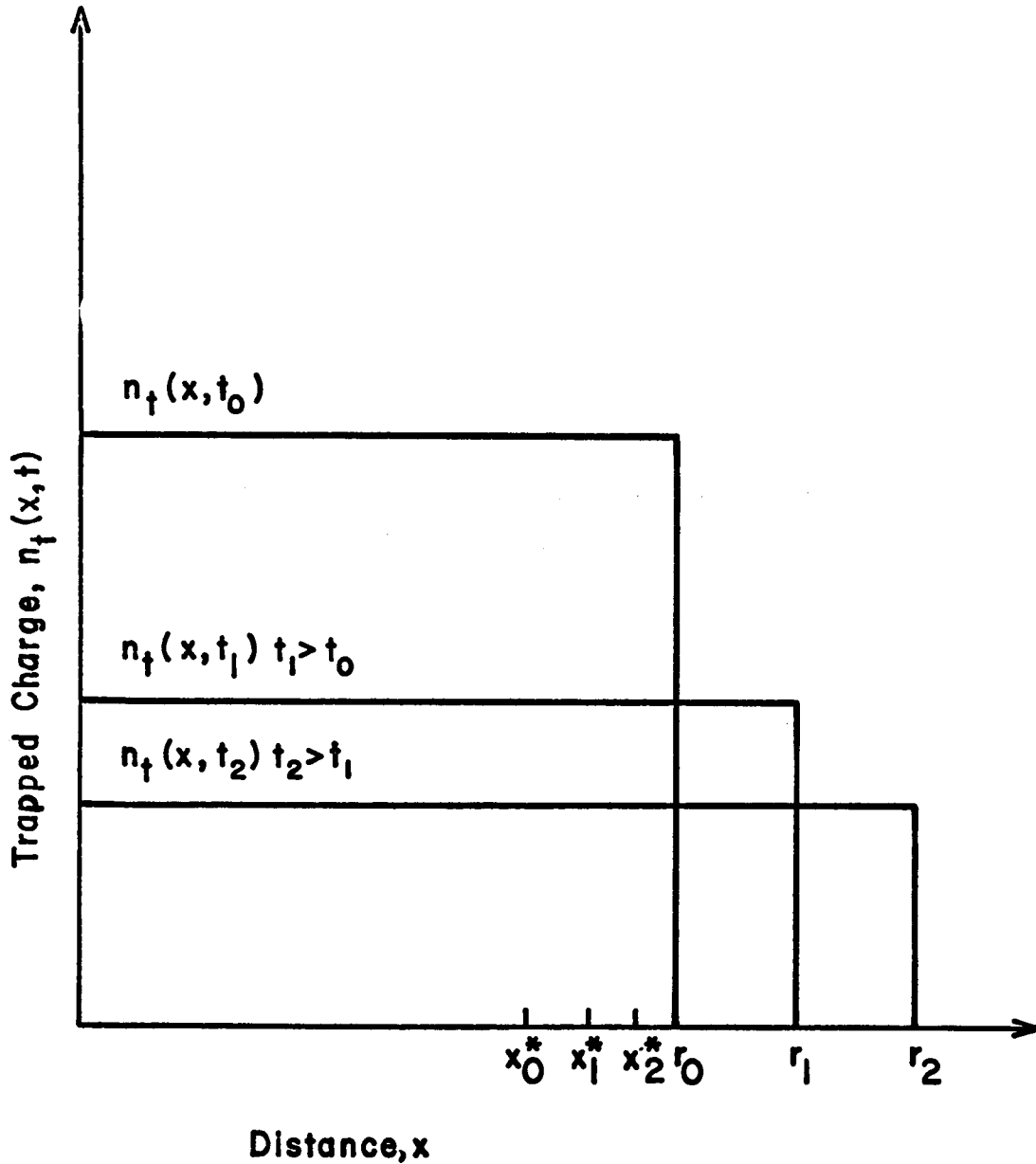
Figure D-5.   The assumed trapped charge distribution during the initial
space charge decay.

Appendix D

Integration of Eq. (D-3) relates the zero field point to the extent of the space charge region and

$$x^* = r - \frac{r^2}{2\ell} \qquad \text{(D-8)}$$

Combining Eqs. (D-7) and (D-8) results in the expression

$$\frac{d\bar{n}(x^*)}{dx^*} = - \frac{\bar{n}(x^*)}{\ell} \left[\frac{2x^*}{\ell} + \left(1 - \frac{x^*}{\ell}\right)\left(1 - \frac{2x^*}{\ell}\right)^{1/2} - 1 \right]^{-1} . \text{(D-9)}$$

The expression in brackets represents the way in which the movement of the zero field point affects the kinetics and magnitude of the external charge transfer. The magnitude of this expression for zero field points of interest is shown in Fig. D-6. Introducing Eq. (D-9) in Eq. (D-5) one obtains

$$dQ_{ext}(t) = - qA \ell \; f(\frac{x^*}{\ell}) \, d\bar{n}(x^*)$$

where

$$f\left(\frac{x^*}{\ell}\right) = \left[\frac{2x^*}{\ell} + \left(1 - \frac{x^*}{\ell}\right)\left(1 - \frac{2x^*}{\ell}\right)^{1/2} - 1 \right] . \qquad \text{(D-10)}$$

Assuming the space charge region is uniformly distributed from the irradiated electrode to the practical range of the primary electrons, the initial values of interest in Fig. D-6 for the 14 kev irradiation are $r/\ell = 0.58$ and $x^*/\ell = 0.41$. For zero field point movement in the range $0.41 \leq x^*/\ell \leq 0.48$ integration of Eq. (D-10) can be approximated by

$$Q_{ext}(t) \simeq \frac{qA\ell}{14} \left[\bar{n}\left(\frac{x^*}{\ell} = 0.41\right) - \bar{n}(x^*) \right] . \qquad \text{(D-11)}$$

However, for the assumed model $\bar{n}(x^*) = n_t(t)$ and

$$Q_{ext}(t) \simeq \frac{qA\ell}{14} n_r(t) \qquad \text{(D-12)}$$

where $n_r(t)$ is the number of electrons released from traps per cm^3.
This approximation applies only for the time interval where $x^*/\ell \leq 0.48$ and $r/\ell \leq 0.8$. Over this time interval, the trapped charge density has

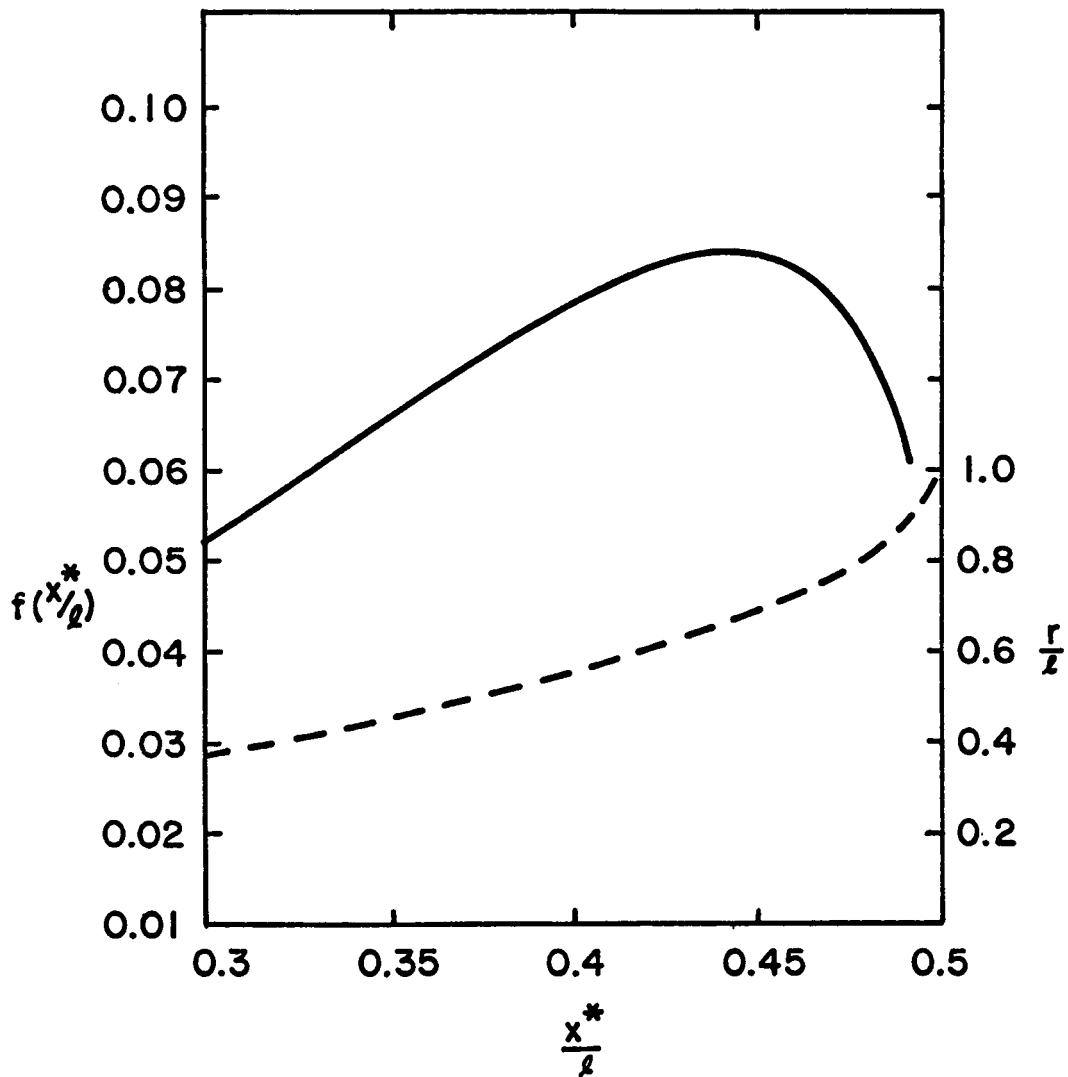Figure D-6. A plot of the functional relationships in équations D-8 and D-10.

decreased such that $\bar{n}(x*/\ell = 0.41) \sim 2.7\ \bar{n}(x*/\ell = 0.48)$ using Eq. (D-9). For the 30 minute irradiation in Fig. D-4,

$$Q_{ext}(t) = 5.4 \times 10^{-9} \ln (t/60) \qquad 60 \leq t \leq 2 \times 10^3 \ . \qquad \text{(D-13)}$$

Introducing this observation into Eq. (D-12) yields

$$n_r(t) = 7.5 \times 10^{14} \ln (t/60) \qquad 60 \leq t \leq 2 \times 10^3 \qquad \text{(D-14)}$$

for the assumed model of space charge decay. Using

$$n_r(t) = n_t(60) - n_t(t) = 7.5 \times 10^{14} \ln (t/60) \quad 60 \leq t \leq 2 \times 10^3 \quad \text{(D-15)}$$

and that over the time interval τ where the release kinetics predominate $n_t(60)/n_t(\tau) \leq 2.7$ a minimum value for $n_t(60)$ can be obtained. Since Eq. (D-13) holds for $60 \leq t \leq 2 \times 10^3$, one can choose $\tau = 2 \times 10^3$ such that $n_t(60) \geq 4 \times 10^{15}$ electrons/cm^3 or a total space charge greater than 2×10^{-7} coulomb.

For the assumption of uniform net charge density from the irradiated surface to the practical range (r) of the primary electrons, the minimum value for the trapped electron density can be used in conjunction with Poisson's equation to obtain a lower limit for the internal electric field at the irradiated surface of the polyethylene terephthalate film. Using the values $r = 3 \times 10^{-4}$ cm, $d = 6 \times 10^{-4}$ cm, $n_t \geq 4 \times 10^{15}$ electrons/cm^3, $\epsilon = 2.83 \times 10^{-13}$ farad/cm yields $|E_x = 0| \geq 5.1 \times 10^5$ volts/cm. Using the 30 minute irradiation in Fig. D-4, the minimum trapped electron density from Eq. (D-1) is $n_t \geq 1.6 \times 10^{15}$ electrons/cm^3 and $|E_x = 0| \geq 2 \times 10^5$ volts/cm. This is approximately an order of magnitude smaller than published values of the field strength (Ref. 22).

It has been possible to gain some confidence in these values of internal electric field using an applied voltage and observing the current flow before irradiation, during irradiation and after irradiation. With no bias applied, the current flow after irradiation has ceased is in a direction such that the irradiated electrode is negative with respect to the unirradiated electrode. An external dc bias was applied to the polyethylene terephthalate capacitor in a manner to oppose the current flow due to space charge decay. At various bias levels, the capacitor was irradiated with 14 kev electrons for 15 minutes at a current density

Appendix D

of 5×10^{-8} amperes/cm^2. For a bias less than 350 volts, the current
flow immediately after irradiation ceased was in the direction consis-
tent with space charge decay to the irradiated electrode for zero bias.
After approximately 10^3 seconds, the current flow was in a direction
consistent with the applied dc bias. However, for a bias greater than
350 volts, the current flow was in the direction determined by the
applied bias. For the 6×10^{-4} cm polyethylene terephthalate the
applied electric field necessary to overcome the space charge effect
is approximately 5.8×10^5 volts/cm for the 15 minute irradiation.

The reproducibility for the measurement of trapped irradiation
electron decay provides additional information about the present work.
In general, the variations from sample to sample for the measurement
of external charge transfer were greater than the estimated experimental
error. However, the results for each sample were qualitatively consis-
tent with those shown in Figs. D-2, D-3, and D-4 which are for three
different samples. The reproducibility of the charge release measure-
ment for repeated irradiations of a given sample depended upon the
number of times the particular sample had been irradiated. For the
initial irradiations on a newly prepared sample, charge release
measurements were not consistent with the measurements obtained from
subsequent irradiations. However, after the initial irradiations, the
reproducibility of the charge release measurements were within the
estimated experimental error. This dependence suggests that the
trapping sites are radiation induced.

REFERENCES

1. Monteith, L. K.: Study on the Electronic Irradiation Effects on
    Capacitor-Type Micrometeoroid Detectors. NASA CR-312, 1965.

2. Staff of Ling-Temco-Vought: Investigation of Electron Energy and
    Intensity Effects on Capacitor Type Micrometeoroid Detectors.
    NAS8-9032, 1964.

3. Storti, G. M.; Phillips, D. H.; and Frank, C. S.: Experimental
    Study of Transient Effects of Electron Irradiation. NASA TN
    D-3032, 1965.

4. Results of Transmission Computations were supplied through
    M. J. Berger, National Bureau of Standards.

5. Evans, R. D.: The Atomic Nucleus. McGraw-Hill Book Co., Inc.,
    1955, pp. 627 - 628.

6. Berger, M. J.; and Seltzer. S. M.: Results of Some Recent
    Transport Calculations for Electronics and Bremsstrahlung.
    NBS Report 8509, Dec. 1964.

7. Schultz, A. A.; and Pomerantz, M. A.: Secondary Electron Emission
    Produced by Relativistic Primary Electrons. Phys. Rev., Vol 130,
    No. 6, June 1963, pp. 2135 - 2141.

8. Kanter, H.: Energy Dissipation and Secondary Electron Emission
    in Solids. Phys. Rev., Vol 121, No. 3, Feb. 1961, pp. 677 - 681.

9. Turner, D.: The Influence of Radiation on Polymers (Polyethylene
    Terephthalate). 2nd Annual Report. NAS1-3183, 1965.

10. Fowler, J. F.: X-ray Induced Conductivity in Insulating Materials.
    Proc. Roy. Soc., No. A236, 1956, pp. 464 - 480.

11. Lengyel, G.: Schottky Emission and Conduction in Some Organic
    Insulating Materials. J. Appl. Phys., Vol. 37, No. 2, Feb. 1966,
    pp. 807 - 810.

12. Amborski, L. E.: H-Film-A New High Temperature Dielectric. Ind.
    Eng. Chem., Vol. 2, No. 5, Sept. 1963, pp. 189 - 194.

13. Rose, A.: Space-Charge-Limited Currents in Solids. Phys. Rev.,
    Vol. 97, No. 6, Mar. 1955, pp. 1538 - 1544.

14. Monteith, L. K.: Trapping and Thermal Irradiation Electrons from
    Polyethylene Terephthalate Films. J. Appl. Phys., Vol. 37, No. 7,
    June 1966, pp. 2633 - 2639.

15. Sternglass, E. J.: Backscattering of Kilovolt Electrons from Solids.
    Phys. Rev., Vol. 95, No. 2, July 1954, pp. 345 - 358.

REFERENCES (continued)

16. Kanter, H.: Contribution of Backscattered Electrons to Secondary Electron Formation. Phys. Rev., Vol. 121, No. 3, Feb. 1961, pp. 681 - 684.

17. Lindmayer, J.: Current Transients in Insulators. J. Appl. Phys., Vol. 36, 1965, p. 196.

18. Berger, M. J.; and Seltzer, S. M.: Tables of Energy Losses and Ranges of Electrons and Positrons. NASA SP-3012, 1964.

19. Young, J. R.: Dissipation of Energy by 2.5 -10 kev Electrons in Al_2O_3. J. Appl. Phys., Vol. 28, No. 5, May 1957, pp. 524 - 525.

20. Spencer, L. V.: Energy Dissipation by Fast Electrons, NBS Monograph 1, 1959.

21. Monteith, L. K.: Spontaneous Discharge from Electron Irradiated Polyethylene Terephthalate Films. Ph.D. Thesis, Duke University, 1965.

22. Yahagi, K.; and Danno, A.: Gamma-Ray Induced Conductivity in Polyethylene and Teflon under Radiation at High Dose Rate. J. Appl. Phys., Vol. 34, No. 4 part 1, Apr. 1963, pp. 804 - 809.

"The aeronautical and space activities of the United States shall be conducted so as to contribute . . . to the expansion of human knowledge of phenomena in the atmosphere and space. The Administration shall provide for the widest practicable and appropriate dissemination of information concerning its activities and the results thereof."

—NATIONAL AERONAUTICS AND SPACE ACT OF 1958

NASA SCIENTIFIC AND TECHNICAL PUBLICATIONS

TECHNICAL REPORTS: Scientific and technical information considered important, complete, and a lasting contribution to existing knowledge.

TECHNICAL NOTES: Information less broad in scope but nevertheless of importance as a contribution to existing knowledge.

TECHNICAL MEMORANDUMS: Information receiving limited distribution because of preliminary data, security classification, or other reasons.

CONTRACTOR REPORTS: Technical information generated in connection with a NASA contract or grant and released under NASA auspices.

TECHNICAL TRANSLATIONS: Information published in a foreign language considered to merit NASA distribution in English.

TECHNICAL REPRINTS: Information derived from NASA activities and initially published in the form of journal articles.

SPECIAL PUBLICATIONS: Information derived from or of value to NASA activities but not necessarily reporting the results of individual NASA-programmed scientific efforts. Publications include conference proceedings, monographs, data compilations, handbooks, sourcebooks, and special bibliographies.

Details on the availability of these publications may be obtained from:

SCIENTIFIC AND TECHNICAL INFORMATION DIVISION

NATIONAL AERONAUTICS AND SPACE ADMINISTRATION

Washington, D.C. 20546